The Dissertation Committee for Scott Andrew Zawko

certifies that this is the approved version of the following dissertation:

HYALURONIC ACID HYDROGEL MATERIALS

Committee:

_____
Christine E. Schmidt, Supervisor

_____
Keith P. Johnston

_____
Krishnendu Roy

_____
Isaac C. Sanchez

_____
Robert O. Williams III

Hyaluronic Acid Hydrogel Materials

by

Scott Andrew Zawko, B.S.

Dissertation

Presented to the Faculty of the Graduate School of

the University of Texas at Austin

in Partial Fulfillment

of the Requirements

for the Degree of

Doctor of Philosophy

The University of Texas at Austin

August 2008

Acknowledgements

I sincerely thank my advisor, Christine Schmidt, for her mentorship and guidance; I thank Shalu Suri for her enthusiastic collaboration on our super-swelling hydrogel project and her generous assistance with confocal and Schwann cell culture; Nathalie Guimard for our many stimulating chemistry discussions and experimental collaborations; Jae Lee for frequently brain-storming research ideas with me and sharing his HA expertise; Quan Truong for her dedication and plenty of enjoyable discussions; and Hyma Durgam for readily helping me innumerable times. I also thank Jon Nickels for donating his time and expertise with AFM; Prinon Hossain for his assistance with the early hydrogel experiments; Klaus Linse for assistance with HPLC and MADLI-MS; and Troy Purvis for assistance with analytical HPLC.

June 20, 2008

Hyaluronic Acid Hydrogel Materials

Publication No. _____

Scott Andrew Zawko, Ph.D.

The University of Texas at Austin, 2008

Supervisor: Christine E. Schmidt

Hyaluronic acid (HA) is one of the primary chemical building blocks of the extracellular matrix and thus is an attractive material for biomedical applications. FDA approved HA-based materials are available as dermal fillers, joint viscosupplements, vitreous substitutes, and abdominal adhesion barriers. The engineering of new HA-based materials and applications is an active area of research. Here we develop several new types of HA-based hydrogels with unique and useful properties. To address the challenge of delivering hydrophobic drugs from hydrophilic hydrogel matrices we have grafted HA hydrogels with β-cyclodextrin to create hydrogels capable of binding poorly water soluble drugs. To create HA hydrogels with unique anisotropic swelling behavior we have developed a dual-crosslinking technique in which a super-swelling chemically crosslinked hydrogel is patterned with low-swelling photocrosslinked domains. When this dual-crosslinked hydrogel is swelled it contorts into a new shape because of differential swelling among

photopatterned regions. To address the challenge of creating hydrogel scaffolds with biomimetic branched porosity we have invented a “crystal templating” technique. This technique grows dendritic crystals throughout a biopolymer solution, crosslinks the biopolymer around the crystals, and washes the crystals away to yield a hydrogel with a dendritic macroporous network. Lastly, we invented a method for patterning a substrate with a microarray of hydrogel compartments. A microarray of living cells is obtained when cells are seeded on the hydrogel patterned substrate. This method addresses the need for an inexpensive, simple method for obtaining living cell microarrays that does not require clean room labs and lithographic expertise. Each of these new materials were based on hyaluronic acid hydrogels but the methods are generalizable to hydrogels of other polymers too. In conclusion, the novel methods in this dissertation are a significant contribution to the engineering of HA-based materials.

Table of Contents

List of Tables

List of Figures

Chapter 1: Introduction to Hydrogels of Hyaluronic Acid

1.1 PROPERTIES OF HYALURONIC ACID

Hyaluronic acid (HA) is one of the primary chemical building blocks of the extracellular matrix and thus is an attractive material for biomedical applications. HA is found naturally in skin, cartilage, intra-articular joint fluid and vitreous humor.[1-3] Its role is to maintain tissue hydration, supply compressive strength, and promote cell quiescence and tissue homeostasis. Medical grade hyaluronic acid that is obtainable by bacterial fermentation is free of immunogenic animal proteins and exhibits excellent biocompatibility and non-immunogenicity.[4] HA is degraded *in vivo* by enzymes (i.e., hyaluronidases) that are prevalent in human tissues.[5] The degradation products of hyaluronidase digestion are non-toxic oligomeric sugars that can be further digested and recycled. Upregulation of HA is observed during development and during embryonic wound healing and is correlated with regeneration of scar-free tissue; thus, HA appears to play a crucial role in non-scar regeneration, the ultimate goal of tissue engineering.[6,7] FDA approved HA-based materials are available in the areas of dermal fillers, joint viscosupplementation, vitreous substitutes, and abdominal adhesion barriers.[8-11] The invention of new HA-based materials and applications is an active area of research.

It is important to recognize that in addition to its attractive qualities HA also exhibits several non-ideal properties that should be carefully considered when engineering HA-based materials. These are insolubility in organic solvents, susceptibility to pH and temperature induced degradation, and high viscosity in aqueous solutions even

at dilute concentrations. These properties can make HA difficult to chemically derivatize and make HA materials difficult to process. Therefore, the creation of novel HA-based materials is dependent on developing synthesis and fabrication techniques that are compatible with HA's unique combination of properties.

The form of HA used in Schmidt lab and throughout this dissertation is a photocrosslinkable derivative (GMHA) synthesized by the reaction of glycidyl methacrylate with hyaluronic acid. GMHA is hyaluronic acid with pendant methacrylate functionalities. Photocrosslinked hydrogels can be prepared by UV exposure of GMHA solutions containing photoinitiator. UV exposure initiates radical polymerization of the pendant methacrylate functionalities and the resulting hydrogel consists of long hyaluronic acid chains crosslinked by short polymethacrylate chains. Previously, Schmidt lab has developed and characterized the basic properties of GMHA hydrogels,[12] functionalized GMHA hydrogels with cell-adhesive peptides,[13] and explored the release of protein from GMHA hydrogels.[14] The new research detailed in this dissertation uses GMHA hydrogels as the starting material in the creation of novel HA-based materials for drug delivery, and tissue engineering, and microarray applications.

1.2 DRUG-BINDING HYALURONIC ACID HYDROGELS FUNCTIONALIZED WITH β-CYCLODEXTRIN

The function of a tissue engineering scaffold is to provide a temporary structural framework that can direct cells to regenerate scar-free healthy tissue. Polymer scaffolds alone are not sufficient for tissue regeneration because they provide only insoluble

structural components without soluble chemical signals. The next generation of polymer scaffolds needs to integrate the delivery of soluble chemical signals to promote tissue regeneration. The aqueous micro-environment and the large mesh size of HA hydrogels is well-suited for the sustained release of high molecular weight water-soluble drugs. Indeed, the release of growth factors from HA matrices has been demonstrated to have beneficial effects on cell viability and scaffold vascularization.[15,16] There are also important low molecular weight (i.e., MW < 1000 Da) poorly water soluble organic molecules that enable aspects of cell signaling. It is challenging to release these types of hydrophobic molecules from HA hydrogels because drug loading is severely limited in the aqueous micro-environment. The goal for this particular project was to design and synthesize an HA hydrogel that can release low molecular weight hydrophobic drug.

The strategy was to functionalize GMHA hydrogels with β-cyclodextrin (βCD) to endow the hydrogels with a drug-binding capability. βCD is a cyclic oligomer of seven glucose units that is obtained from the bacterial degradation of starch. Each βCD molecule is a cup-shaped nano-container with a hydrophobic cavity ~6 Å in diameter and ~260 $Å^3$ in volume.[17] In aqueous solution the βCD molecule can host a guest hydrophobic molecule within this cavity. The exterior of the βCD molecule is rendered hydrophilic by an array of hydroxyls that surround the hydrophobic cavity and guest. Formulations of βCD-drug complexes have been used by pharmaceutical scientists for many years to increase the solubility of poorly water soluble drugs.[18] The interactions between βCD and drug are non-covalent; thus, complexes in solution are at equilibrium

with free βCD and free drug. Conditions favorable to complexation are low drug solubility and high complementarity between the sizes of the drug and the cavity.

The objectives of this project, detailed in Chapter 3, were to (i) synthesize a methacryloyl-βCD monomer; (ii) synthesize GMHA hydrogels functionalized with the methacryloyl-βCD monomer; (iii) demonstrate enhanced drug absorption and drug release by GMHA-βCD hydrogels relative to ordinary non-functionalized GMHA hydrogels; and (iv) prove unambiguously the existence of drug-hydrogel complexes within the GMHA-βCD hydrogel system.

1.3 DUAL-CROSSLINKED HYDROGELS EXHIBITING ANISOTROPIC SWELLING

Swelling is a characteristic property of hydrogels caused by the diffusion of hydrogel polymer chains in solution. A swelling hydrogel increases in both weight and volume due to uptake of water. Total dissolution of the hydrogel is prevented by the presence of chemical crosslinks. The inverse relationship between crosslink density and swelling is the basis for this project.

The goal of this project was to synthesize a hydrogel that exhibits anisotropic swelling. The strategy consisted of synthesizing chemically crosslinked hydrogels and, before swelling them, patterning with photocrosslinks. The addition of photocrosslinks within the hydrogel increases the local crosslink density and decreases local equilibrium swelling. When the hydrogel is placed in solution the chemically crosslinked domains

will swell to a high degree and the dual-crosslinked domains (i.e., domains with both chemical crosslinks and photocrosslinks) will swell to a low degree. Anisotropic swelling will permit the hydrogel to contort and evolve a shape different from that of the unswollen hydrogel. Such shape changing hydrogels with patterned anisotropic swelling have not been reported. A biodegradable HA-based hydrogel with this type of swelling behavior would yield a new, unexplored type of shape changing tissue engineering scaffold.

The objectives of this project, detailed in Chapter 4, were (i) characterize the swelling of HA hydrogels chemically crosslinked by butanediol diglycidyl ether; (ii) characterize the swelling of photocrosslinked GMHA hydrogels; and (iii) combine chemical and photocrosslinking within a single hydrogel system to create hydrogels with anisotropic swelling.

1.4 HYALURONIC ACID HYDROGELS WITH DENDRITIC POROSITY OBTAINED BY CRYSTAL TEMPLATING

There are two kinds of porosity within a hydrogel. Micro-porosity consists of the pores among individual polymer chains. This porosity is a result of the solvation of HA by water which induces HA chains to swell. The length scale of microporosity is on the order of 10 nm to 100 nm which is sufficient for the diffusion of water, oxygen, salts, and low molecular weight metabolites. Macro-porosity is on the length scale of 1 μm to 100 μm. Tissue engineered scaffolds require macro-porosity to permit rapid protein diffusion, cellular migration, and ingress of microvessels from surrounding tissue.

Several methods have been developed to create polymeric scaffolds with macro-porous networks. Rapid prototyping techniques (e.g., 3D printing and stereolithography) use software to plot the porous networks which are precisely sculpted in three dimensions by a method suitable to the polymer of interest.[19-21] Simpler techniques use a particulate leeching strategy such as leeching of salt crystals or microspheres from crosslinked polymer scaffolds.[22-24] Another method is the freezing of a polymer solution followed by sublimation of solvent (e.g., lyophilization of PLGA-dioxane solutions).[25-27]

A limitation of these methods is that they are incompatible with HA hydrogels because they require extreme temperature or pH, polymer solubility in organic solvent, or concentrated low viscosity solutions. A further limitation is that the above methods are unable to create the dendritic porous architecture that is exhibited by microvasculature, glandular epithelial ducts, and networks of nerve endings.

This project concerns the invention of a "crystal templating" technique for patterning biopolymer hydrogels with dendritic macro-porous networks. Large dendritic crystals (i.e., crystal templates) were grown within aqueous HA solutions. The biopolymer was then crosslinked around the template and the template was washed out with water. The advantages of this technique are that it creates unique branched networks, requires no extreme temperature or pH, can be scaled and performed in parallel, and has no requirement for expensive machines and instruments such as those that are necessary for rapid prototyping.

The objectives of this project, detailed in Chapter 5, were (i) develop a crystal-templating technique to pattern HA hydrogels; (ii) characterize the morphology of the

patterned hydrogel; and (iii) identify the key parameters that determine the resulting macroporous network structure.

1.5 LIVING CELL MICROARRAYS OBTAINED BY PATTERNED HYDROGEL MESHES

Highly developed technologies have been invented in recent years for the fabrication of DNA microarrays.[28] The microarrays consist of biological molecules covalently tethered to a substrate in a defined grid pattern. The microarray facilitates high throughput data acquisition and image analysis and has permitted a number of new diagnostic assays to be developed. In contrast to the advances of biomolecule microarrays the development of living cell microarrays has not progressed as far. The fundamental hurdle of creating cell microarrays is obtaining a grid of cell-adhesive compartments. Current methods use clean room equipment and lithographic techniques to fabricate grid patterns, but access to this equipment has been identified as a significant impediment to the spread of living cell microarrays to many research groups.[29]

This project describes the invention of an extremely simple method for patterning living cell microarrays. This invention fulfills the need for a simple cell patterning technique that can be easily disseminated to other research labs without transference of custom made apparatuses, clean room expertise, and specialized technical and chemical synthetic skills. The key insight to our invention is that nylon mesh in the desired appropriate grid pattern is abundantly available, off-the-shelf, and inexpensive. We

developed a method for transferring the grid pattern from nylon mesh to a hydrogel mesh adhered to a cell culture substrate. The hydrogel mesh is non-cell adhesive and delineates individual microarray compartments. Biological cells that are seeded on the patterned substrate adhere to the individual compartments but not the hydrogel partitions. This patterning method can array both cell clusters and single-cells thus paving the way for truly single-cell assays and diagnostics.

Cell microarrays are applicable as cell-based sensors of environmental toxins and pathogens, cell-based medical diagnostics, and *in vitro* drug screening assays.[30] Furthermore, cell microarrays and biomolecule microarrays can be expected to be highly synergistic technologies. For example, cell microarrays overlaid on DNA microarrays can be used to create transfection arrays, loss of function arrays, and other assays of cell response to the underlying biomolecules.[31, 32]

The objectives of this project, detailed in Chapter 6, were (i) develop a method for creating hydrogel meshes from nylon meshes; and (ii) evaluate the ability of the meshes to create living cell microarrays.

1.6 REFERENCES

1. Bishop, P.N. Structural macromolecules and supramolecular organization of the vitreous gel. *Prog. Retin. Eye Res.,* **19**, 323-344 (2000).
2. Huber, M., Trattnig, S., Lintner, F. Anatomy, biochemistry, and physiology of articular cartilage. *Invest. Radiol.,* **35**, 574-580 (2000).
3. Price, R.D., Myers, S., Leigh, I.M., Navsaria, H.A. The role of hyaluronic acid in wound healing. *Am. J. Clin. Dermatol.* **6**, 393-402 (2005).
4. Agerup, B., Berg, P., Akermark, C. Non-animal stabilized hyaluronic acid. *BioDrugs,* **19**, 23-30 (2005).
5. Stern, R. Devising a pathway for hyaluronan catabolism: are we there yet? *Glycobiology,* **13**, 105R-115R (2003).
6. Chen, W.Y., Abatangelo, G. Functions of hyaluronan in wound repair. *Wound Repair Regen.,* **7**, 79-89 (1999).
7. Estes, J.M., Adzick, N.S., Harrison, M.R., Longaker, M.T., Stern, R. Hyaluronate metabolism undergoes an ontogenic transition during fetal development: implications for scar-free wound healing. *J. Pediatr. Surg.,* **28**, 1227-31 (1993).
8. Reijnen, M.M.P.J., Bleichrodt, R.P., van Goor, H. Pathophysiology of intra-abdominal adhesion and abscess formation, and the effect of hyaluronan. *Brit. J. Surg.,* **90**, 533-541 (2003).
9. Monheit, G.D., Coleman, K.M. Hyaluronic acid fillers. *Dermatol. Ther.,* **19**, 141-150 (2006).

10. Arshinoff, S.A. Dispersive-cohesive viscoelastic soft shell technique. *J. Cataract Refract. Surg.,* **25**, 167-173 (1999).

11. Kirchner, M., Marshall, R.N. A double-blind randomized controlled trial comparing alternate forms of high molecular weight hyaluronan for the treatment of osteoarthritis of the knee. *Osteoarthritis Cartilage,* **14**, 154-162 (2006).

12. Leach, J.B., Bivens, K.A., Patrick, C.W., Schmidt, C.E. Photocrosslinked hyaluronic acid hydrogels: natural, biodegradable tissue engineering scaffolds. *Biotechnol. Bioeng.,* **82**, 578-589 (2003).

13. Leach, J.B., Bivens, K.A., Collins, C.N., Schmidt, C.E. Development of photocrosslinkable hyaluronic acid-polyethylene glycol-peptide composite hydrogels for soft tissue engineering. *J. Biomed. Mater. Res.,* **70**, 74-82 (2004).

14. Leach, J.B., Schmidt, C.E. Characterization of protein release from photocrosslinkable hyaluronic acid-polyethylene glycol hydrogel tissue engineering scaffolds. *Biomaterials,* **26**, 125-135 (2005).

15. Peattie, R.A., Rieke, E.R., Hewett, E.M., Fisher, R.J., Shu, X.J., Prestwich, G.D. Dual growth factor-induced angiogenesis in vivo using hyaluronan hydrogel implants. *Biomaterials,* **27**, 1868-1875 (2006).

16. Pike, D.B., Cai, S., Pomraning, K.R., Firpo, M.A., Fisher, R.J., Shu, X.Z., Prestwich, G.D., Peattie, R.A. Heparin-regulated release of growth factors in vitro and angiogenic response in vivo to implanted hyaluronan hydrogels containing VEGF and bFGF *Biomaterials,* **27**, 5242-5251 (2006).

17. Uekama, K. Design and evaluation of cyclodextrin-based drug formulation. *Chem. Pharm. Bull.,* **52**, 900-915 (2004).

18. Szente, L., Szejtli, J. Highly soluble cyclodextrin derivatives: chemistry, properties, and trends in development. *Adv. Drug Deliver. Rev.,* **36**, 17-28 (1999).

19. Yang, S.F., Leong, K.F., Du, Z., Chua, C.K. The design of scaffolds for use in tissue engineering. Part II. Rapid prototyping techniques. *Tissue Eng.,* **8**, 1-11 (2002).

20. Lu, Y., Mapili, G., Suhali, G., Chen, S., Roy, K. A digital micro-mirror device-based system for the microfabrication of complex, spatially patterned tissue engineering scaffolds. *J. Biomed. Mater. Res.,* **77A**, 396-405 (2006).

21. Tsang, V.L., Chen, A.A., Cho, L.M., Jadin, K.D., Sah, R.L., DeLong, S., West, J.L., Bhatia, S.N. Fabrication of 3D hepatic tissue by additive photopatterning of cellular hydrogels. *FASEB J.,* **21**, 790-801 (2007).

22. Mikos, A.G., Thorsen, A.J., Czerwonka, L.A., Bao, Y., Langer, R., Winslow, D.N., Vacanti, J.P. Preparation and characterization of poly(L-lactic acid) foams. *Polymer,* **35**, 1068-1077 (1994).

23. Ma, P.X., Choi, J.W. Biodegradable polymer scaffolds with well-defined interconnected spherical pore network. *Tissue Eng.,* **7**, 23-33 (2001).

24. Murphy, W.L., Dennis, R.G., Kileny, J.L., Mooney, D.J. Salt fusion: an approach to improve pore interconnectivity within tissue engineering scaffolds. *Tissue Eng.,* **8**, 43-52 (2002).

25. Cho, C.H, Eliason, J.F., Matthew, H.W.T. Application of porous glycosaminoglycan-based scaffolds for expansion of human cord blood stem cells in perfusion culture. *J. Biomed. Mater. Res.,* **86**, 98-107 (2008).

26. Schugens, Ch., Maquet, V., Grandfils, C., Jerome, R., Teyssie, Ph. Biodegradable and macroporous polylactide implants for cell transplantation: 1. Preparation of macroporous polylactide supports by solid-liquid phase separation. *Polymer,* **37**, 1027-1038 (1996).

27. Teng, Y.D., Lavik, E.B., Qu, X., Park, K.I., Ourednik, J., Zurakowski, D., Langer, R., Snyder, E.Y. Functional recovery following traumatic spinal cord injury mediated by a unique polymer scaffold seeded with neural stem cells. *PNAS,* **99**, 3024-3029 (2002).

28. Dufva, M. Fabrication of high quality microarrays. *Biomol. Eng.,* **22**, 173-184 (2005).

29. Falconnet, D., Csucs, G., Grandin, H.M., Textor, M. Surface engineering approaches to micropattern surfaces for cell-based assays. *Biomaterials*, **27**, 3044-3063 (2006).

30. Kim, H., Cohen, R.E., Hammond, P.T., Irvine, D.J. Live lymphocyte arrays for biosensing *Adv. Funct. Mater.,* **16**, 1313-1323 (2006).

31. Ziauddin, J., Sabatini, D.M. Microarrays of cells expressing defined cDNAs *Nature*, **411**, 107-110 (2001).

32. Wheeler, D.B., Carpenter, A.E., Sabatini, D.M. Cell microarrays and RNA interference chip away at gene function. *Nature Genetics*, **37**, S25-S30 (2005).

Chapter 2: Photocured Hydrogel Films of Hyaluronic Acid

Abstract

This chapter discusses two protocols that are used throughout the remaining chapters. These protocols and experimental data comprise the early preliminary work of this dissertation. The first protocol is the synthesis of photocrosslinkable glycidyl methacrylate modified hyaluronic acid (GMHA). This derivative was synthesized by the reaction of glycidyl methacrylate with HA in a solvent mixture of water and acetone. The novelty of this protocol is that it used an organic water mixture to increase the degree of methacryloyl substitution. The second protocol is the synthesis of photocured GMHA hydrogel films. The literature describes many methods for creating films of hyaluronic acid. These methods typically consist of mixing HA with a chemical crosslinker in solution, adjusting the pH, casting the solution, and evaporating the solvent. This method has the advantage of simplicity but lacks reproducibility of film properties. To address the lack of reproducibility we developed a novel method of synthesizing photocured GMHA films. These films were prepared by mixing GMHA with a photoinitiator and casting the solution. After solvent evaporation the film was crosslinked by one minute exposure to UV light. This photocrosslinking method produced hydrogel films with a greater degree of control over the crosslinking reaction than is possible with chemical crosslinking methods. The photocured GMHA films were transparent, low swelling, and resistant to cell adhesion.

2.1 Introduction

In this dissertation a hydrogel *film* refers to a thin, planar, free-standing, water-swelling material. Hydrogel films resist protein adsorption and cell adhesion because they are surrounded by a layer of tightly bound water molecules. These properties permit hydrogels to evade cellular detection and exhibit high degrees of non-immunogenicity and biocompatibility. The porous, hydrated properties of hydrogels permit the diffusion of oxygen, ions, metabolites, nutrients, and even proteins if hydrogel pores are large enough.[1] Hydrogel films may be applied as tissue engineered scaffolds and drug delivery reservoirs.[2,3] Some hydrogel films are used as abdominal adhesion barriers to prevent the formation of scar tissue between intra-abdominal surfaces that are wounded during surgery.[4] Genzyme's Seprafilm™ is an adhesion barrier partially composed of hyaluronic acid.[5] Hydrogel films of hyaluronic acid (HA) have the additional properties of biodegradability by hyaluronidases that are found in human tissues *in vivo*.[6]

The literature describes many methods for producing HA films. Common chemical crosslinkers are diglycidyl ethers and divinyl sulfone.[7] Crosslinking typically consists of mixing HA with the crosslinker, adjusting the pH, casting the solution, and evaporating the solvent. This evaporation step can require several days or longer depending on the desired thickness of the film. After evaporation the films are neutralized with dilute acid or base and washed with organic solvents to remove excess crosslinker. The advantage of this technique is its simplicity. The primary disadvantage is extremely poor reproducibility of hydrogel properties due to several factors. First, the concentration, viscosity, and pH of the solution changes dramatically during solvent evaporation;

therefore, the crosslinking reaction is uncontrolled. Second, HA is sensitive to acid and base conditions; therefore, there is simultaneous uncontrolled degradation of the HA backbone during solvent evaporation. Third, the ambient humidity and temperature can radically affect the rate of evaporation and the final water content of the cast films, thus further impairing control of the crosslinking reaction. Lastly, neutralization of the pH is difficult because it is not possible to accurately predict the pH of the evaporated films nor is it possible to accurately measure the pH within the hydrogel. An additional disadvantage is the inability to encapsulate proteins and drugs within the hydrogels due to cross-reactivity with the crosslinker and pH-induced degradation.

We have used the technique of photoinitiated crosslinking to circumvent the disadvantages of chemical crosslinking. We prepared an aqueous solution of a methacryloyl-derivative of hyaluronic acid (GMHA) and photoinitiator (Irgacure 2959). The solution was cast into a dish and evaporated at ambient conditions. After evaporation the hydrogel films were exposed for one minute to 365 nm UV light to initiate polymerization of methacryloyl functionalities. The reproducibility of this method was much improved compared to chemical crosslinking in several respects. First, the pH did not need to be altered. Second, there was no chemical reaction during the lengthy evaporation step which was the primary source of heterogeneity in the chemical crosslinking reaction. Third, there was no degradation of hyaluronic acid due to acidic and basic conditions. Fourth, no pH neutralization step was required. Fifth, organic solvents were not needed to rinse out oily chemical crosslinkers; water was sufficient for removing the aqueous-soluble Irgacure 2959. Sixth, the photocrosslinking reaction was

easily controlled by modulating the duration of UV exposure. Lastly, the method is more compatible with encapsulated drugs and proteins.

A limitation of the photocuring method is that a chemical synthetic step is required to render HA photocrosslinkable; whereas, chemical crosslinking can be performed with unmodified HA directly off-the-shelf. An important parameter that impacts the success of photocuring is the hygroscopicity of the evaporated hyaluronic acid films. The air-dried films possess a water content that is in equilibrium with the ambient humidity. This water content has a decisive effect on the diffusion of photoinitiator and methacryloyl groups within the air-dried films. We found that dessicated films exposed to UV did not crosslink and rapidly dissolved in water. Therefore, to ensure reproducibility of the hydrogel properties it is important to equilibrate the ambiently dried films at a well-defined humidity until immediately prior to UV exposure.

Another important consideration is the number of methacryloyl groups grafted to the HA backbone. HA can be reacted with either methacrylic anhydride or with glycidyl methacrylate (GMHA) to produce a photocrosslinkable derivative.[8,9] The grafting reaction must be performed in aqueous solution because HA is insoluble in organic solvents. The exclusion of organic solvents is problematic because the methacryloyl reactants are poorly water soluble and high concentrations are needed for the grafting reaction. Therefore, we investigated the reaction of glycidyl methacrylate with HA in mixtures of water and acetone that we predicted would be more effective at solubilizing both HA and glycidyl methacrylate than water alone. To perform this reaction a base,

triethylamine, was used to activate the primary hydroxyls of HA. The activated hydroxyls attack the epoxide ring of the glycidyl methacrylate. The resulting GMHA derivative consists of hyaluronic acid with methacryloyl functionalities linked through epoxy spacers to the primary hydroxyls of HA. The degree of substitution (DS) is the percentage of HA disaccharides that are substituted with a methacryoyl functionality. The goal of our first experiments was to maximize the DS of the GMHA derivative by changing the solvent composition. The goal of the remaining experiments in this chapter was to use the GMHA thus obtained to create photocured hydrogel films.

2.2 Results and Discussion

2.2.1 Water/Acetone mixtures for HA modification. The chemical structures of hyaluronic acid and glycidyl methacrylate are given in **Figure 2.1**. The HA molecule is highly water soluble because of the high density of hydroxyls and carboxyls along the HA backbone. In organic solvents HA undergoes strong intramolecular hydrogen bonding and precipitates from solution. Water is a polar protic solvent whereas acetone is a polar aprotic solvent. We predicted that water/acetone mixtures would facilitate the reaction of glycidyl methacrylate with hyaluronic acid by solubilizing the reactants more effectively than water alone. Furthermore, polar aprotic solvents favor S_N2 reactions such as the base catalyzed ring-opening of epoxides. Increasing the proportion of acetone in the solvent mixture decreases the mixture's protic character and will increase the solubility of glycidyl methacrylate; however, if the protic character of the mixture is decreased too much the HA will precipitate. Therefore, our first step was to test the

solubility of HA in mixtures of water and acetone. We found that HA was soluble up to 1% w/v in solvent mixtures of up to 50% acetone but not soluble in mixtures with greater proportions of acetone.

The reaction of glycidyl methacrylate with HA was performed in either pure water (GMHA00), 70/30 water/acetone (GMHA30) or 50/50 water/acetone (GMHA50). The DS was determined from ^{1}H NMR spectra by taking the ratio of glycidyl methacrylate methyl protons to HA methyl protons (**Figure 2.2**). GMHA00 had a DS of 11 ± 2.8% (average of two synthesis batches); GMHA30 had a DS of 24 ± 1.2% (average of three synthesis batches); and GMHA50 had a DS of 33 ± 1.0% (average of three synthesis batches). Based on NMR data the addition of acetone facilitated the reaction of glycidyl methacrylate with HA.

Hydrogels synthesized from GMHA with increasing DS should have a greater density of poly(methacrylate) crosslinks and reduced swelling. We found that GMHA00 hydrogels swelled to 55 ± 3.0 g PBS/g polymer; GMHA30 hydrogels swelled to 36 ± 1.9 g PBS/g polymer; and GMHA50 hydrogels swelled to 31 ± 1.5 g PBS/g polymer (**Figure 2.3**). Thus, these results supported the hypothesis that increasing acetone would facilitate methacryloyl substitution and decrease swelling.

We reasoned that GMHA hydrogels with a greater DS would exhibit slower degradation rates due to increased crosslink density. Hydrogels were degraded in solutions containing hyaluronidase, an enzyme that degrades HA *in vivo*. Degradation was followed by measuring the weights of the hydrogels. The time to 50% weight loss of GMHA00 hydrogels was 0.66 ± 0.06 hours; for GMHA30 hydrogels the time was 4.5 ±

0.46 hours; and for GMHA50 hydrogels the time was 13 ± 1.6 hours (**Figure 2.4**). Thus, these results supported the hypothesis that increasing acetone composition in the reaction mixture facilitates methacryloyl substitution. In conclusion, we demonstrated that a mixture of 50/50 water/acetone maximizes the number of methacryloyl groups grafted to HA. Complementary data obtained by NMR, swelling, and degradation consistently supported this conclusion. Similar results in which a GMHA derivative was synthesized with a 90% DS in a 50/50 co-solvent of water/DMF are support our hypothesis that polar aprotic solvent mixtures can facilitate the reaction of HA with hydrophobic reagents.[10]

2.2.2 Photocuring of GMHA hydrogel films. The GMHA derivative synthesized in 50:50 water/acetone was used to create both solvent cast photocured hydrogel films as well as hydrogels photocrosslinked in solution. Photographs of a GMHA hydrogel film (left) and solution photocrosslinked hydrogels (right) are depicted in **Figure 2.5**. The solution photocrosslinked hydrogels are the basis of the cyclodextrin-HA hydrogels in Chapter 3. The hydrogel films are used throughout Chapter 5 and are the basis of the hydrogel meshes in Chapter 6. These hydrogel films were optically transparent, flexible, and mechanically robust to handling.

The synthesis conditions of photocured films were optimized with respect to duration of UV exposure and concentration of photoinitiator. First, hydrogel films were prepared from solutions of 1% w/v GMHA50 in water with Irgacure 2959 at a concentration of 5% w/w with respect to GMHA. After solvent casting and evaporation, the hydrogel films were exposed to various durations of UV exposure ranging from 15 seconds to 5 minutes. The goal was to find the minimum amount of UV exposure

required to produce mechanically stable photocured hydrogel films. Films that were exposed to 15 seconds of UV dissolved rapidly in water indicating that insufficient crosslinks had formed. Films that were crosslinked with 30 seconds of UV exposure did not dissolve. Quantitative measurements of swelling based on weight (i.e., swelling ratio) and diameter (i.e., % linear swelling) indicated that swelling was not strongly dependent on UV exposure in the range of 30 seconds to 5 minutes (**Figure 2.6a**); however, qualitative assessment of mechanical stability indicated that films exposed to only 30 seconds of UV were more fragile than films exposed to UV for longer durations. UV exposures beyond 1 minute did not appear to have an effect on the stability of the hydrogel films. Based on these results, we used 1 minute of UV exposure as the default exposure time for photocured hydrogel film synthesis.

Next, hydrogel films were prepared with various concentrations of photoinitiator ranging from 1% to 10% w/w. All films were exposed to 1 minute of UV. The trends in swelling ratio and % linear swelling were similar. Films with 2.5% and 1.0% w/w photoinitiator absorbed more solution and swelled to greater diameters than films with 5% and greater photoinitiator (**Figure 2.6b**). Based on these results, the optimum photoinitiator concentration was determined to be 5% w/w because it minimized swelling.

HA has a high density of hydroxyls and carboxyls on the backbone. These groups tightly bind water molecules and permit hydrogels produced from HA to resist protein adsorption and cell adhesion. This is a useful property for applications such as adhesion barriers, drug delivery matrices, and protective coatings for which non-biofouling

surfaces are desired. To rigorously challenge the ability of the photocured films to resist cell adhesion we selected experimental conditions that strongly favor cell adhesion. Normal human dermal fibroblasts (nHDF) are a cell type that is particularly durable, secretes many extracellular matrix molecules that support adhesion, and robustly adheres to a variety of surfaces. Furthermore, we used cell culture media supplemented with 10% fetal bovine serum; thus, the media had a high concentration of proteins that can adsorb to the hydrogel surface and support cell adhesion. Hydrogel films were incubated in media with 10% serum for 24 hours prior to cell seeding. Cell adhesion was assessed 24 hours after cell seeding by staining cells with calcein, a fluorescent dye that labels live cells. Fibroblasts failed to adhere to photocured GMHA films proving that these films can resist cell adhesion even under conditions that strongly favor adhesion (**Figure 2.7**). Positive control substrates of tissue culture polystyrene supported the growth of fibroblasts.

Surprisingly, previous work on photocured HA hydrogel films appears to be limited to a series of US patents issued to Seikagaku Corporation (US Patent #5,462,976, #5,763,504, #6,602,859). Their chemical synthetic strategy was to functionalize HA with cinnamic acid, uracil, and thymine chemical groups. Irradiation by UV light induces these functionalities to undergo dimerization through cyclobutane linkages. A recent patent application by Seikagaku Corporation (US Patent Application 20060057098) claims photocured HA films obtained by acryloyl and methacryloyl polymerization in addition to the cyclobutane dimerization chemistries. This patent application also describes performing the methacrylate functionalization of HA in aqueous solvent

mixtures of up to 50% organic solvent. This similar line of research indicates the utility and potential commercial use of these protocols for engineering HA-based materials.

In conclusion, this chapter describes two protocols: one protocol for synthesizing GMHA and another protocol for creating photocured GMHA films. In subsequent chapters, GMHA always indicates that the photocrosslinkable HA derivative was prepared in 50/50 water/acetone and has an average DS of 33%. All GMHA hydrogel films in later chapters (i.e., Chapter 5 and Chapter 6) were cast from 1% GMHA solutions with 5% w/w Irgacure 2959 and 1 minute of UV exposure.

2.3 Materials and Methods

2.3.1 Materials. High molecular weight sodium hyaluronate from *Streptococcus equi* of molecular weight 1.6×10^6 Da and bovine testicular hyaluronidase (1000 U/mg) were obtained from Sigma-Aldrich (St. Louis, MO). Irgacure 2959 was obtained from Ciba Specialty Chemicals (Basel, Switzerland). All other chemicals and reagents were obtained from Sigma-Aldrich. Circular silicone rubber molds (Grace Bio-Labs, Bend, OR) of 9 mm diameter and 2 mm thickness were used for making hydrogels. A longwave UV lamp filtered around 365 nm and with an intensity of 22 mW/cm^2 was used to initiate photopolymerization (Blak-Ray B-100A, UVP, Upland, CA).

2.3.2 Methacryloyl modification of hyaluronic acid (GMHA). Hyaluronic acid was conjugated with photopolymerizable methacryloyl groups by reaction with glycidyl methacrylate. The reaction was performed in either pure water (GMHA00), 70/30 water/acetone (GMHA30) or 50/50 water/acetone (GMHA50). A 1% w/v solution of HA

was prepared in the appropriate solvent and stirred 24 hours. Twenty molar equivalents of triethylamine as base catalyst and twenty molar equivalents of glycidyl methacrylate were added to the solution and stirred for 24 hours at room temperature. The glycidyl methacrylate-modified hyaluronic acid (GMHA) was precipitated into a 20-fold volumetric excess of acetone, dissolved in water for 24 hours, precipitated a second time, redissolved in water for another 24 hours, and lyophilized.

2.3.3 NMR. ^{1}H NMR samples were dissolved in deuterium oxide at 10 mg/mL and the spectra recorded on a Varian Unity +300 spectrometer. The degree of substitution (DS) was calculated by integration of HA methyl protons (1.90 ppm, 3 H atoms) and methacrylate methyl protons (1.85 ppm, 3 H atoms).

2.3.4 Preparation of photocrosslinked GMHA hydrogels. Gelation solutions of 20 mg/mL GMHA were prepared in phosphate buffered saline (PBS, 10 mM, pH 7.4) containing 1% w/v Irgacure 2959 and 0.3% N-vinyl pyrrolidone. Hydrogels were each prepared from 100 μL of gelation solution and 5 minutes of UV exposure. The hydrogels were then swelled to equilibrium in PBS and rinsed with several exchanges of PBS to remove photoinitiator.

2.3.5 Hydrogel swelling ratio measurements. A small portion of each swollen gel, 10-15 mg, was placed in a thermogravimetric analyzer (Perkin Elmer TGA 7) and heated at 100°C until all water was evaporated and a constant dry weight obtained. The mass of residual PBS salts contributing to the dry weight was determined from the mass of evaporated water and was subtracted to obtain the dry weight of the polymer alone. The swelling ratio was calculated according to Equation 3, where SR [g PBS / g polymer]

is the swelling ratio, W_S [g] is the swollen weight of the hydrogel, and W_D [g] is the dry weight of the hydrogel. Three hydrogels were analyzed per condition.

$$SR = \frac{W_S - W_D}{W_D} \quad [1]$$

2.3.6 Enzymatic degradation of GMHA hydrogels. A stock solution of hyaluronidase (500 U/mL) was prepared in citrate buffer. Hydrogels were swollen to equilibrium in citrate buffer. The swollen weight of the hydrogels was measured on an analytical balance. The hydrogels were then transferred to hyaluronidase solution and incubated at 37°C. The hydrogels were removed at various timepoints, carefully blotted, and reweighed. The hydrogels were then placed in fresh hyaluronidase solution. Hydrogels were degraded until complete dissolution. The percent degradation was calculated by Equation 2. Eight hydrogels were analyzed per condition but some hydrogels broke into small pieces at later time points due to degradation and were discarded.

$$\%Degradation = \frac{W_0 - W_t}{W_0} \text{ x } 100\% \quad [2]$$

2.3.7 Preparation of photocured GMHA hydrogel films. Aqueous solutions were prepared containing 1% w/v GMHA and 0.05% w/v Irgacure 2959. All steps were performed sterilely to prevent bacterial growth in the hyaluronic acid solutions. The solution was filter sterilized (0.22 μm PVDF, Millipore) and dispensed into sterile, non-tissue culture treated 12-well plates. Each well was 2.2 cm in diameter and a volume of 2.6 mL of sterile solution was dispensed per well. The solvent was evaporated in a sterile

horizontal flow hood in the dark for four days at ambient temperature and humidity. After evaporation, the films were humidified for four days in humid chambers equilibrated with saturated salt solutions. The films were photocrosslinked by exposure to UV light for 30 seconds to 5 minutes.

2.3.8 Photocured film swelling studies. After photocrosslinking, hydrogel films were dessicated and weighed on an analytical balance. The films were then swelled in PBS at 37°C for 24 hours. The swollen films were carefully blotted to remove excess liquid and reweighed. The swelling ratio was calculated by Equation 1 given above. The diameter of the films was measured with electronic calipers. The % linear swelling was calculated by Equation 3 in which the swollen and dry diameters are D_S and D_D respectively.

$$\%LinearSwelling = \frac{D_S - D_D}{D_D} \text{ x } 100\% \qquad [3]$$

2.3.9 Cell adhesion study. Normal human dermal fibroblasts were obtained from Cambrex and cultured in DMEM with 10% fetal bovine serum (FBS). The fibroblasts were seeded onto either tissue culture polystyrene (positive control) or onto photocured GMHA hydrogels films. Hydrogel films were incubated in DMEM with 10% FBS for 24 hours prior to cell seeding. After 24 hours the cells were stained with 4 mM calcein AM (Live/Dead Viability Kit, Molecular Probes) and imaged by epifluorescence.

2.4 References

1. Tessmar, J.K., Gopferich, A.M. Matrices and scaffolds for protein delivery in tissuse engineering. *Adv. Drug Deliver. Rev.,* **59**, 274-291 (2007).
2. Hoare, T.R., Kohane, D.S. Hydrogels in drug delivery: progress and challenges. *Polymer*, **49**, 1993-2007 (2008).
3. Drury, J.L., Mooney, D.J. Hydrogels for tissue engineering: scaffold design variables and applications. *Biomaterials* **24**, 4337-4351 (2003).
4. Yeo, Y., Kohane, D.S. Polymers in the prevention of peritoneal adhesions *Eur. J. Pharm. Biopharm.,* **68**, 57-66 (2008).
5. Seprafilm Package Insert (Genzyme Corporation) http://www.seprafilm.com/pdf/seprafilm_package_insert.pdf
6. Stern, R. Devising a pathway for hyaluronan catabolism: are we there yet? *Glycobiology,* **13**, 105R-115R (2003).
7. Collins, M.N., Birkinshaw, C. Comparison of the effectiveness of four different crosslinking agents with hyaluronic acid hydrogel films for tissue-culture applications. *J. Appl. Polym. Sci.,* **104**, 3183-3191 (2007).
8. Leach, J.B., Bivens, K.A., Patrick, C.W., Schmidt, C.E. Photocrosslinked hyaluronic acid hydrogels: natural, biodegradable tissue engineering scaffolds. *Biotechnol. Bioeng.,* **82**, 578-589 (2003).
9. Burdick, J.A., Chung, C., Jia, X.Q., Randolph, M.A., Langer, R. Controlled degradation and mechanical behavior of photopolymerized hyaluronic acid networks. *Biomacromolecules*, **6**, 386-391 (2005).

10. Bencherif, S.A., Srinivasan, A., Horkay, F., Hollinger, J.O., Matyjaszewski, K., Washburn, N.R. Influence of the degree of methacrylation on hyaluronic acid hydrogels properties. *Biomaterials* **29**, 1739-1749 (2008).

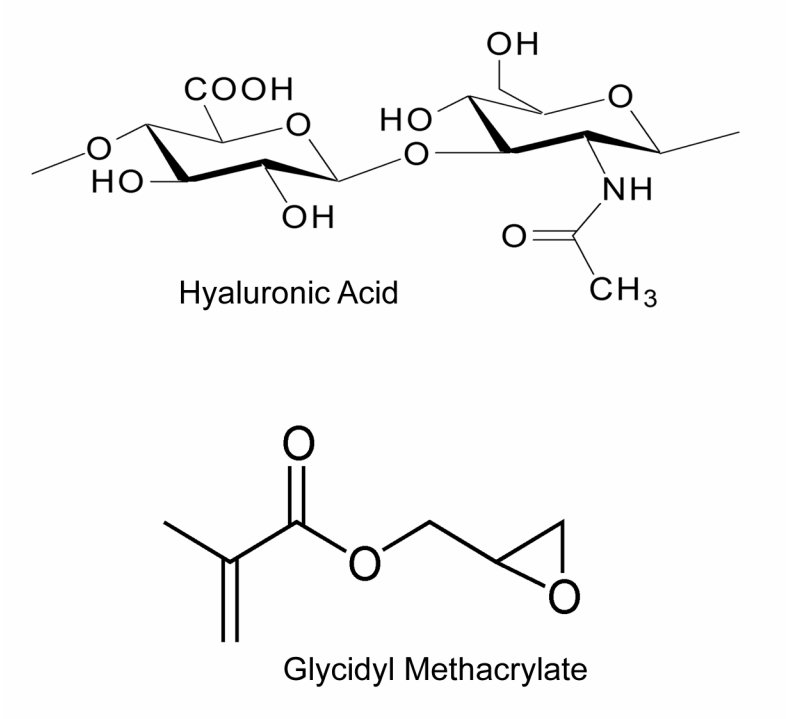

Figure 2.1 Chemical structures of hyaluronic acid and glycidyl methacrylate. Photocrosslinkable hyaluronic acid is prepared by conjugation of glycidyl methacrylate.

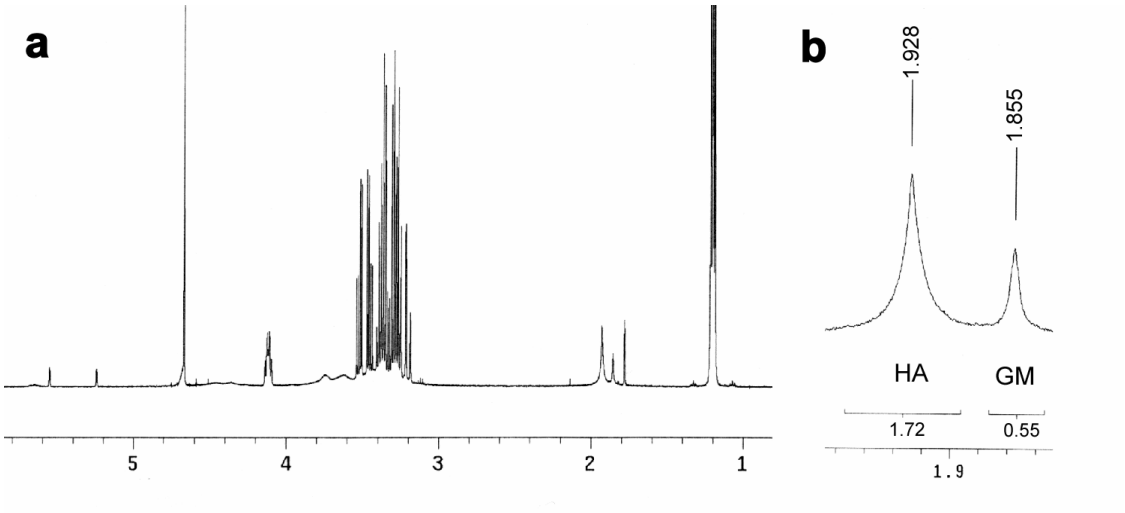

Figure 2.2 Full spectrum ^{1}H NMR spectra of GMHA50 (**a**) and expansion of methyl proton signals (**b**). The DS was determined by integrating the signals at 1.855 ppm and 1.928 ppm and calculating the ratio. The DS was 0.32 methacryloyl groups per disaccharide of hyaluronic acid.

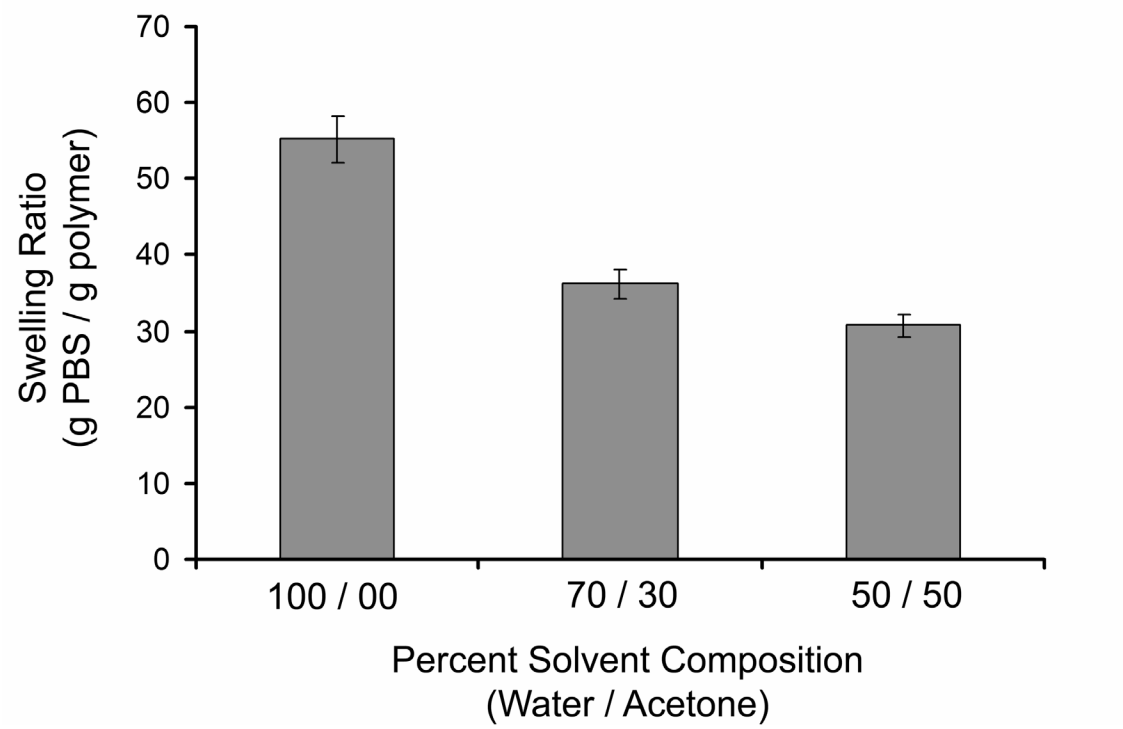

Figure 2.3 Swelling ratios of GMHA hydrogels in PBS. GMHA was synthesized in solvents containing different compositions of water and acetone. GMHA synthesized in solvents with greater percentages of acetone produced hydrogels with greater crosslink density and less swelling; therefore, increasing amounts of acetone facilitated the grafting of glycidyl methacrylate to hyaluronic acid. Data are average ± standard deviation of three specimens.

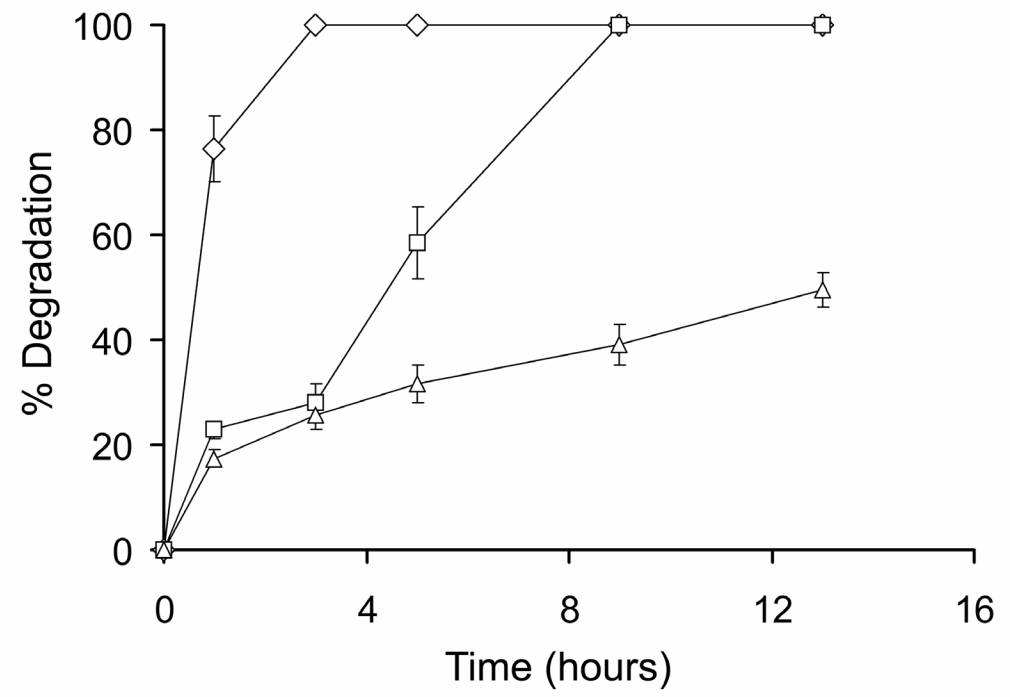

Figure 2.4 Enzymatic degradation of GMHA hydrogels by hyaluronidase at 37°C. GMHA was synthesized in solvents containing different compositions of water and acetone. GMHA synthesized in solvents with greater percentages of acetone produced hydrogels with greater crosslink density and slower rates of degradation; therefore, increasing amounts of acetone facilitated the grafting of glycidyl methacrylate onto hyaluronic acid. GMHA00 = diamonds. GMHA30 = squares. GMHA50 = triangles. Data are average ± standard deviation of eight specimens.

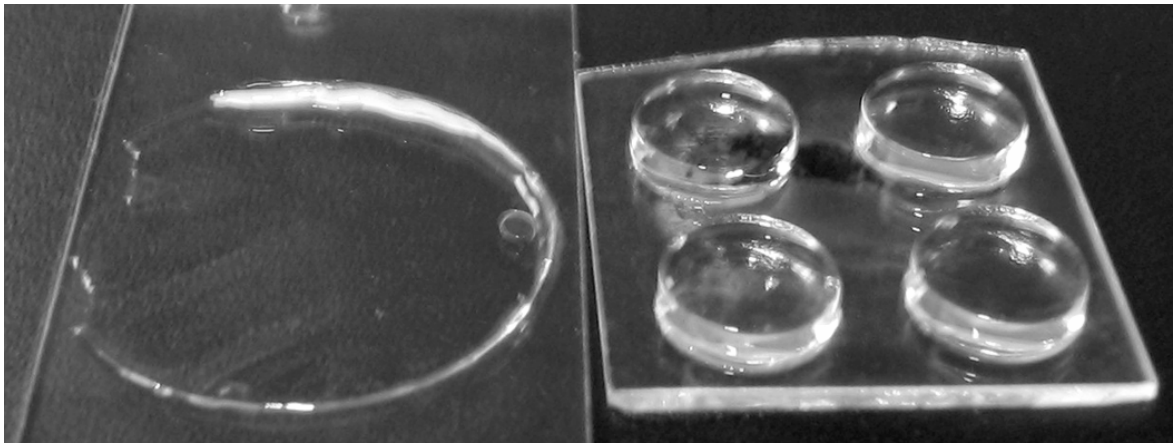

Figure 2.5 Photograph of photocured GMHA hydrogel films (left) and solution photocrosslinked GMHA hydrogels (right). GMHA hydrogel films are flexible, thin, and have a very high polymer concentration. Film dimensions are 2.2 cm in diameter and ~500 μm in thickness. Solution photocrosslinked GMHA hydrogels are rigid, thick, and have a lower polymer concentration. Their dimensions are 8 mm in diameter and 2 mm in thickness.

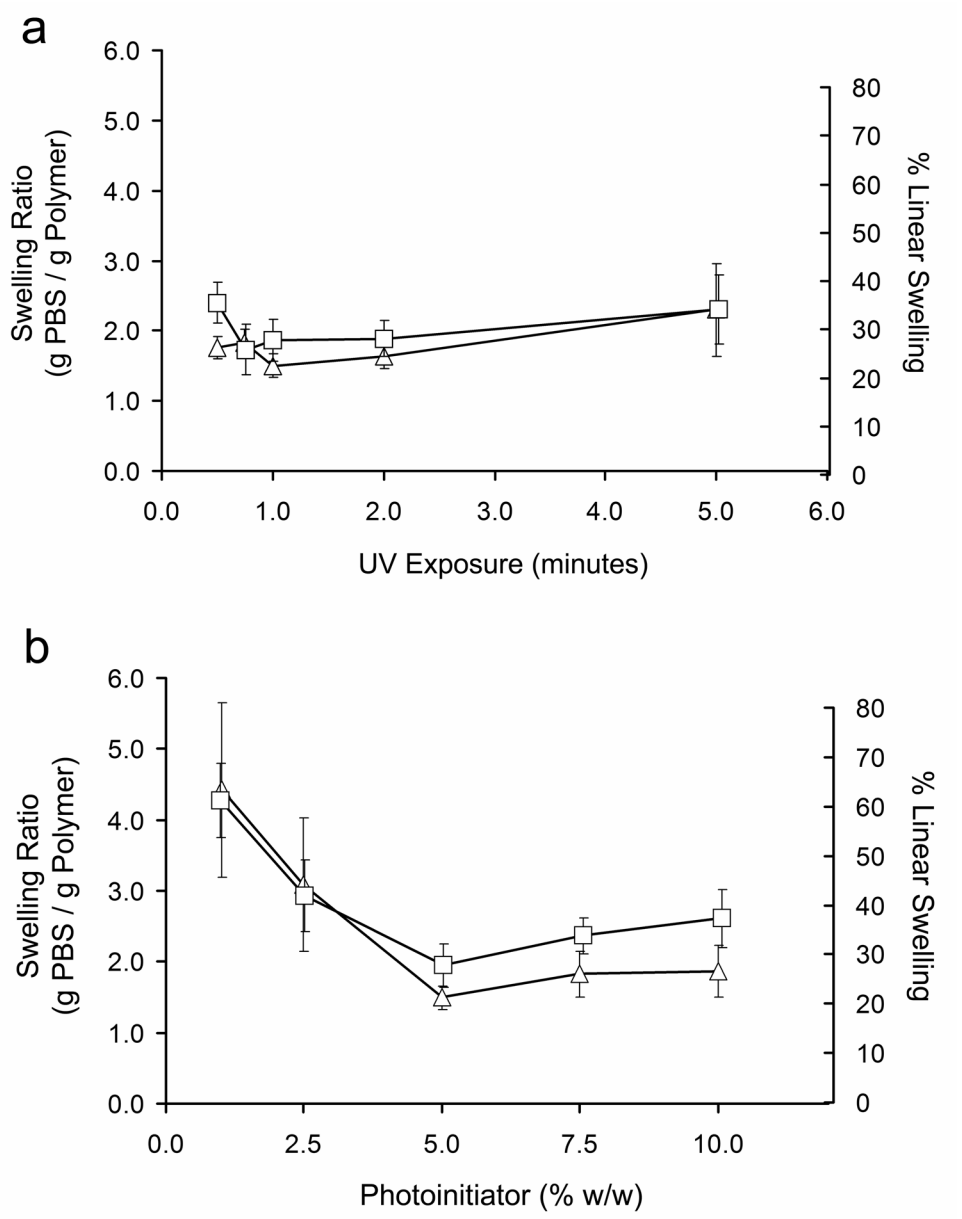

Figure 2.6 Swelling of photocured GMHA films as a function of UV exposure (**a**) and concentration of photoinitiator (**b**). Swelling ratio (Δ) is the amount of solution absorbed by the hydrogels. % linear swelling (□) is the change in diameter of the swollen hydrogels. Photoinitiator was held constant at 5% w/w in (a) and UV exposure was held constant at 1 minute in (b). Swelling was not strongly dependent on UV exposure for durations longer than 30 seconds. Swelling was minimized by photoinitiators concentrations greater than 5% w/w with respect to GMHA.

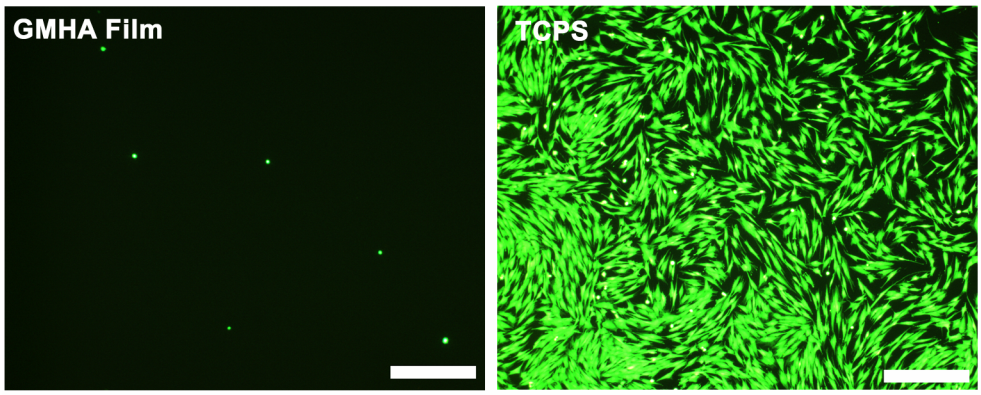

Figure 2.7 GMHA photocured films resist cellular adhesion. Human dermal fibroblasts were unable to adhere to GMHA films (left) but exhibited high adhesion to tissue culture polystyrene (right). Scale bars are 500 μm.

Chapter 3: Drug-binding Hydrogels of Hyaluronic Acid Functionalized with β-Cyclodextrin*

Abstract

Hyaluronic acid (HA) hydrogels are attractive materials for biomedical applications because they are porous, water-swelling, biocompatible, biodegradable, and resistant to non-specific cell adhesion. A limitation of HA hydrogels is that incorporation of bioactive drugs is restricted by low solubility of drug within the hydrogel environment. Our goal was to synthesize HA hydrogels that bind drug through hydrophobic interactions as a method for increasing drug loading. We functionalized photocrosslinked HA hydrogels with a methacryloyl derivative of β-cyclodextrin (βCD). βCD is a molecular "basket" with a hydrophilic exterior and a hydrophobic cavity. Inclusion complexes are formed when βCD hosts all or part of a hydrophobic drug within the cavity. HA hydrogels functionalized with methacryloyl-βCD monomer gained the property of inclusion complexation which greatly enhanced the uptake of a model hydrophobic drug, hydrocortisone. Pre-incubation of the hydrogels with adamantane carboxylic acid (ACA) inhibited hydrocortisone uptake by competition for βCD cavities. In addition, HA hydrogels functionalized with αCD monomer were not efficient at hydrocortisone uptake because the αCD cavity is too small for efficient complexation.

* Portions of the figures and text in this chapter are taken from the following journal article: Zawko, S.A., Truong, Q., Schmidt, C.E. Drug-binding hydrogels of hyaluronic acid functionalized with β-cyclodextrin. *J. Biomed. Mater. Res. A*, In Press.

These experiments confirmed that the βCD monomer enhances drug loading by the mechanism of inclusion complexation. Drug binding HA-βCD hydrogels may be further engineered to create HA-based biomaterials with a built in drug delivery capability.

3.1 Introduction

Hyaluronic acid (HA) is a linear biopolymer found ubiquitously in the tissues of the body and particularly in synovial fluid, skin and vitreous.[1] Aqueous solutions of HA can be crosslinked to produce insoluble hydrogels that exhibit high water content, high porosity, degradability by hyaluronidases, and resistance to cell adhesion. Commercial HA-based products include dermal fillers, adhesion barriers, and intra-articular viscosupplements.[2-4] HA tissue engineering scaffolds have been designed for cartilage, skin, adipose and vocal cord.[5-11] Hydrogel matrices are uniquely suited for biomedical applications because they resemble natural tissues with respect to mechanical properties, porosity, and water content.[12] It is desirable to find methods for building drug delivery capability into hydrogels to permit them to locally deliver bioactive agents while also functioning as adhesion barriers, wound dressings, tissue engineering scaffolds, and other devices.[13] However, incompatibility between hydrophobic drugs with the aqueous hydrogel environment may induce drug crystallization which can result in poor hydrogel properties and irregular release kinetics. In addition, hydrophobic drugs may migrate to the surface of the hydrogel upon drying and result in burst release.[14] Hydrophobic peptides and proteins within hydrogels may aggregate causing poor bioavailability.

Steroidal drugs in particular are widely applicable to biomedical applications of HA hydrogels such as adhesion barriers and wound dressings. Covalent conjugation has been used to solubilize steroids by tethering to HA through hydrolytically labile bonds, but this requires chemical modification of the drug and makes the drug's release dependent on environmental pH.[15-17] Our goal is to synthesize a complexing hydrogel based on hyaluronic acid that will bind drug non-covalently and improve drug-hydrogel interactions and drug loading. We have synthesized a photocrosslinkable monomer based on cyclodextrin which can form inclusion complexes with hydrophobic drugs. When this monomer is copolymerized with a photocrosslinkable HA derivative the result is an HA hydrogel with drug binding property.

There are several types of commercially available cyclodextrins (CD) and derivatives but the types used in this paper are αCD and βCD. The αCD is a cyclic oligomer of six glucopyranose units and βCD is composed of seven glucopyranose units. CD resembles a molecular "basket" with a hydrophilic exterior and a hydrophobic cavity. The cavity is accessible to small poorly water soluble drugs in aqueous solution. An inclusion complex is formed when CD wholly or partially includes a drug within the hydrophobic cavity **(Figure 3.1)**. Inclusion complexes are typically more soluble than the uncomplexed drug; therefore, the formulation of inclusion complexes is a method of drug solubilization.[18] CDs also interact with peptides and proteins such as cyclosporin, insulin and human growth hormone through complexation of hydrophobic amino acids.[19] Such interactions inhibit aggregation, degradation and denaturation.

The equilibrium concentrations of drug, CD, and complex in aqueous solution are given by an association constant, K_a, which is dependent on the solubility, size, and shape of the drug and CD cavity. The diameters of αCD and βCD are ~5 Å and ~6 Å, respectively; consequently, some drugs that complex with βCD are too big to complex with αCD.[19,20] The range of cyclodextrin-ligand association constants spans several orders of magnitude. At the high end is the interaction of βCD with adamantane derivatives which are roughly spherical hydrocarbons with poor water solubility and a size complementary to the βCD cavity. The association constant of adamantane carboxylic acid with βCD is on the order of 10^4 M^{-1}.[21]

The corticosteroid hydrocortisone was chosen as our model drug because its interactions with both βCD and αCD have been well characterized. Hydrocortisone is classified by USP as "very slightly soluble" in water (i.e., one part soluble in 1,000 - 10,000 parts solvent).[22] Hydrocortisone forms strong complexes with βCD with an association constant on the order of 10^3 M^{-1}.[20,23,24] With αCD, however, it forms very weak complexes (K_a ~10 M^{-1}) because the αCD cavity is too small for efficient complexation.[20] We hypothesized that hydrogels functionalized with βCD but not αCD would efficiently bind hydrocortisone through inclusion complexation. We further predicted that hydrogels functionalized with βCD and inhibited with adamantane carboxylic acid would be unable to bind hydrocortisone. Experimental confirmation of these hypotheses will prove that our HA-βCD hydrogels bind drug by inclusion complexation.

3.2 Results

3.2.1 Characterization of methacryloyl-cyclodextrin. To make drug-binding GMHA hydrogels we first needed to synthesize a polymerizable βCD monomer. A methacryloyl-cyclodextrin monomer was synthesized by the base-catalyzed reaction of βCD with methacrylic anhydride **(Figure 3.2)**. The reaction of methacrylic anhydride with βCD may occur at any of the 21 hydroxyls and produces a mixture of methacryloyl-β-cyclodextrin derivatives that have different numbers of methacryloyl groups. The degree of substitution (DS) is defined as the moles of methacryloyl groups per mole of CD. The average DS of the product mixture was measured by MALDI-MS and ^{1}H NMR. The DS of methacryloyl-βCD and methacryloyl-αCD was controlled by adjusting the molar equivalents of methacrylic anhydride to CD. Increasing the equivalents of methacrylic anhydride produced a product mixture with increasing methacryloyl substitution a decreasing proportion of unsubstituted cyclodextrin (**Table I**). We found that 4.7 molar equivalents of methacrylic anhydride per mole of βCD yielded a product (M4βCD) with an average DS of 3.1. Likewise, 6.4 molar equivalents of methacrylic anhydride per mole of αCD yielded a product (M6αCD) with an average DS of 3.4. Neither product contained more than a few percent of unsubstituted CD detected by MALDI-MS.

There were two considerations guiding the synthesis of methacryloyl-CD. First, the product should be free of unsubstituted CD which would be unpolymerizable. Second, highly substituted methacryloyl-CD should be avoided because methacryloyl groups may occlude CD's cavity and inhibit complexation.[31] M4βCD and M6αCD were

compromises between these constraints because they contained little unsubstituted CD and the DS between 3 and 4 was relatively low.

Methacrylic acid oligomer impurities were removed from the crude product mixtures by reverse phase HPLC. To determine the effectiveness of HPLC purification, the mass and average DS were measured for each of the thirty-two eluate fractions **(Figure 3.3)**. Mass recovered in the first three fractions was shown to consist of methacrylic oligomers by NMR. The methacryloyl-CDs eluted separately from the impurities and in order of increasing DS. Unsubstituted CDs and CDs with DS greater than six were discarded. The remaining fractions were combined and analyzed by MALDI-MS which showed that no unsubstituted CD remained (**Figure 3.4**). The ^{1}H NMR spectra of purified M4βCD has vinyl peaks at 5.6 and 6.1 ppm and a methyl peak at 1.9 ppm **(Figure 3.5)**. These peaks indicate the presence of methacryloyl groups. Average DS values of 3.2 and 3.6 for M4βCD and M6αCD, respectively, were determined from NMR spectra and are consistent with MALDI measurements.

3.2.2 Inclusion complexes of methacryloyl cyclodextrins. Phase solubility diagrams were constructed to assess the strength of complexation between CD and hydrocortisone. A phase solubility diagram is a plot of drug solubility against CD concentration. The association constant, K_a, can be calculated from the slope of the solubility curve using Equation 2. A steep slope indicates a large K_a. Use of Equation 2 requires the following assumptions: (i) 1:1 complexation of drug and CD; (ii) saturation of the solution with uncomplexed drug; (iii) equilibrium concentrations of drug, CD, and complex; and (iv) equivalent molar absorptivity of complexed drug and uncomplexed

drug at the analyzed wavelength. The K_a is a nonlinear function of the slope and is sensitive to small differences in concentration measurements. The K_a for hydrocortisone has been reported as 1720, 2683, and 4170 M^{-1} reflecting the variability of this measurement.[20,23,24]

The solubility curves of hydrocortisone in solutions of βCD and M4βCD are plotted in **Figure 3.6**. The K_a for βCD and M4βCD were 5422 M^{-1} and 1268 M^{-1} respectively. The shape of the βCD solubility curve is linear at low concentrations and plateaus at high concentrations. Solubility curves of this shape are classified as B-type and they suggest the formation of soluble 1:1 complexes at low βCD concentrations and precipitation of insoluble complexes at high concentrations.[20,28] These results are consistent with previously reported βCD-hydrocortisone solubility curves.[20,23,24] The shape of the M4βCD solubility curve was linear throughout. Linear solubility curves are classified as A-type and are consistent with the formation of soluble 1:1 complexes.[20] The magnitude of the association constant, K_a ~10^3 M^{-1}, confirms that M4βCD complexes effectively with hydrocortisone. The partial decrease in association constant for M4βCD relative to βCD may have been caused by steric hindrance by methacryloyl groups. Similarly, commercial hydroxypropyl derivatives of βCD have a diminished affinity for hydrocortisone because of steric hindrance; K_a has been reported as both 636 M^{-1} and 1040 M^{-1}.[32,33]

Phase solubility curves of hydrocortisone with αCD and M6αCD are plotted too **(Figure 3.6)**. The K_a for αCD and M6αCD were 94 M^{-1} and 164 M^{-1} respectively. These

weak association constants indicate that neither αCD nor M6αCD complex effectively with hydrocortisone. These results are consistent with the mismatch of hydrocortisone's size and the volume of αCD's cavity.

3.2.3 Swelling ratios of hyaluronic acid-cyclodextrin hydrogels. Hydrogels of HA and CD were crosslinked by photopolymerization and swelled to equilibrium in PBS. The dry and swollen weights were measured by thermogravimetry. Hydrogel swelling was strongly dependent on cyclodextrin concentration but not cyclodextrin type (i.e., α or β). The close similarity in both swelling ratio and composition establishes that the GMHA-M4βCD and GMHA-M6αCD hydrogels are physico-chemically similar except for the property of CD cavity size. The volume of solvent absorbed per unit mass of polymer decreased with increasing concentration of cyclodextrin **(Figure 3.7)**. Addition methacryloyl cyclodextrin to the GMHA matrix increases the concentration of methacryloyl groups and results in greater crosslink density and decreased swelling. These results strongly support the successful incorporation of methacryloyl-CD derivatives into the GMHA matrix.

3.2.4 Hydrocortisone uptake by hyaluronic acid-cyclodextrin hydrogels. This experiment measured the capability of GMHA-M4βCD hydrogels to absorb hydrocortisone. The molar quantity of absorbed hydrocortisone was plotted against the moles of hydrogel M4βCD functionalities **(Figure 3.8A)**. This plot is analogous to the phase solubility diagram in Figure 3.4. Absorption in terms of mass (mg drug / g polymer) is also plotted (**Figure 3.8B**). Unfunctionalized GMHA hydrogels correspond

to the data points located at the y-axis intercept (i.e. hydrogels with 0 μmol of cyclodextrin functional groups). Unfunctionalized GMHA hydrogels absorbed 30.0 ± 2.0 μg hydrocortisone whereas GMHA-M4βCD with the highest level of functionalization absorbed 79.8 ± 4.6 μg hydrocortisone. M4βCD functionalities and hydrocortisone uptake show a statistically strong and positive correlation (Pearson correlation coefficient, r = 0.972). These results demonstrate that incorporation of M4βCD functionalities in the GMHA hydrogel enhanced drug-hydrogel interactions and increased hydrocortisone loading.

Drug-hydrogel interactions are a complicated phenomena that depend on variables including the hydrogel charge density, polymer-solvent interactions, hydrogen bonding, and crosslink density. We wanted to determine conclusively whether inclusion complexation rather than any non-inclusion effect was the mechanism of increased hydrocortisone uptake. If inclusion complexation is indeed the dominant mechanism then hydrocortisone uptake should be inhibited by a strong βCD-binding ligand. Consistent with this hypothesis, we found that pre-incubation of GMHA-M4βCD hydrogels with adamantane carboxylic acid abolished all additional hydrocortisone uptake. The inhibited GMHA-M4βCD hydrogels absorbed only 29.3 ± 0.5 μg hydrocortisone which is statistically no different than pure GMHA hydrogels. The Pearson correlation coefficient, –0.142, further indicates that there is no correlation between M4βCD functionalities and hydrocortisone uptake when complexation is inhibited by adamantane carboxylic acid.

The mechanism of inclusion complexation was corroborated by a second experiment in which parallel hydrogels of GMHA functionalized with M6αCD were tested for hydrocortisone absorption. Uptake by GMHA-M6αCD hydrogels should be substantially lower because M6αCD is less effective at hydrocortisone complexation than M4βCD as shown in Figure 3.6. Consistent with this hypothesis, we found that GMHA-M6αCD hydrogels absorbed much less hydrocortisone than GMHA-M4βCD hydrogels. GMHA-M6αCD hydrogels absorbed up to 46.0 ± 3.1 μg hydrocortisone (equivalent to 16.4 mg/g polymer) compared to 79.8 ± 4.6 μg hydrocortisone (equivalent to 29.3 mg/g polymer) for GMHA-M4βCD hydrogels. These experiments establish that inclusion complexation is the dominant mechanism of hydrocortisone uptake by GMHA-M4βCD hydrogels.

3.2.5 Hydrocortisone release by hyaluronic acid-cyclodextrin hydrogels. The stability of the hydrogel-hydrocortisone complex was assessed by examining the kinetics of hydrocortisone release. Four compositions of hydrogel were investigated spanning a range of pure GMHA to GMHA functionalized with 14 mg/mL M4βCD. The hydrogels containing more M4βCD functionalities released more hydrocortisone as was expected **(Figure 3.9A)**. The duration of release was modestly but significantly extended by increasing M4βCD functionalization (ANOVA, α=0.05). The pure GMHA hydrogels released 100% of hydrocortisone within the first hour whereas the GMHA hydrogels with 14 mg/mL M4βCD released only 70% **(Figure 3.9B)**. Cyclodextrin functionalization enhanced drug loading but had little effect on the kinetics of release.

3.3 Discussion

Drug loading of a hydrogel is dependent on the solubility of drug in the absorbed solvent and by interactions of drug with the polymer.[34] We engineered HA hydrogels with enhanced drug-polymer interactions by incorporating a functional βCD monomer. This permitted the hydrogels to uptake more hydrocortisone from aqueous solution. An important aspect of this work is that the mechanism of absorption was unambiguously established as inclusion complexation. Confirmation of the mechanism of drug loading is necessary to rationally optimize the hydrogels and further engineer them for target applications.

The slope of the GMHA-M4βCD line in Figure 3.8A is 0.156 μmol hydrocortisone per μmol M4βCD. This indicates that about 1 in 6 of the hydrogel M4βCD moieties formed inclusion complexes; therefore, hydrogel M4βCD was less efficient at complexation than soluble M4βCD. This difference may be explained because hydrocortisone must first partition into the gel phase before complexing with hydrogel M4βCD functionalities. Methods that shift cyclodextrin-drug equilibrium towards complexation (e.g., lyophilization, kneading, spray-drying) can be used to prepare M4βCD-hydrocortisone complexes prior to photopolymerization and circumvent the gel phase barrier of post-gelation complexation.[35]

The time release profiles of hydrocortisone from GMHA-M4βCD hydrogels are a preliminary assessment of the stability of the hydrogel-drug complexes. The release profiles were similar in terms of percent release across all four hydrogel compositions

despite that the mass of hydrocortisone released was very different. Thus the amount of hydrocortisone delivered by GMHA-M4βCD hydrogels can be tuned without altering the kinetics of release under these conditions. For a given application it may be desirable to prepare drug-loaded GMHA-M4βCD hydrogels in a dried state; therefore, the kinetics of release could be very different from the kinetics observed here for which solvent penetration and hydrogel swelling played no role.

Biomedical applications of HA hydrogels include drug delivery, adhesion barriers, wound dressings, dermal fillers, and tissue engineering scaffolds that could benefit from the capability to locally deliver bioactive agents. GMHA-M4βCD hydrogels may be engineered to fit the requirements of such applications. The model drug used in these experiments, hydrocortisone, is structurally similar to a large number of steroidal drugs that can be expected to complex with the GMHA-M4βCD hydrogel. Furthermore, any of the great number of drugs known to complex with βCD may complex with these hydrogels. Development of peptide and protein complexation with GMHA-M4βCD hydrogels will further expand the versatility of the hydrogels and adapt them more fully to tissue engineering applications. It is possible to synthesize HA hydrogel microparticles and it is likely that GMHA-M4βCD hydrogel could be adapted to particle-based drug delivery.[36,37]

3.4 Materials and Methods

3.4.1 Materials. High molecular weight sodium hyaluronate from *Streptococcus equi* of molecular weight $1.6x10^6$ Da was obtained from Sigma-Aldrich (St. Louis, MO). Dialysis tubing was obtained from Spectrum Laboratories Inc. and Irgacure 2959 was obtained from Ciba Specialty Chemicals (Basel, Switzerland). All other chemicals and reagents were obtained from Sigma-Aldrich. Circular silicone rubber molds (Grace Bio-Labs, Bend, OR) of 9 mm diameter and 2 mm thickness were used for making hydrogels. A longwave UV lamp filtered around 365 nm and with an intensity of 22 mW/cm^2 was used to initiate photopolymerization (Blak-Ray B-100A, UVP, Upland, CA).

3.4.2 Synthesis of methacryloyl cyclodextrin. A 15 mM solution of cyclodextrin was prepared in deionized, distilled water. Methacrylic anhydride was added dropwise and 10 M sodium hydroxide was added to adjust the pH to 8.0. The solution was stirred and the pH was continually adjusted for 6 hours until the pH stabilized. The reaction mixture was then transferred to cellulose ester dialysis tubing of 500 molecular weight cut-off and dialyzed against deionized distilled water for 48 hours. The dialyzed solution was frozen in liquid nitrogen and lyophilized.

3.4.3 HPLC purification of methacryloyl-cyclodextrin. Crude methacrylated CD was purified by reverse phase HPLC with an ÄKTA Purifier and Source 5RPC ST 4.6/150 column (Amersham Pharmacia Biotech, Piscataway, NJ). A linear gradient of 98:2 to 45:55 water-acetonitrile and flowrate 0.8 mL/min was used for the mobile phase. The injection volume was 1 mL of 100 mg/mL solution. The recovered purified product was lyophilized and stored dessicated in the dark until use.

To assess the efficacy of the separation, the HPLC eluate was collected in thirty-two 1 mL fractions. The collection tubes were weighed before collection. After collection the fractions were lyophilized to dryness and reweighed to determine the mass recovered in each fraction. Fractions were screened by MALDI-MS to detect the presence of cyclodextrins. The purified M4βCD and M6αCD used in subsequent experiments consisted of fractions 8-22 and 7-22, respectively.

3.4.4 NMR and MALDI. ^{1}H NMR samples were dissolved in deuterium oxide and the spectra recorded on a Varian Unity +300 spectrometer. The degree of substitution (DS) was calculated by integration of all cyclodextrin ^{1}H peaks (49 H atoms) and integration of the vinyl peaks at 5.6 and 6.1 ppm (2 H atoms). Matrix-assisted laser desorption/ionization mass spectrometry (MALDI-MS) was also used to characterize the DS of derivatized cyclodextrin.[25-27] Spectra were recorded with a PerSeptive Biosystems Voyager MALDI-MS instrument. The matrix solution was 2.5 mg/mL α-cyano-hydroxycinammic acid in 50:50 water:acetonitrile and was spotted in equal volumes with aqueous CD solutions. Methacryloyl cyclodextrins were detected in positive ion mode as singly charged sodium adducts that were separated by 68 m/z which corresponds to the molecular weight of one methacryloyl-group. The average DS of the product mixtures was calculated from MALDI-MS spectra by Equation 1, where I is the intensity measured by peak height and d.s. is the degree of substitution corresponding to the peak.

$$\text{Average DS} = \frac{\sum I(d.s.)}{\sum I} \qquad [1]$$

3.4.5 Phase solubility diagrams. Phase solubility diagrams were constructed by the method of Higuchi and Connors to determine the association constants of native αCD and βCD, and of their methacrylated derivatives.[28] Triplicate samples of 300 μL of aqueous CD solutions were prepared in 0.65 mL tubes. An excess of hydrocortisone (~5 mg) was added to each sample. The solutions were sonicated for 5 minutes and then incubated at room temperature and rotated end over end for 6 days to achieve equilibrium concentrations of hydrocortisone, CD and complex. After 6 days the solutions were syringe filtered to remove undissolved solid phase hydrocortisone. The filtrate was diluted and the absorbance measured at 248 nm. This absorbance is a measure of the total concentration of hydrocortisone in both the complexed and uncomplexed form. The concentration of hydrocortisone was plotted against the concentration of CD and a regression line was fit to the linear portion of each solubility curve. The association constant was calculated from the slope of the regression line according to Equation 2, where K_a [M^{-1}] is the association constant and C_0 [1.04 x 10^{-3} M] is the solubility of hydrocortisone in water determined by experiment.

$$K_a = \frac{slope}{(1 - slope)C_0} \qquad [2]$$

3.4.6 Methacryloyl modification of hyaluronic acid. Hyaluronic acid was conjugated with photopolymerizable methacryloyl groups following a modified protocol of a procedure described previously.[29] A 1% w/v solution of HA was prepared in a 50:50 mixture of acetone:water and stirred 24 hours. Twenty molar equivalents of triethylamine as base catalyst and twenty molar equivalents of glycidyl methacrylate

were added to the solution and stirred for 24 hours at room temperature. The glycidyl methacrylate-modified hyaluronic acid (GMHA) was precipitated into a 20-fold volumetric excess of acetone, dissolved in water, precipitated a second time, redissolved in water, and lyophilized. The average degree of methacrylate substitution was determined by ^{1}H NMR and was 0.32 moles of methacryloyl groups per mole of HA disaccharides.

3.4.7 Hydrogel swelling ratio measurements. Gelation solutions of 20 mg/mL GMHA and 5, 10 or 15 mg/mL M4βCD and M6αCD were prepared in phosphate buffered saline (PBS, 10 mM, pH 7.4) containing 1% w/v Irgacure 2959 and 0.3% N-vinyl pyrrolidone. Hydrogels were each prepared from 100 μL of gelation solution and 5 minutes of UV exposure. The hydrogels were then swelled to equilibrium in PBS and rinsed with several exchanges of PBS to remove photoinitiator. A small portion of each swollen gel, 10-15 mg, was placed in a thermogravimetric analyzer (Perkin Elmer TGA 7) and heated at 100°C until all water was evaporated and a constant dry weight was obtained. The mass of residual PBS salts contributing to the dry weight was determined from the mass of evaporated water and was subtracted to obtain the dry weight of the polymer alone. The swelling ratio was calculated according to Equation 3, where SR [g PBS / g polymer] is the swelling ratio, W_S [g] is the swollen weight of the hydrogel, and W_D [g] is the dry weight of the hydrogel. Three hydrogels per composition were analyzed.

$$SR = \frac{W_S - W_D}{W_D} \qquad [3]$$

3.4.8 Uptake of hydrocortisone by GMHA hydrogels. These experiments assessed the GMHA-M4βCD hydrogel's ability to uptake hydrocortisone. Pre-gelation solutions of 20 mg/mL GMHA and 3-15 mg/mL M4βCD and M6αCD were prepared in phosphate buffered saline (PBS) containing 1% w/v Irgacure 2959. Eight hydrogels per composition were prepared with 80 μL of pre-gelation solution and 5 minutes of UV exposure. Hydrogels were swollen to equilibrium in PBS and rinsed with several exchanges of PBS to remove photoinitiator. Hydrogels were then incubated at room temperature for 7 days in 3 mL of PBS saturated with hydrocortisone. To determine the amount of hydrocortisone uptake the hydrogels were transferred to fresh PBS and placed on an orbital platform for release for 48 hours. The concentration of released hydrocortisone in the buffer was determined spectrophotometrically.

An additional experiment tested whether adamantane carboxylic acid could inhibit hydrocortisone uptake by binding βCD functionalities. GMHA-M4βCD hydrogels were each pre-incubated in 3 mL of PBS saturated with adamantane carboxylic acid for 48 hours and then transferred to PBS saturated with both hydrocortisone and adamantane carboxylic acid and incubated for 7 days. These hydrogels were transferred to fresh PBS and the concentration of released hydrocortisone was determined spectrophotometrically.

3.4.9 Release of hydrocortisone from GMHA hydrogels. The stability of the hydrogel-hydrocortisone complexes was assessed by examining the kinetics of hydrocortisone release into PBS buffer at 37°C. Six hydrogels per composition were prepared as described previously for the uptake experiment. Gels were rinsed thoroughly

to remove photoinitiator and then incubated for 1 week in PBS saturated with hydrocortisone. After incubation the gels were transferred to Eppendorf tubes containing 15 mL of PBS. The tubes were incubated at 37°C and rotated end over end. Aliquots of 500 μL were collected from each sample at each time point and replaced with 500 μL of fresh buffer.

The concentration of released hydrocortisone in each aliquot was measured by HPLC.[30] The column was a Waters Spherisorb ODS1 column with diameter 4.6 mm, length 150 mm, and 5 μm particles (Waters Corporation, Milford, MA). The mobile phase was 60/40 methanol/water at flowrate of 1 mL/min. Hydrocortisone was detected at 245 nm and had a retention time of 4.6 minutes. Injection volume was 25 μL. The equipment was a Waters Dual HPLC Pump 515, Waters 996 Photodiode Array Detector, and Waters 717 Plus Autosampler. The concentration of hydrocortisone was calculated by peak area using Waters Empower Pro Software. A series of seven standards spanning the full range of hydrocortisone concentrations was analyzed at the beginning and end of the assay and confirmed the linearity and stability of the assay.

3.4.10 Statistical analysis. Regression lines, Pearson correlation coefficients (r), and 95% confidence intervals (95% CI) were calculated with SPSS 14.0 software (SPSS Inc., Chicago, IL). Slopes of the regression lines are given as slope ± standard error. All other results are reported as mean ± standard deviation. Significant differences in the release experiment were determined by ANOVA with $\alpha = 0.05$.

3.5 References

1. Fraser, J.R.E., Laurent, T.C., Laurent, U.B.G. Hyaluronan: It's nature, distribution, functions and turnover. *J. Intern. Med.* **242**, 27-33 (1997).
2. Marshall, K.W. Intra-articular hyaluronan therapy. *Curr. Opin. Rheumatol.* **12**, 468-474 (2000).
3. Reijnen, M.M.P.J., Bleichrodt, R.P., van Goor, H. Pathophysiology of intra-abdominal adhesion and abscess formation, and the effect of hyaluronan. *Brit. J. Surg.* **90**, 533-541 (2003).
4. Monheit, G.D., Coleman, K.M. Hyaluronic acid fillers. *Dermatol. Ther.* **19**, 141-150 (2006).
5. Yoo, H.S., Lee, E.A., Yoon, J.J., Park, T.G. Hyaluronic acid modified biodegradable scaffolds for cartilage tissue engineering. *Biomaterials* **26**, 1925-1933 (2005).
6. Nettles, D.L., Vail, T.P., Morgan, M.T., Grinstaff, M.W., Setton, L.A. Photocrosslinkable hyaluronan as a scaffold for articular cartilage repair. *Ann. Biomed. Eng.* **32**, 391-397 (2004).
7. Chung, C., Mesa, J., Miller, G.J., Randolph, M.A., Gill, T.J., Burdick, J.A. Effects of auricular chondrocyte expansion on neocartilage formation in photocrosslinked hyaluronic acid networks. *Tissue Eng.* **12**, 2665-2673 (2006).
8. Park, S.N., Kim, J.K., Suh, H. Evaluation of antibiotic-loaded collagen-hyaluronic acid matrix as a skin substitute. *Biomaterials* **25**, 3689-3698 (2004).

9. Price, R.D., Das-Gupta, V., Leigh, I.M., Navsaria, H.A. A comparison of tissue-engineered hyaluronic acid dermal matrices in a human wound model. *Tissue Eng.* **12**, 2985-2995 (2006).

10. Jia, X.Q., Burdick, J.A., Kobler, J., Clifton, R.J., Rosowski, J.J., Zeitels, S.M., Langer, R. Synthesis and characterization of in situ cross-linkable hyaluronic acid-based hydrogels with potential application for vocal fold regeneration. *Macromolecules* **37**, 3239-3248 (2004).

11. Hemmrich, K., von Heimburg, D., Rendchen, R., Bartolo, C.D., Milella, E., Pallua, N. Implantation of preadipocyte-loaded hyaluronic acid-based scaffolds into nude mice to evaluate potential for soft tissue engineering. *Biomaterials* **26**, 7025-7037 (2005).

12. Peppas, N.A., Bures, P., Leobandung, W., Ichikawa, H. Hydrogels in pharmaceutical formulations. *Eur. J. Pharm. Biopharm.* **50**, 27-46 (2000).

13. Saltzman, W.M., Olbrich, W.L. Building drug delivery into tissue engineering. *Nat. Rev. Drug Discov.* **11**, 177-186 (2002).

14. Huang, X., Brazel, C.S. On the importance and mechanisms of burst release in matrix-controlled drug delivery systems. *J. Control Release* **73**, 121-136 (2001).

15. Payan, E., Jouzeau, J.Y., Lapicque, F., Bordji, K., Simon, G., Gillet, P., O'Regan, M., Netter, P. In-vitro drug-release from HYC-141, a corticosteroid ester of high-molecular-weight hyaluronan. *J Control Release* **34**, 145-153 (1995).

16. Prestwich, G.D., Marecak, D.M., Marecek, J.F., Vercruysse, K.P., Ziebell, M.R. Controlled chemical modification of hyaluronic acid: synthesis, applications and biodegradation of hydrazide derivatives. *J. Control Release* **53**, 93-103 (1998).

17. Ito, T., Fraser, I.P., Yeo, Y., Highley, C.B., Bellas, E., Kohane, D.S. Anti-inflammatory function of an in situ cross-linkable conjugate hydrogel of hyaluronic acid and dexamethasone. *Biomaterials* **28**, 1778-1786 (2007).

18. Challa, R., Ahuja, A., Ali, J., Khar, R.K. Cyclodextrins in drug delivery: An updated review. *AAPS PharmSciTech* **6**, 329-357 (2005).

19. Uekama, K. Design and evaluation of cyclodextrin-based drug formulation. *Chem. Pharm. Bull.* **52**, 900-915 (2004).

20. Uekama, K., Fujinaga, T., Hirayama, F., Otagiri, M., Yamasaki, M. Inclusion complexations of steroid-hormones with cyclodextrins in water and in solid-phase. *Int. J. Pharm.* **10**, 1-15 (1982).

21. Cromwell, W.C., Bystrom, K., Eftink, M.R. Cyclodextrin adamantanecarboxylate inclusion complexes – Studies of the variation in cavity size. *J. Phys. Chem.* **89**, 326-332 (1985).

22. The United States Pharmacopeia. The National Formulary 2004.

23. Liu, F.Y., Kildsig, D.O., Mitra, A.K. Beta-cyclodextrin steroid complexation – Effect of steroid structure on association equilibria. *Pharm. Res.* **7**, 869-873 (1990).

24. Szeman, J., Fenyvesi, E., Szejtli, J., Ueda, H., Machida, Y., Nagai, T. Water-soluble cyclodextrin polymers – Their interaction with drugs. *J. Inclusion Phenom.* **5**, 427-431 (1987).

25. Bartsch, H., Konig, W.A., Strassner, M., Hintze, U. Quantitative determination of native and methylated cyclodextrins by matrix-assisted laser desorption/ionization time-of-flight mass spectrometry. *Carbohyd. Res.* **286**, 41-53 (1996).

26. Chankvetadze B, Endresz G, Blaschke G, Juza M, Jakubetz H, Schurig V. Analysis of charged cyclomalto-oligosaccharides (cyclodextrin) derivatives by ion-spray, matrix-assisted laser-desorption/ionization time-of-flight and fast-atom bombardment mass spectrometry, and by capillary electrophoresis. *Carbohyd. Res.* **287**, 139-155 (1996).

27. Jacquet, R., Favetta, P., Elfakir, C., Lafosse, M. Characterization of a new methylated beta-cyclodextrin with a low degree of substitution by matrix-assisted laser desorption/ionization mass spectrometry and liquid chromatography using evaporative light scattering detection. *J. Chromatogr. A* **1083**, 106-112 (2005).

28. Higuchi, T., Connors, K.A. Phase solubility techniques. *Adv. Anal. Chem. Instru.* **4**, 117 (1965).

29. Leach, J.B., Bivens, K.A., Patrick, C.W. Jr, Schmidt, C.E. Photocrosslinked hyaluronic acid hydrogels: Natural, biodegradable tissue engineering scaffolds. *Biotechnol. Bioeng.* **82**, 578-589 (2003).

30. Brondsted, H., Andersen, C., Hovgaard, L. Crosslinked dextran - a new capsule material for colon targeting of drugs. *J. Control Release* **53**, 7-13 (1998).

31. Buvari-Barcza, A., Barcza, L. Influence of the guests, the type and degree of substitution on inclusion complex formation of subsituted β-cyclodextrins. *Talanta* **49**, 577-585 (1999).

32. Davies, N.M., Wang, G., Tucker, I.G. Evaluation of a hydrocortisone/hydroxypropyl-beta-cyclodextrin solution for ocular drug delivery. *Int. J. Pharm.* **156**, 201-209 (1997).

33. Loftsson, T., Frioriksdottir, H., Sigurdardottir, A.M., Ueda, H. The effect of water-soluble polymers on drug-cyclodextrin complexation. *Int. J. Pharm.* **110**, 169-177 (1994).

34. Kim, S.W., Bae, Y.H., Okano, T. Hydrogels – Swelling, drug loading, and release. *Pharm. Res.* **9**, 283-290 (1992).

35. Hedges, A.R. Industrial applications of cyclodextrins. *Chem. Rev.* **98**, 2035-2044 (1998).

36. Yun, Y.H., Goetz, D.J., Yellen, P., Chen, W. Hyaluronan microspheres for sustained gene delivery and site-specific targeting. *Biomaterials* **25**, 147-157 (2004).

37. Jia, X., Yeo, Y., Clifton, R.J., Jiao, T., Kohane, D.S., Kobler, J.B., Zeitels, S.M., Langer, R. Hyaluronic acid-based microgels and microgel networks for vocal fold regeneration. *Biomacromolecules* **7**, 3336-3344 (2006).

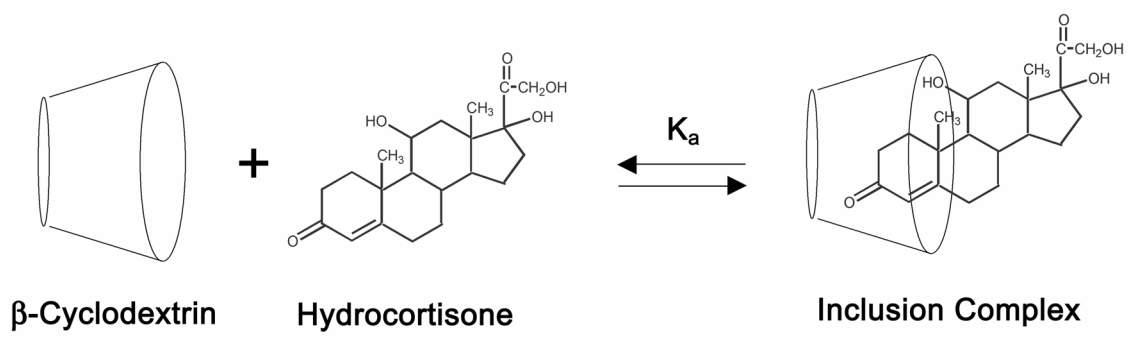

Figure 3.1 Equilibrium association of β-cyclodextrin, hydrocortisone, and complex.

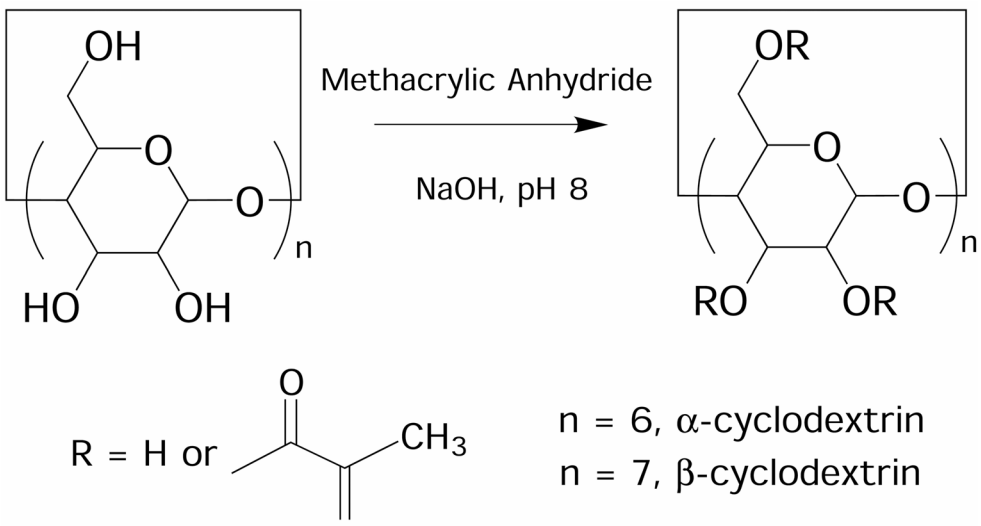

Figure 3.2 Chemical synthesis of methacryloyl-cyclodextrin.

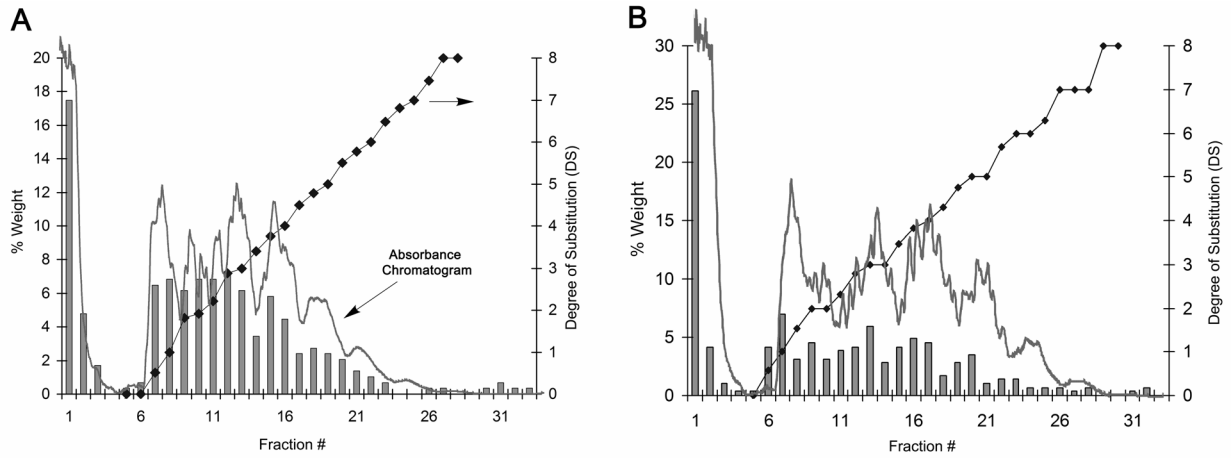

Figure 3.3 Purification of (A) M4βCD and (B) M6αCD by reverse phase HPLC. Bars are the weight percentage of total recovered mass in each fraction of eluate. The dark solid line is the average degree of substitution of cyclodextrin in each fraction as determined by MALDI-MS. The light line is the absorbance chromatogram. The methacrylic oligomer impurities eluted in fractions #1-3 and the methacryloyl cyclodextrins eluted in order of increasing substitution beginning with fraction #6.

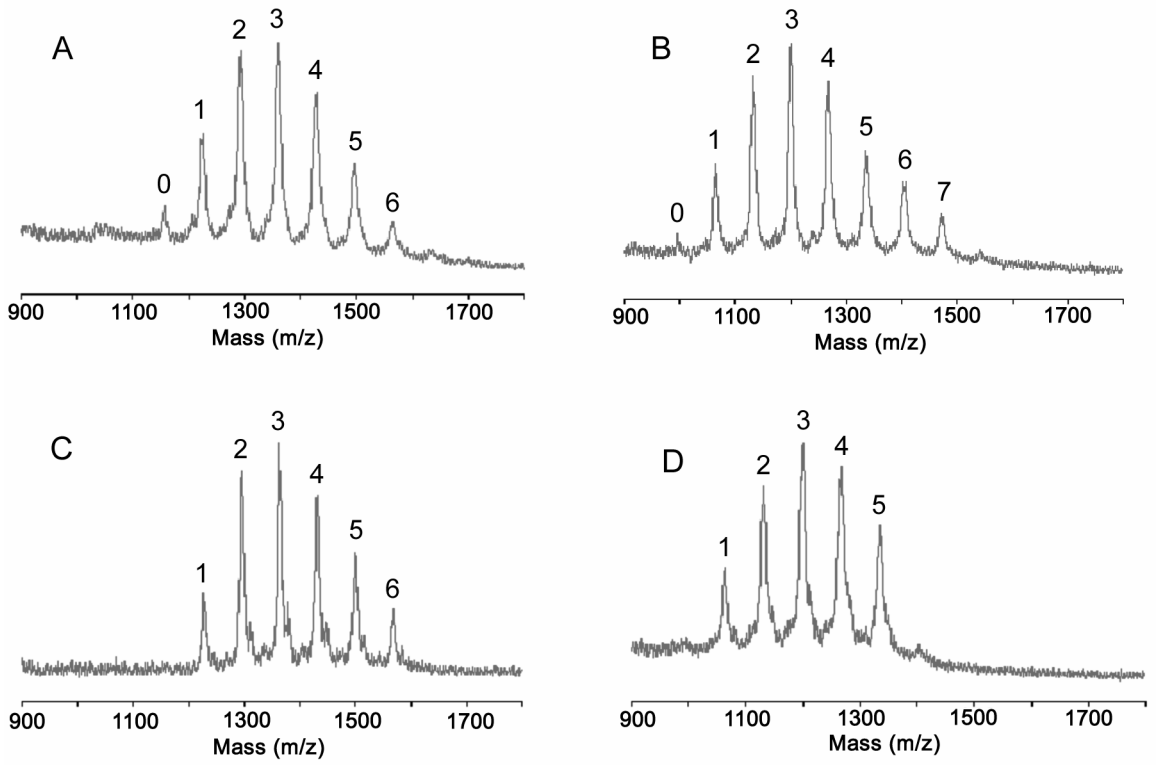

Figure 3.4 MALDI-MS spectra of (A) crude M4βCD; (B) crude M6αCD; (C) purified M4βCD and (D) purified M6αCD. The peaks are labeled with the degree of substitution. Peaks correspond to singly charged sodium adducts of cyclodextrin and are separated by 68 m/z which is the molecular weight of one methacryloyl-group. Unsubstituted cyclodextrin (DS 0) and small amounts of highly substituted cyclodextrin (DS > 6) were removed by HPLC.

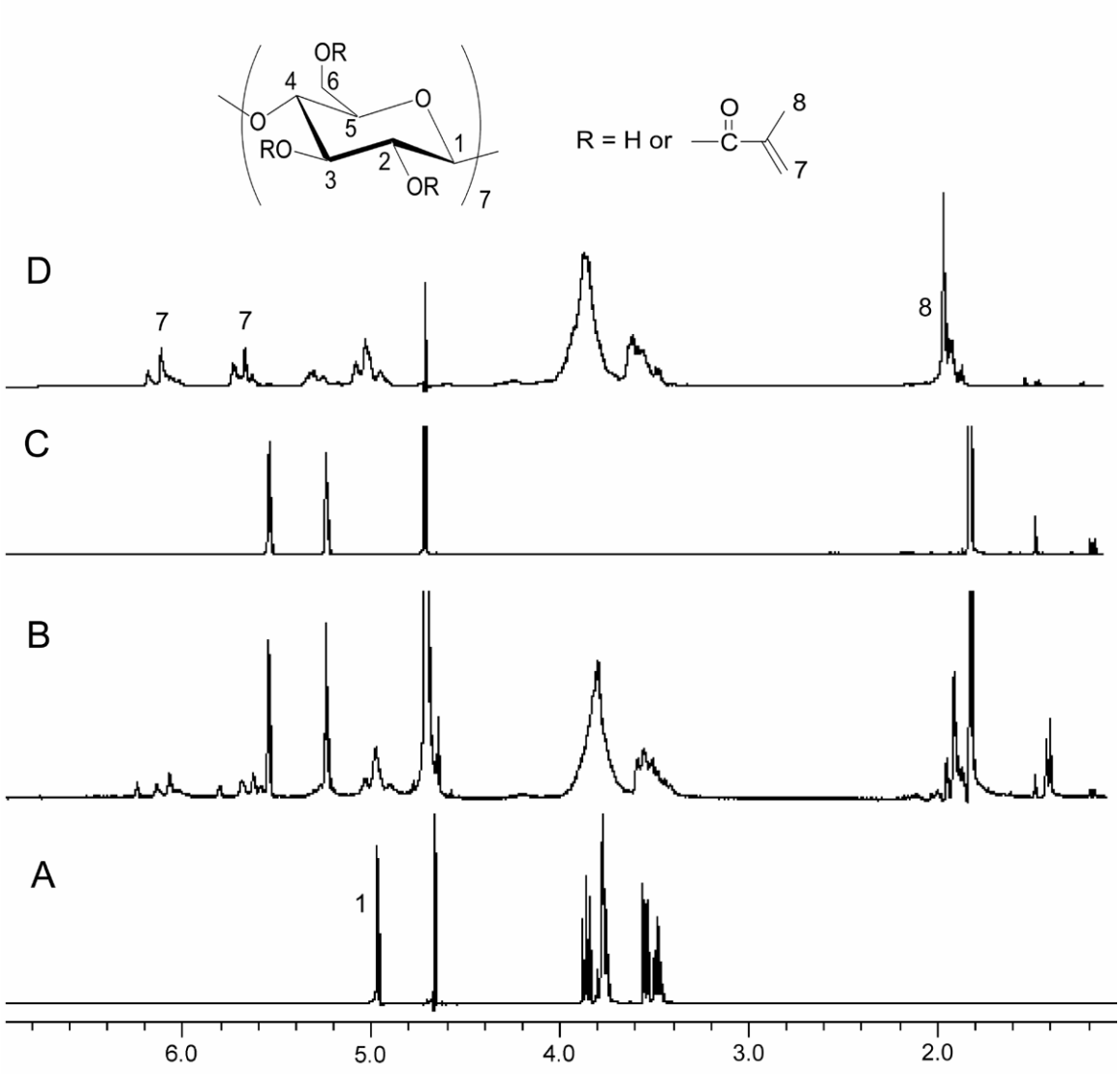

Figure 3.5 ^{1}H NMR spectra of (A) βCD; (B) crude M4βCD; (C) methacrylic impurities; and (D) purified M4βCD. Vinyl (5.6 and 6.1 ppm) and methyl (1.9 ppm) peaks in the spectra of M4βCD indicate the presence of methacryloyl groups. All of the impurity peaks in spectra C are absent from the purified M4βCD in spectra D.

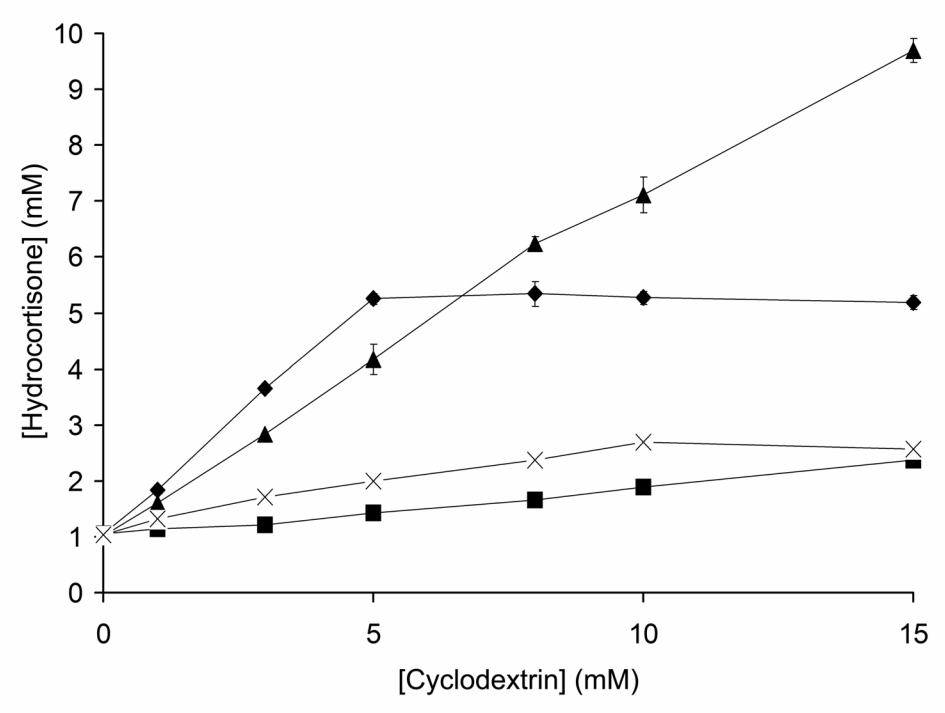

Figure 3.6 Phase solubility diagram of hydrocortisone with underivatized and derivatized cyclodextrins. Association constants were calculated from the linear portions of each curve. (♦) βCD, K_a = 5422 M^{-1}; 95% confidence interval (CI) = [4484, 6750]; (▲) M4βCD, K_a = 1268 M^{-1}, 95% CI = [1149, 1408]; (■) αCD, K_a = 94 M^{-1}, 95% CI = [86, 104]; (**x**) M6αCD, K_a = 164 M^{-1}; 95% CI = [159, 169]. Data points are mean ± standard deviation of three measurements.

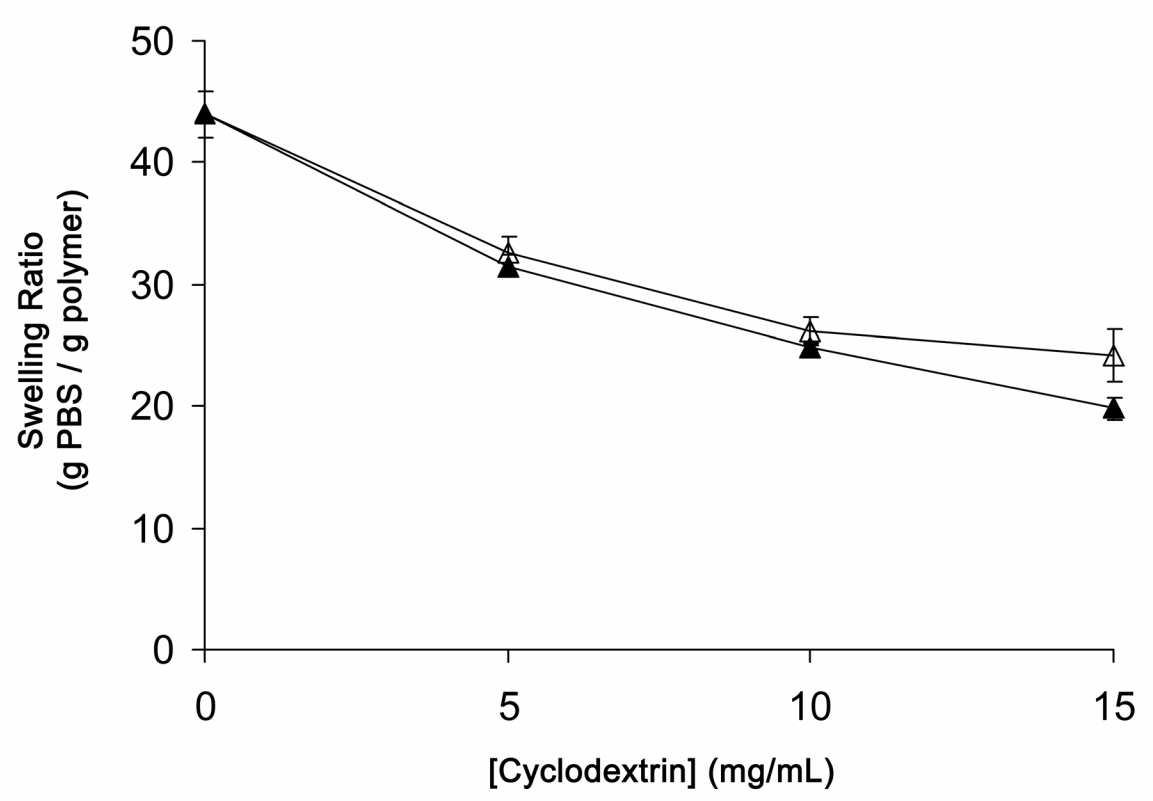

Figure 3.7 Swelling ratio in phosphate buffered saline (PBS) as a function of cyclodextrin concentration. Hydrogels were composed of 20 mg/mL GMHA functionalized with 0, 5, 10 or 15 mg/mL M4βCD (▲) or M6αCD (Δ). These data demonstrate that hydrogel swelling was dependent on cyclodextrin concentration but not type of cyclodextrin. Data points are mean ± standard deviation of three measurements.

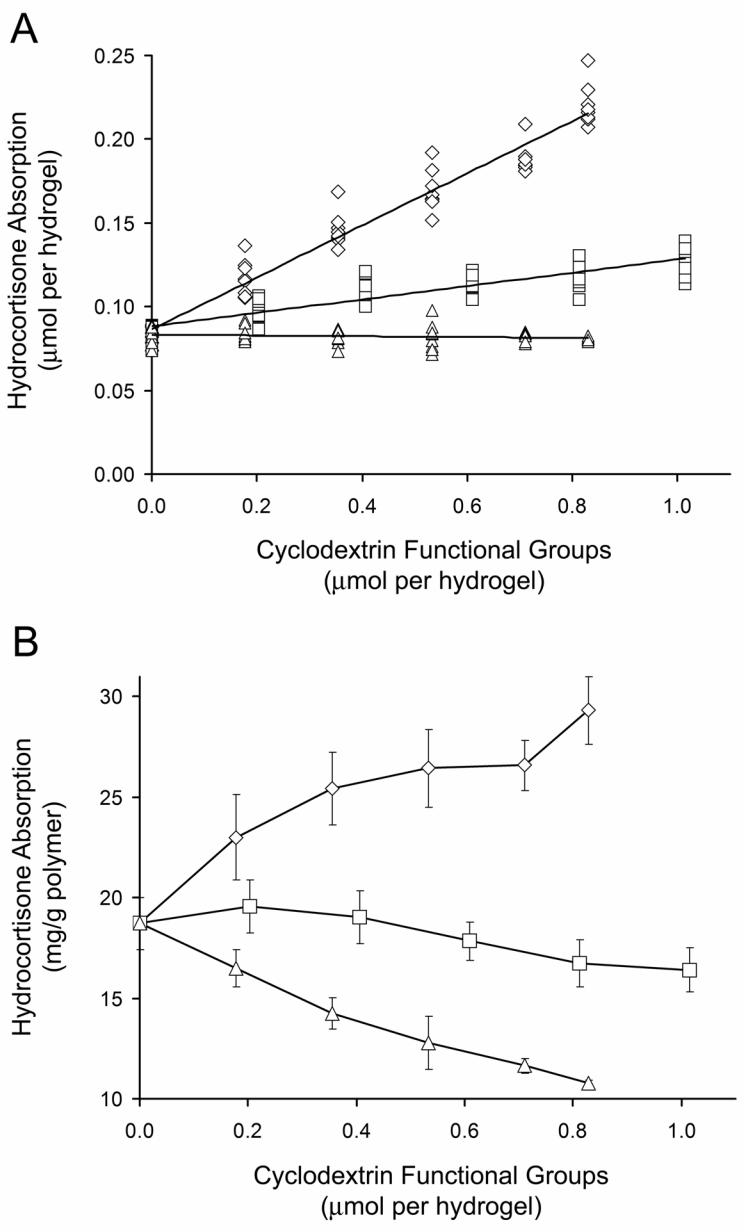

Figure 3.8 Hydrocortisone absorption by hyaluronic acid-cyclodextrin hydrogels. (◊) GMHA-M4βCD, slope ± standard error = 0.156 ± 0.006, Pearson correlation coefficient (r) = 0.972; (□) GMHA-M6αCD, m = 0.040 ± 0.003, r = 0.872; (Δ) GMHA-M4βCD inhibited with adamantane carboxylic acid, m = -0.002 ± 0.002, r = -0.142. (A) Hydrocortisone uptake in moles is plotted against moles of cyclodextrin functional groups. The slope of the regression line represents the additional moles of hydrocortisone absorbed by the hydrogel per mole of cyclodextrin functional groups. (B) The drug loading of hydrocortisone is plotted against moles of cyclodextrin hydrogel functionalities. Data are presented as mean ± standard deviation of eight measurements.

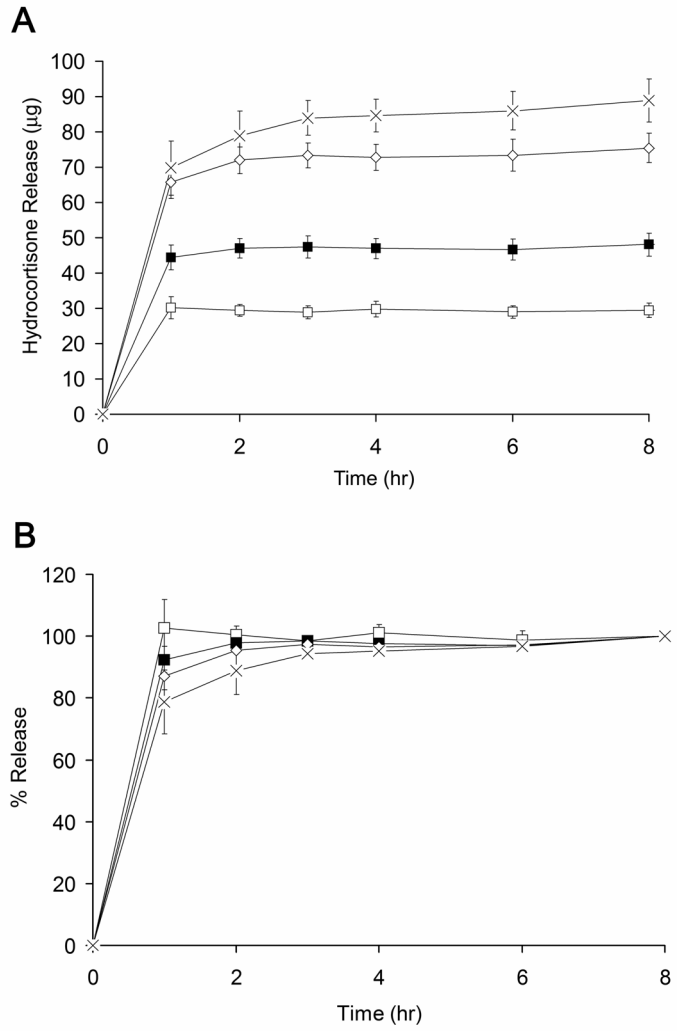

Figure 3.9 Release of hydrocortisone from GMHA-M4βCD hydrogels in terms of (A) mass and (B) % release. Hydrogel compositions are (□) 20 mg/mL GMHA; (■) 20 mg/mL GMHA with 3 mg/mL M4βCD; (◊) 20 mg/mL GMHA with 9 mg/mL M4βCD; (**x**) 20 mg/mL GMHA with 14 mg/mL M4βCD. The compositions with greater cyclodextrin functionalization released more hydrocortisone as shown in (A) and this had a modest but statistically significant effect (ANOVA, α=0.05) on the duration of release as shown in (B). Data points are mean ± standard deviation of six measurements.

Table I. Degree of substitution of methacryloyl-cyclodextrin and the percentage of unreacted cyclodextrin.

	Code Name[a]	CD	Equivalents of MA	Average DS[b]	Percent Unsubstituted[b]	Average DS[c]
Crude Products						
	M4αCD	α	4.2	2.6	4	--
	M6αCD #1	α	6.4	3.4	2	--
	M6αCD #2	α	6.4	3.3	1	--
	M9αCD	α	9.6	4.8	0	--
	M4βCD #1	β	4.7	3.1	3	--
	M4βCD #2	β	4.7	3.1	3	--
	M4βCD #3	β	4.7	3.0	5	--
	M7βCD	β	7.1	4.2	1	--
	M10βCD	β	10.6	5.2	0	--
Purified Products						
	M6αCD #1	α	6.4	3.6	0	3.1
	M4βCD #1	β	4.7	3.2	0	3.2

CD = cyclodextrin.
MA = methacrylic anhydride.
DS = degree of substitution (moles of methacryloyl groups per mole of cyclodextrin).
[a] Numbers after the codenames M6αCD and M4βCD denote individual batch numbers and show reproducibility of the synthesis.
[b] Calculated from MALDI mass spectra.
[c] Calculated from ^{1}H NMR spectra.

Chapter 4: Super-Swelling and Dual-Crosslinked Hydrogels of Hyaluronic Acid with Patterned Anisotropic Swelling

Abstract

In this chapter, we have engineered dual-crosslinked hyaluronic acid hydrogel scaffolds with novel anisotropic swelling which yields a new, unexplored type of shape changing tissue engineering scaffold. First, we synthesized super-swelling chemically crosslinked hyaluronic acid hydrogels. When these hydrogels were placed in solution they absorbed water and swelled to a great extent while faithfully maintaining their original shape. There is an inverse relationship between the crosslink density and swelling of a hydrogel. We found that adding photocrosslinks to chemically crosslinked super-swelling hydrogels yielded a greater crosslink density and diminished swelling. A hydrogel with anisotropic swelling was obtained by spatially patterning the photocrosslinks. The photopatterned regions exhibited low swelling because they contained both photocrosslinks and chemical crosslinks. The non-photopatterned regions exhibited high swelling because they contained only chemical crosslinks. When an unswelled dual-crosslinked hydrogel is placed in solution it swells anisotropically because of differential swelling between the high and low swelling regions. This differential swelling produces a dynamic pattern of crosslink density, water content, and viscoelasticity at the macro- and micro-scale that changes during anisotropic swelling.

4.1 Introduction

TE scaffolds of HA are being developed for cartilage, skin, adipose, and other tissues; however, regeneration of fully natural tissue is not yet possible.[1-4] The purpose of a tissue engineered (TE) scaffold is to provide a support structure that can replace, repair, or aid in the regeneration of damaged tissue. Currently existing TE scaffolds are structurally simple and have homogeneous bulk properties that are unable to induce cells to regenerate architecturally complex healthy tissue. Thus, there is a need for methods that can replicate the structural complexity of natural tissues within TE scaffolds. For example, engineered skin substitutes are effective at performing the barrier function of skin but suffer from impaired vascularization and enervation and are unable to support the regeneration of hair follicles, sweat glands, and natural appearing pigmentation.[5] Injectable HA gels can fill tissue defects, but their effect is temporary because they are gradually resorbed without replacement by regenerated adipose tissue.[6] A limiting factor is the incongruence between the homogeneous structures of TE scaffolds and the complex patterns of mechanical properties, water content, porosity, and chemical ligands within natural tissues. A challenge for the next generation of TE scaffolds is to incorporate biomimetic spatial patterns of these properties.

Several of the techniques that have been developed to address this challenge share a strategy in which a homogeneous bulk hydrogel is used as a foundational material within which photopatterning is used to obtain spatial distributions of material properties. For example, a homogeneous agarose gel modified with photolabile 2-nitrobenzyl-cysteine functionalities was photopatterned with the cell-adhesive peptide motif, RGD, to

guide neurite infiltration.[7] In another example, a homogeneous poly(ethylene glycol) diacrylate (PEGDA) hydrogel was photopatterned with a second interpenetrating network of photocrosslinked PEGDA to produce spatially defined regions of high and low crosslink density, porosity, and diffusion.[8] Our dual-crosslinking approach is differentiated from this previous work because we perform the photopatterning step before the hydrogel is fully swelled. Thus, our dual-crosslinked hydrogels have patterned regions of high and low crosslink density, porosity, and diffusion that changes dynamically during anisotropic swelling.

The first element of our anisotropic hydrogel design is a homogeneous base hydrogel of chemically crosslinked HA. The most common crosslinking agents are diglycidyl ethers,[9-11] divinyl sulfone,[12-14] and glutaraldehyde.[15,16] We selected butanediol diglycidyl ether (BDDE) because it is less toxic than other crosslinking agents. BDDE is a bifunctional crosslinker that reacts with HA's primary hydroxyls. Crosslinking is accomplished by mixing HA with BDDE in aqueous solution and appropriately adjusting the temperature and pH. The reaction of HA with BDDE is analogous to the reaction of HA with glycidyl methacrylate. In both instances, the glycidyl functionalities are attacked by base activated hydroxyls on HA (chemical structures are depicted in **Figure 4.1**).

Concentrations of HA hydrogels are typically limited to less than 2% w/v because higher concentrations are too viscous for adequate mixing. At very high concentrations, such as 10% and 20% w/v, HA solutions solidify and can neither be mixed nor poured. We circumvented the problem of HA's viscosity by preparing individual hydrogels from

lyophilized high molecular weight HA powder sealed within silicone rubber molds **(Figure 4.2)**. The crosslinker solution, consisting of BDDE and sodium hydroxide, was injected through the rubber mold and rapidly dissolved the HA powder. By this method semisolid 10% w/v solutions of high molecular weight HA were obtained in the shape of simple disc molds. Chemical crosslinking was initiated by placing the solutions in an oven and incubating for 8 hours at 40°C.

4.2 Results

4.2.1 Chemically crosslinked HA hydrogels. Chemically crosslinked HA hydrogels were synthesized from concentrated high molecular weight HA. Simple disc molds were used to prepare hydrogels for swelling, rheology, and degradation experiments. The representative super-swelling hydrogels depicted in **Figure 4.3a** were prepared from 10% w/v HA crosslinked with 250 μL BDDE/g HA. Before swelling, the hydrogel matched the size of the mold. When the hydrogel was swollen in saline it absorbed 100 times its weight of solution. When the hydrogel was swollen in deionized distilled water it absorbed 1000 times its weight while retaining the disc shape.

It was surprising to find that the super-swelling HA hydrogels maintained their original shape even after swelling so extensively. We are interested in bulk hydrogels that have defined shapes and structures to be used as TE scaffolds. To test shape retention of a complex structure, we created hand-shaped PDMS molds. HA hydrogels were chemically crosslinked within the hand molds and then swelled in water and saline. The super-swelling hydrogels successfully preserved the complex hand shape even while swelling

to many times their original size (**Figure 4.3b**). Ideally, a TE scaffold should be implantable through a small surgical incision and expand *in vivo* to conform to the shape of a tissue defect. The super-swelling property of these HA hydrogels and their ability to maintain shape addresses this issue.

The swelling ratio is an indirect measure of the extent of crosslinking and, for a given hydrogel system, the swelling ratio will decrease as the extent of crosslinking increases. The swelling behavior of these HA hydrogels was dependant on the concentrations of HA and BDDE (**Figure 4.4**). Increasing concentrations of BDDE and HA produced hydrogels with less swelling. The equilibrium swelling ratio of 10% HA hydrogels decreased from 2600 g water/g polymer to 400 g/g when the volume of crosslinker was increased from 150 μL/g to 500 μL/g. The swelling ratios of 10% and 20% w/v HA hydrogels differed by an order of magnitude. The swelling ratio of 20% HA hydrogels decreased from 105 g/g to 24 g/g when the volume of crosslinker was increased from 150 μL/g to 500 μL/g. The swelling ratio of the HA hydrogels in water is the maximum attainable swelling; but swelling in saline more closely resembles *in vivo* conditions. The time profiles of 10% HA hydrogels in saline reveal that they swell rapidly during the first 8 hours and then swell slowly (**Figure 4.5**). Equilibrium swelling was achieved within 48 hours for 10% hydrogels. The lesser swelling 20% hydrogels reached equilibrium swelling within 10 hours.

Rheological characterization of the chemically crosslinked hydrogels was performed to examine the effect of crosslinking on hydrogel stiffness. All rheological measurements were performed on hydrogels at equilibrium swelling in saline. The

storage modulus was plotted as a function of frequency (**Figure 4.6**). There is a pronounced increase in the storage modulus with increasing BDDE concentrations because a higher degree of crosslinking increased the stiffness of the hydrogels. Among 10% w/v hydrogels, the moduli of 500 μL/g hydrogels are almost two orders of magnitude greater than the 150 μL/g hydrogels. Furthermore, as the HA concentration increases from 10% to 20% w/v, the value of G′ becomes much greater. The increase in HA concentration results in denser crosslinking and greater entanglement. Thus, the rigidity of the hydrogel is dependent on both polymer concentration and crosslinker concentration.

The degradation of chemically crosslinked hydrogels was performed with hyaluronidase, a mammalian enzyme that acts upon HA *in vivo*. Among chemically crosslinked hydrogels, the degradation rate decreased with an increase in BDDE concentration (**Figure 4.7**). Furthermore, the degradation rate was considerably less for 20% w/v HA concentrations compared to 10% w/v concentrations. The results of the swelling, rheological, and degradation studies of the chemically crosslinked hydrogels demonstrate that increasing crosslink density produces hydrogels with less swelling, greater storage moduli, and slower rates of degradation.

4.2.2 Photocrosslinked HA hydrogels. The next element of our design was to introduce photocrosslinks into the super-swelling chemically crosslinked hydrogels. For this purpose, we synthesized a glycidyl methacrylate derivative of hyaluronic acid (GMHA).[17] GMHA has pendant methacrylate functionalities that can be polymerized by mixing GMHA with photoinitiator and exposing to UV light. The photocrosslinks consist

of polymethacrylate chains linked to many HA chains. Spatial control of photocrosslinking is possible with the use of photomasks.[7,18]

The conditions of photocrosslinking were optimized to minimize hydrogel swelling (**Figure 4.8**). Irgacure 2959 is among the most biocompatible of photoinitiators yet exhibits cytotoxicity at sufficiently high concentrations;[19,20] therefore, an optimum photoinitiator concentration is the minimum that is required for maximal crosslinking inferred from the swelling ratio. The swelling ratio was found to be largely independent of photoinitiator concentration over the range of 0.05-1.0% w/v; thus, the least concentration tested, 0.05% w/v, was selected for further experiments. Hydrogel swelling was strongly dependent on UV exposure for durations less than 5 minutes but not for durations greater than 5 minutes. This indicates that most crosslinks are formed within the first 5 minutes of UV exposure and this time was selected as the optimum duration.

The effects of these two parameters, photoinitiator concentration and UV exposure time, on the rate of degradation were examined. These two parameters impact the crosslink density and therefore should impact the degradation rate. Five combinations of photoinitiator concentration and UV exposure were examined by enzymatic degradation. Among these hydrogels, the combination (1% photoinitiator and 0.5 min UV) with the fastest rate of degradation exhibited the greatest swelling (**Figure 4.9**). The combination (1% photoinitiator and 20 min UV) with the slowest rate of degradation exhibited the least swelling. All hydrogels were degradable by hyaluronidase and therefore should degrade *in vivo*. After investigating the synthesis conditions of

chemically-crosslinked and photocrosslinked hydrogels individually, we turned our attention to dual-crosslinked hydrogels.

4.2.3 Dual-crosslinked HA hydrogels. Dual-crosslinked hydrogels possess two kinds of crosslinks: chemical crosslinks and photocrosslinks. First, photocrosslinks are formed by exposure to UV light and then chemical crosslinks are formed by adjusting the pH and temperature (see schematic in Figure 4.1c). To investigate the contributions made by chemical crosslinks and photocrosslinks to the viscoelastic properties of dual-crosslinked hydrogels, rheological comparisons were made among the following samples: (i) dual-crosslinked hydrogels; (ii) chemically crosslinked hydrogels; and (iii) photocrosslinked hydrogels. The individual contributions of photocrosslinks and chemical crosslinks to the viscoelasticity of dual-crosslinked hydrogels are depicted in the plot of storage modulus and loss modulus in **Figure 4.10**. The dual-crosslinked hydrogels exhibited a greater storage modulus (1370 Pa) than either chemically crosslinked hydrogels (450 Pa) or photocrosslinked hydrogels (140 Pa). This demonstrates that the two crosslinking methods are synergistic and were combined within the dual-crosslinked hydrogel to obtain a greater crosslink density and viscoelasticity.

Chemical crosslinking, but not photocrosslinking, requires alkaline pH and elevated temperatures. For consistency, the photocrosslinked hydrogels in this rheological experiment were exposed to eight hours of alkaline pH and elevated temperature to match the synthesis conditions of the dual-crosslinked and chemically crosslinked hydrogels. Therefore, the differences in viscoelastic properties in Figure 4.10

reflect the effect of crosslink density alone and not incidental degradation by different temperature and pH treatments.

The dual-crosslinking method was adapted to photopatterning by use of a photomask. There are two kinds of regions in patterned dual-crosslinked hydrogels: (i) high-swelling chemically crosslinked regions and (ii) low-swelling dual-crosslinked regions. We created a patterned dual-crosslinked hydrogel in which half was exposed to UV and half was unexposed. This hydrogel exhibited anisotropic swelling when swollen to equilibrium in saline (**Figure 4.11**). The high swelling chemically crosslinked region swelled expansively and the low swelling dual-crosslinked region swelled very little. The differential swelling caused distortions in the shape of the hydrogel because the high swelling chemically crosslinked region was partially restrained by the adjacent low swelling dual-crosslinked region. The two regions of the patterned dual-crosslinked hydrogels tended to fracture when the degrees of swelling were highly mismatched.

Fluorescent labeling by fluorescein-acrylate was used to visualize photopatterning. The dual-crosslinked regions fluoresced green because fluorescein-acrylate was incorporated into the polymethacrylate photocrosslinks during UV-initiated radical polymerization. Dual-crosslinked hydrogels were patterned on the micro-scale with a stereolithography system and digital micro-mirror array.[21] A hexagonal lattice photomask was used to pattern anisotropic swelling hydrogels in which low swelling dual-crosslinked regions coincided with the lattice and high-swelling regions coincided with the interstices. The unswelled dual-crosslinked hydrogel possessed a featureless flat surface; however, when placed in a solution the featureless surface evolved a series of

regularly repeating bumps that were induced by anisotropic swelling (**Figure 4.11d**). These patterned hydrogels demonstrate that the dual-crosslink methodology can produce continuous bulk materials with macro- and micro-scale distributions of crosslink density, water content, and viscoelasticity. Furthermore, these hydrogels can contort into predefined shapes upon contact with water.

4.3 Discussion

Others have reported a method for producing anisotropically swelling hydrogel constructs by using soft lithography to stamp bilayer films of swellable poly(methacrylic acid) and non-swellable poly(hydroxyethyl methacrylate).[22] In solution the swellable layer curled around the edges of the non-swellable layer to produce a folding hydrogel that could grip tissue surfaces. In our method we use two modes of crosslinking within a single continuous hydrogel to achieve anisotropic swelling of a bulk three-dimensional structure. Our material of choice is HA which is well suited to biomedical and tissue engineering applications. We confirmed that the hydrogels were enzymmatically biodegradable by hyaluronidase; thus, our anisotropically swelling hydrogels are entirely composed of a biodegradable and non-immunogenic biopolymer.

Future refinement of anisotropically swelling and super-swelling HA hydrogels should be directed toward three goals. The first goal is a tunable rate of swelling. A hydrogel that swells quickly can rapidly imbibe water that supports mechanical stability. Fast-swelling superabsorbent hydrogels of polyacrylate and other synthetic monomers have been cleverly designed by introducing macropores through acid foaming of

effervescent sodium bicarbonate salts.[23] Macropores facilitate the influx of water and increase the rate of swelling; however, this method is not directly applicable to HA hydrogels because HA is acid sensitive and its solutions are highly viscous. Therefore, inventing a compatible method for creating macropores within HA hydrogels is necessary. The second goal is an environmental stimulus to trigger swelling. Currently, these HA hydrogels begin to swell immediately upon contact with water. Triggered swelling would permit the unswelled hydrogels to be easily rinsed, neutralized, and further processed *ex vivo* prior to implantation and triggered swelling *in vivo*. The third goal is a method for preventing the fracture of dual-crosslinked hydrogels at interfaces between high and low swelling regions. Addition of a fibrillar component to hydrogels may relieve some of the tensile stresses that can cause mechanical failure. This is analogous to the collagen fibers in cartilage that are the natural source of tensile strength that complements the compressive strength of HA.[24]

In conclusion, we have found that crosslinking concentrated solutions of HA with BDDE yields super-swelling hydrogels that greatly increase in size and maintain their initial shape. The addition of photocrosslinks to these super-swelling hydrogels increased the crosslink density and diminished swelling. Patterning of the photocrosslinks produced dual-crosslinked anisotropically swelling hydrogels. Unswelled dual-crosslinked hydrogels in solution swell and contort into new predefined shapes due to the differential swelling between photopatterned regions. This dual-crosslink methodology expands the types of material properties that are achievable with hyaluronic acid tissue engineering scaffolds.

4.4 Materials and Methods

4.4.1 Materials. High molecular weight sodium hyaluronate from *Streptococcus equi* of molecular weight $1.6x10^6$ Da was obtained from Sigma-Aldrich (St. Louis, MO). Photoinitiator Irgacure 2959 (I2959) was obtained from Ciba Specialty Chemicals (Basel, Switzerland). Bovine testicular hyaluronidase of 999 U/mg and all other chemical reagents were obtained from Sigma-Aldrich. Circular silicone rubber molds (Grace Bio-Labs, Bend, OR) of 8 mm diameter, 2 mm thickness, and 100 μL volume were used for making hydrogels. A longwave UV lamp filtered around 365 nm and with an intensity of 22 mW/cm^2 was used to initiate photopolymerizations (Blak-Ray B-100A, UVP, Upland, CA).

4.4.2 Methacryloyl modification of hyaluronic acid. HA was conjugated with photopolymerizable methacryloyl groups following a protocol that has been described previously with modifications.[25] A 1% w/v solution of HA was prepared in a 50:50 mixture of acetone:water and stirred 24 hours. Twenty molar equivalents of triethylamine as base catalyst and glycidyl methacrylate were added to the solution and stirred for 24 hours at room temperature. The glycidyl methacrylate modified hyaluronic acid (GMHA) was precipitated into a 20-fold volumetric excess of acetone, dissolved in water, precipitated a second time, redissolved in water and lyophilized. The dry GMHA product was dessicated and stored at –20 °C in the dark until use. The average degree of methacrylate substitution was determined by ^1H NMR and found to be 0.32 moles of methacryloyl groups per mole of HA disaccharides.

4.4.3 Synthesis of chemically crosslinked hydrogels. These hydrogels were prepared by the method depicted in Figure 4.2a. For each hydrogel either 10 mg or 20 mg of sodium hyaluronate powder were dispensed into a circular silicone rubber mold. The molds were sandwiched between two glass microscope slides and tightly secured. Crosslinking solutions consisted of 0.2 M NaOH containing butanediol diglycidyl ether (BDDE). This solution was injected through the side of each rubber mold by a syringe equipped with a 25 gauge needle. A second needle provided an exit for air and care was taken to minimize entrapment of bubbles. A volume of crosslinking solution was added to completely fill each mold. The molds were approximately 100 μL in volume and yielded an HA concentration of 10% or 20% w/v. HA and crosslinking solution were then incubated at 40°C for eight hours. The crosslinked hydrogels were removed from the molds and transferred to a large volume of either distilled deionized (ddI) water or saline (0.9% NaCl) for swelling.

4.4.4 Synthesis of photocrosslinked hydrogels. These hydrogels were prepared by the method depicted in Figure 4.2b. For each hydrogel an appropriate mass of GMHA was placed into a silicone rubber mold. The mold was secured between two glass microscope slides. Crosslinking solutions consisted of aqueous solutions of 0.05–1.0% w/v I2959. 100 μL of crosslinking solution was injected through the side of each rubber mold. The GMHA was permitted to dissolve overnight. The hydrogels were photocrosslinked by exposure to UV light for 0.5 – 20 minutes. The hydrogels were then removed from the molds and transferred to a large volume of either ddI water or saline solution for swelling.

4.4.5 Synthesis of dual-crosslinked hydrogels. These hydrogels were prepared by the method depicted in Figure 4.2c. For each hydrogel 10 mg of GMHA was dispensed into a silicone rubber mold secured between two glass microscope slides. Crosslinking solutions consisted of aqueous solutions with an appropriate volume of BDDE and 0.05% w/v I2959. 100 μL of crosslinking solution was injected through the side of each mold. The GMHA was permitted to dissolve in the crosslinking solution overnight. The hydrogels were photocrosslinked by 5 minutes exposure to UV light. To initiate chemical crosslinking 2 μL of 10 M NaOH was added to each hydrogel to yield a final concentration of 0.2 M NaOH. The hydrogels were transferred to an oven and incubated for eight hours at 40°C. After crosslinking the hydrogels were moved to a large volume of ddI water for swelling. Patterned dual-crosslinked hydrogels were synthesized as described above with a photomask used during the UV exposure step.

4.4.6 Rheological measurements. The rheological properties of the HA hydrogels were quantified in terms of the storage modulus (G′) and the loss modulus (G″). G′ gives the elastic component of the material whereas the viscous component is given by G″ and both of these parameters represent the relative stiffness. Hydrogel samples were swollen in saline overnight and all measurements were performed in triplicate at room temperature. Dynamic viscoelastic measurements were performed with an MRC 300 modular compact rheometer (Paar Physica, Ashland, VA) using parallel plate geometry with a plate diameter of 25 mm and gap size of 1 mm. The moduli were measured at the deformation value of 0.1-10 mrad and a frequency sweep of 0.05-10 Hz.[17]

4.4.7 Hydrogel swelling ratio measurements. After synthesis, hydrogels were swelled to equilibrium in either water or saline consisting of 0.9% NaCl. The hydrogels were weighed after swelling. The swelling ratio was calculated according to Equation 1, where SR is the swelling ratio, W_S [mg] is the swollen weight of the hydrogel, and W_D [mg] is the dry weight of the hydrogel. The dry weight of the hydrogels was assumed as either 10 mg or 20 mg depending on the mass of dry HA powder that was placed in the mold.

$$SR = \frac{W_S - W_D}{W_D} \quad [1]$$

4.4.8 Degradation of hydrogels. Hydrogels were swollen to equilibrium in saline and then transferred to saline containing 500 U/mL of hyaluronidase. These hydrogels were incubated at 37°C. At selected time points the hydrogels were removed from solution, weighed, and returned to solution. The percentage of degradation was calculated by Equation 2, where W_0 [mg] is the initial wet weight of the hydrogel and W_t [mg] is the wet weight of the hydrogel at time t.

$$\%Degradation = \frac{W_0 - W_t}{W_0} \times 100\% \quad [2]$$

4.4.9 Patterned dual-crosslinked hydrogels. The spatial patterning of photocrosslinking in the dual-crosslinked hydrogels was visualized by confocal fluorescence (Figure 4.11b) and epifluorescence (Figure 4.11c) microscopy. Fluorescent hydrogels were prepared by the method depicted in Figure 4.2c with fluorescein-acrylate mixed into the crosslinking solution and injected into the mold. The hydrogels were then

exposed to a photomasked UV source. Micro-patterns were created with a stereolithographic laser system.[21] The hydrogels were chemically crosslinked by adding sodium hydroxide and incubating eight hours at 40°C. The hydrogels were swollen in saline for 24 hours and uncrosslinked fluorescein-acrylate was removed by washing.

4.4.10 Statistical analysis. All data are presented as mean ± standard deviation.

4.5 References

1. Nettles, D.L., Vail, T.P., Morgan, M.T., Grinstaff, M.W., Setton, L.A. Photocrosslinkable hyaluronan as a scaffold for articular cartilage repair. *Ann. Biomed. Eng.* **32**, 391-397 (2004).
2. Chung, C., Mesa, J., Miller, G.J., Randolph, M.A., Gill, T.J., Burdick, J.A. Effects of auricular chondrocyte expansion on neocartilage formation in photocrosslinked hyaluronic acid networks. *Tissue Eng.* **12**, 2665-2673 (2006).
3. Price, R.D., Das-Gupta, V., Leigh, I.M., Navsaria, H.A. A comparison of tissue-engineered hyaluronic acid dermal matrices in a human wound model. *Tissue Eng.* **12**, 2985-2995 (2006).
4. Hemmrich, K., von Heimburg, D., Rendchen, R., Bartolo, C.D., Milella, E., Pallua, N. Implantation of preadipocyte-loaded hyaluronic acid-based scaffolds into nude mice to evaluate potential for soft tissue engineering. *Biomaterials* **26**, 7025-7037 (2005).

5. Metcalfe, A.D., Ferguson, M.W.J. Tissue engineering of replacement skin: the crossroads of biomaterials, wound healing, embryonic development, stem cells and regeneration. *J. R. Soc. Interface,* **4**, 413-437 (2007).

6. Johl, S.S., Burgett, R.A. Dermal filler agents: a practical review. *Curr. Opin. Ophthalmol.,* **17**, 471-479 (2006).

7. Luo, Y., Shoichet, M.S. A photolabile hydrogel for guided three-dimensional cell growth and migration. *Nat. Mater.* **3**, 249-253 (2004).

8. Hahn, M.S., Miller, J.S., West, J.L. Three-dimensional biochemical and biomechanical patterning of hydrogels for guiding cell behavior. *Adv. Mater.,* **18**, 2679-2684 (2006).

9. Agerup, B. Polysaccharide gel composition. US Patent 5,827,937, 1998.

10. Malson, T., Lindqvist, B.L. Gel of crosslinked hyaluronic acid for use as a vitreous humor substitute. US Patent 4,716,154, 1987.

11. Collins, M.N., Birkinshaw, C. Comparison of the effectiveness of four different crosslinking agents with hyaluronic acid hydrogel films for tissue-culture applications. *J. Appl. Polym. Sci.* **104**, 3183-3191 (2007).

12. Hahn, S.K., Jelacic, S., Maeir, R.V., Stayton, P.S., Hoffman, A.S. Anti-inflammatory drug delivery from hyaluronic acid hydrogels. *J. Biomat. Sci. Polym. E.* **15**: 1111-1119 (2004).

13. Sannino, A., Madaghiele, M., Conversano, F., Mele, G., Maffezzoli, A., Netti, P.A., Ambrosio, L., Nicolais, L. Cellulose derivative-hyaluronic acid-based microporous hydrogels cross-linked through divinyl sulfone (DVS) to modulate

equilibrium sorption capacity and network stability. *Biomacromolecules* **5**, 92-96 (2004).

14. Balazs, E.A., Leshchiner, A. Cross-linked gels of hyaluronic acid and products containing such gels. US Patent 4,582,865, 1986.

15. Tomihata, K., Ikada, Y. Crosslinking of hyaluronic acid with glutaraldehyde. *J. Polym. Sci. A. Polym. Chem.* **35**, 3553-3559 (1997).

16. Crescenzi, V., Francescangeli, A., Taglienti, A., Capitani, D., Mannina, L. Synthesis and partial characterization of hydrogels obtained via glutaraldehyde crosslinking of acetylated chitosan and of hyaluronan derivatives. *Biomacromolecules* **4**, 1045-1054 (2003).

17. Leach, J.B., Bivens, K.A., Patrick, C.W., Schmidt, C.E. Photocrosslinked hyaluronic acid hydrogels: natural, biodegradable tissue engineering scaffolds. *Biotechnol. Bioeng.,* **82**, 578-589 (2003).

18. Albrecht, D.R., Tsang, V.L., Sah, R.L., Bhatia, S.N. Photo- and electropatterning of hydrogel-encapsulated living cell arrays. *Lab Chip* **5**, 111-118 (2005).

19. Williams, C.G., Malik, A.N., Kim, T.K., Manson, P.N., Elisseeff, J.H. Variable cytocompatibility of six cell lines with photoinitiators used for polymerizing hydrogels and cell encapsulation. *Biomaterials* **26**, 1211-1218 (2005).

20. Bryant, S.J., Nuttelman, C.R., Anseth, K.S. Cytocompatibility of UV and visible light photoinitiating systems on cultured NIH/3T3 fibroblasts in vitro. *J. Biomater. Sci. Polym. Ed.* **11**, 439-457 (2000).

21. Mapili, G., Lu, Y., Chen, S.C., Roy, K. Laser-layered microfabrication of spatially patterned functionalized tissue engineering scaffolds. *J. Biomed. Mater. Res.* **75B**, 414-424 (2005).

22. Hongyan, H., Guan, J., Lee, J.L. An oral delivery device based on self-folding hydrogels. *J. Control Release* **110**, 339-346 (2006).

23. Omidian, H., Rocca, J.G., Park, K. Advances in superporous hydrogels. *J. Control Release* **102**, 3-12 (2005).

24. Almarza, A.J., Athanasiou, K.A. Design characteristics for the tissue engineering of cartilaginous tissues. *Ann. Biomed. Eng.* **32**, 2-17 (2004).

25. Smeds, K.A., Grinstaff, M. Photocrosslinkable polysaccharides for in situ hydrogel formation. *J. Biomed. Mater. Res. A* **54**, 115-121 (2001).

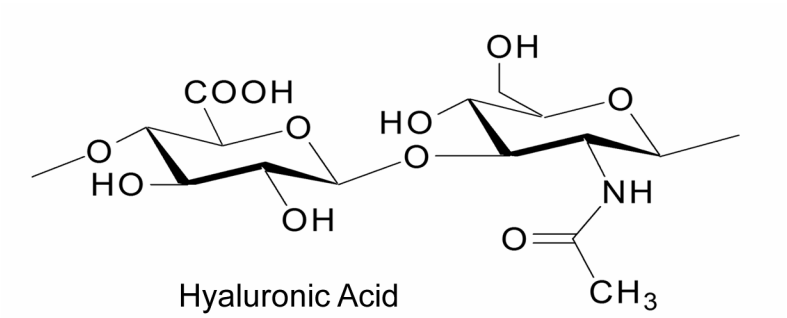

Hyaluronic Acid

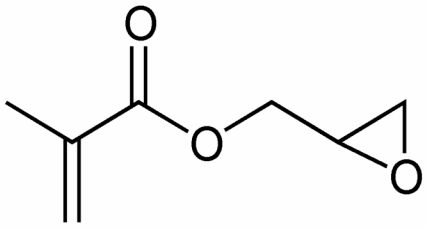

Glycidyl Methacrylate

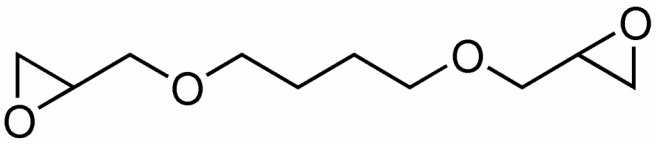

Butanediol Diglycidyl Ether

Figure 4.1 Chemical structures of hyaluronic acid (HA), glycidyl methacrylate, and butanediol diglycidyl ether (BDDE). Glycidyl methacrylate was used to functionalize HA with methacrylate functional groups that could undergo photocrosslinking. BDDE was used to synthesize chemically crosslinked HA hydrogels.

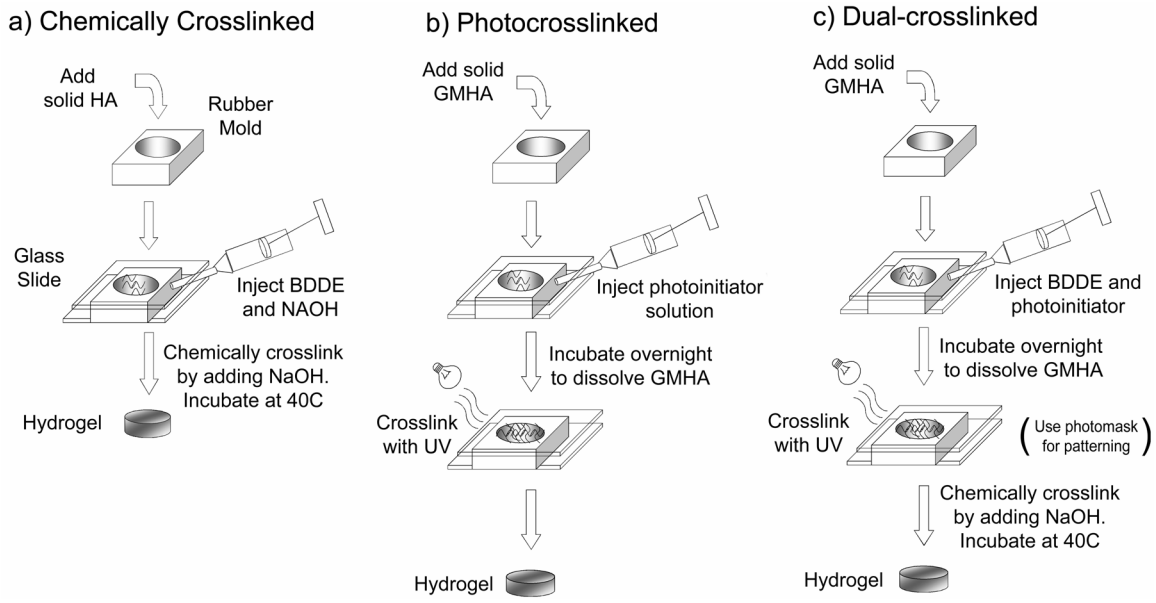

Figure 4.2 Procedure for synthesizing (**a**) chemically crosslinked hydrogels; (**b**) photocrosslinked hydrogels; and (**c**) dual-crosslinked hydrogels.

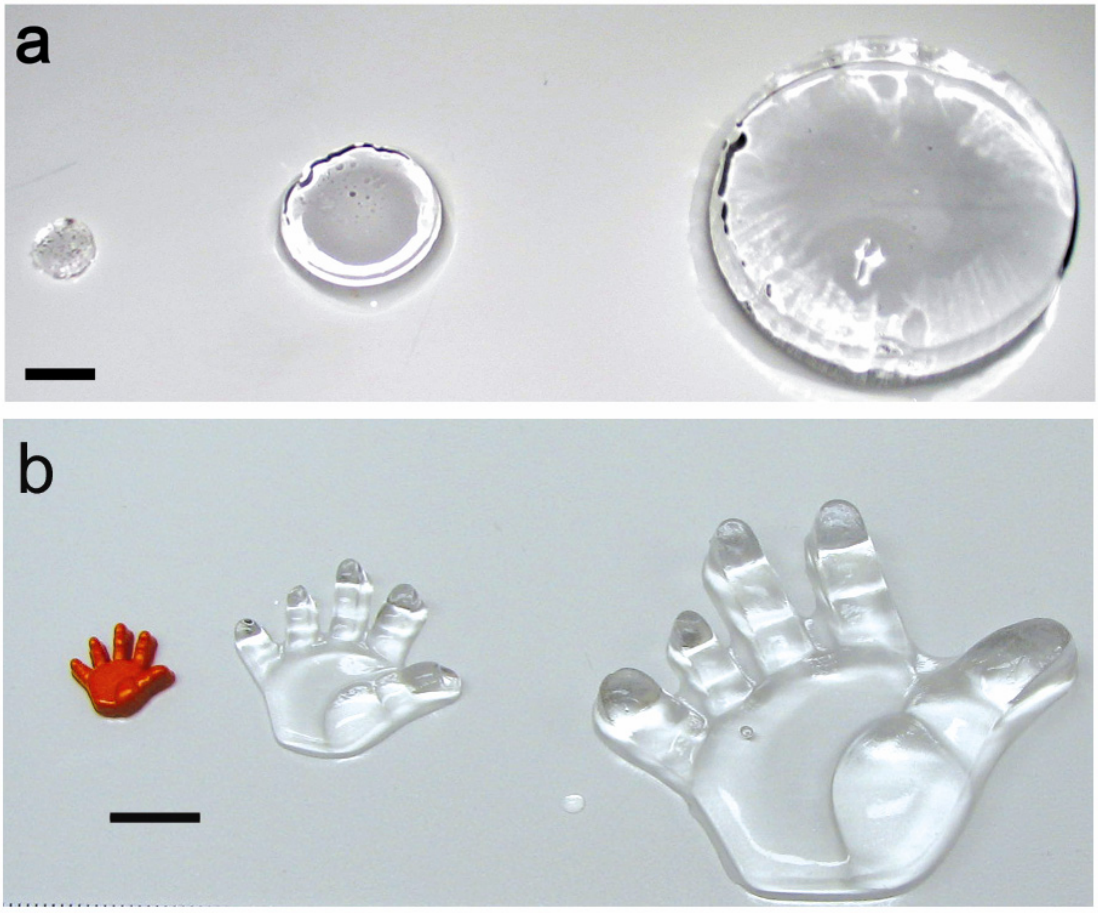

Figure 4.3 Images of chemically crosslinked super-swelling hydrogels of hyaluronic acid. These images demonstrate the ability of the hydrogels to maintain shape during swelling. Scale bars = 1 cm. (**a**) Disc-shaped hydrogels before swelling (left), after swelling in saline (middle), and after swelling in water (right). (**b**) Hand-shaped button that was used to cast the PDMS mold (left), hydrogel after swelling in saline (middle), and hydrogel after swelling in water (right).

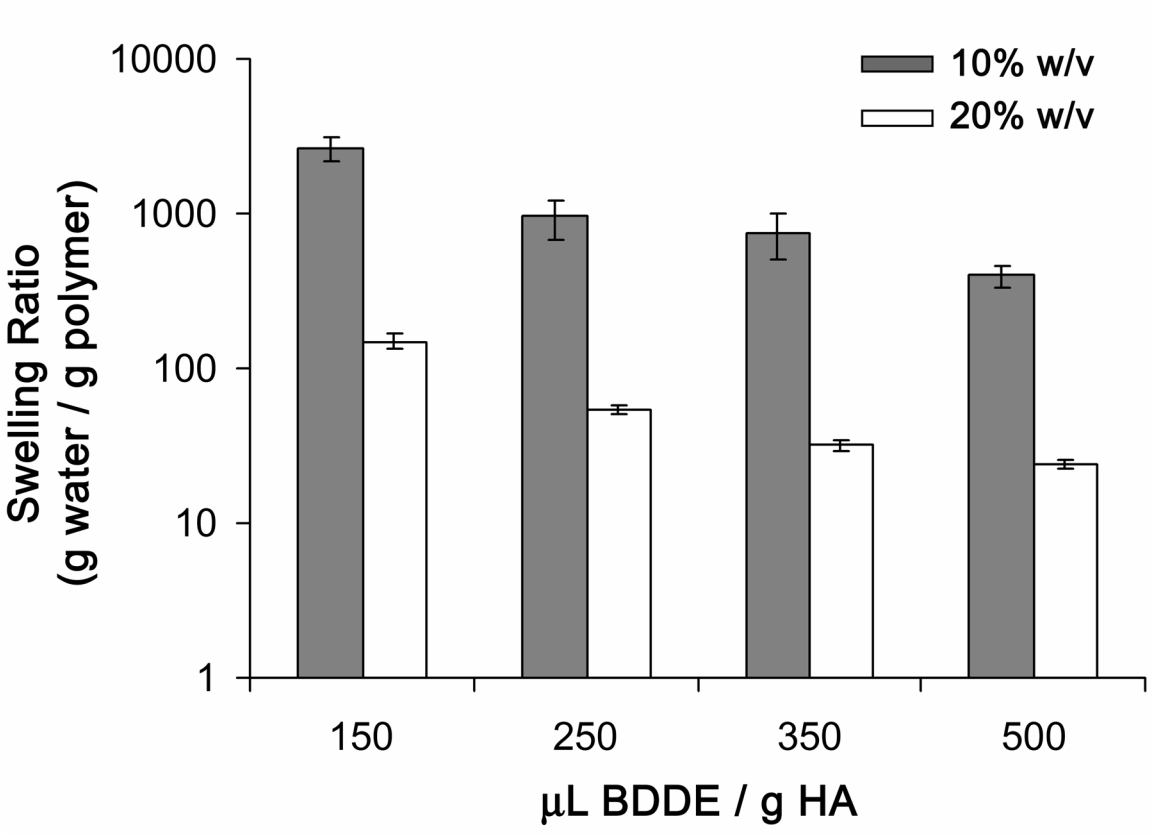

Figure 4.4 Equilibrium swelling ratios of chemically crosslinked hyaluronic acid hydrogels swollen in water. The hydrogels exhibit super-swelling. Dark bars correspond to 10% w/v HA hydrogels and light bars correspond to 20% w/v HA hydrogels. Increasing concentrations of chemical crosslinker (i.e., butanediol diglycidyl ether, BDDE) and HA decreased the swelling ratio. Note that the y-axis is plotted on log scale. Data points are the mean ± standard deviation of at least six measurements.

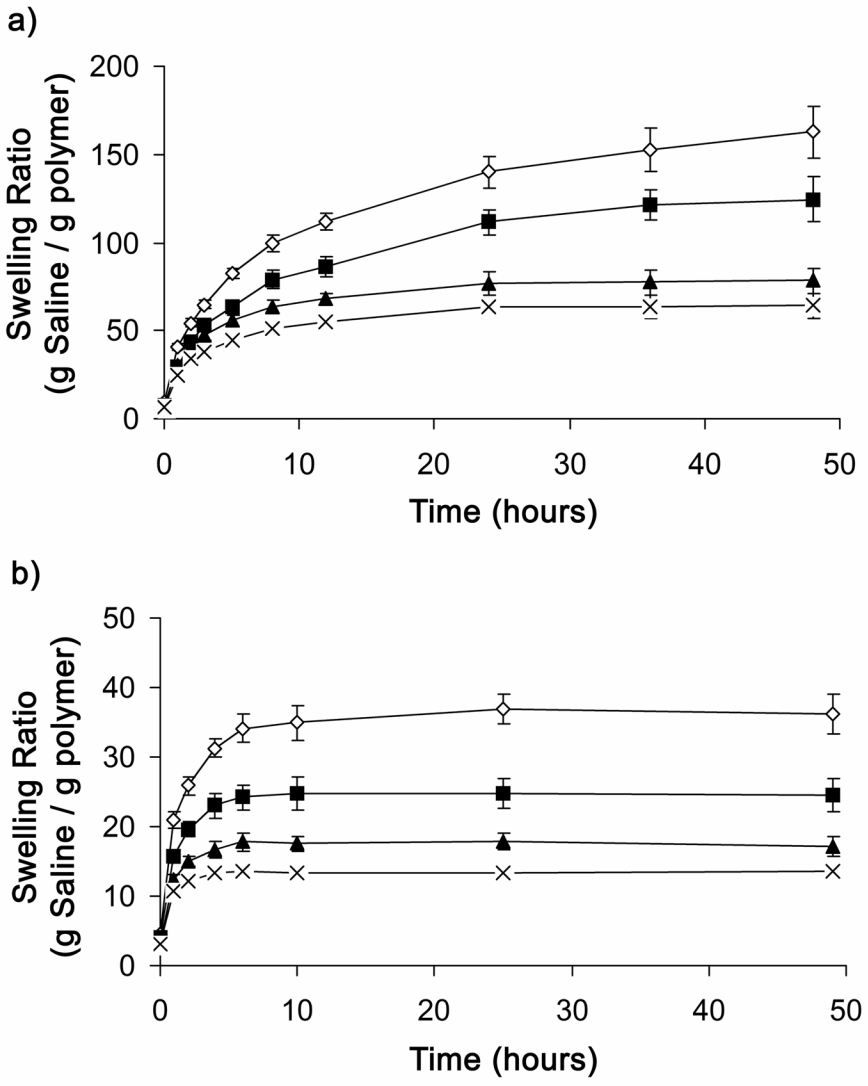

Figure 4.5 Time-dependant profile of swelling in saline. Equilibrium swelling was attained within 48 hours for 10% hydrogels and 10 hours for 20% hydrogels. (**a**) 10% w/v HA hydrogels chemically crosslinked with (◊) 150 μL BDDE/g HA; (■) 250 μL/g; (▲) 350 μL/g; (**x**) 500 μL/g; (**b**) 20% w/v HA hydrogels chemically crosslinked with (◊) 125 μL/g; (■) 250 μL/g; (▲) 350 μL/g; (**x**) 500 μL/g. Data points are the mean ± standard deviation of at least seven measurements.

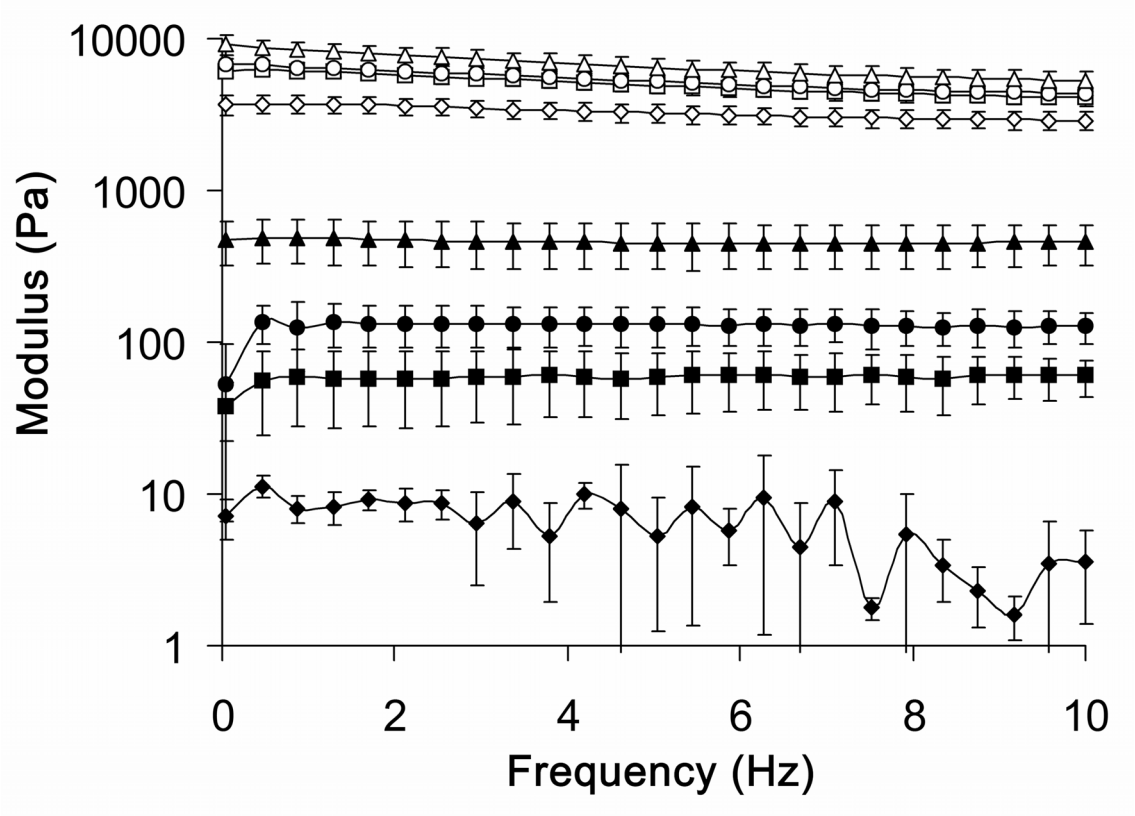

Figure 4.6 Effects of HA and BDDE concentration on the storage modulus of chemically crosslinked hydrogels. The rigidity of the hydrogels was dependent on polymer and crosslinker concentration. Storage modulus (G′) is plotted as a function of frequency. (♦) 10% w/v HA hydrogel crosslinked with 150 μL BDDE/g HA; (■) 10% HA, 250 μL/g; (●) 10% HA, 350 μL/g; (▲) 10% HA, 500 μL/g; (◊) 20% HA, 125 μL/g; (□) 20% HA, 250 μL/g; (○) 20% HA, 350 μL/g; (∆) 20% HA, 500 μL/g. Data points are the mean ± standard deviation of three measurements.

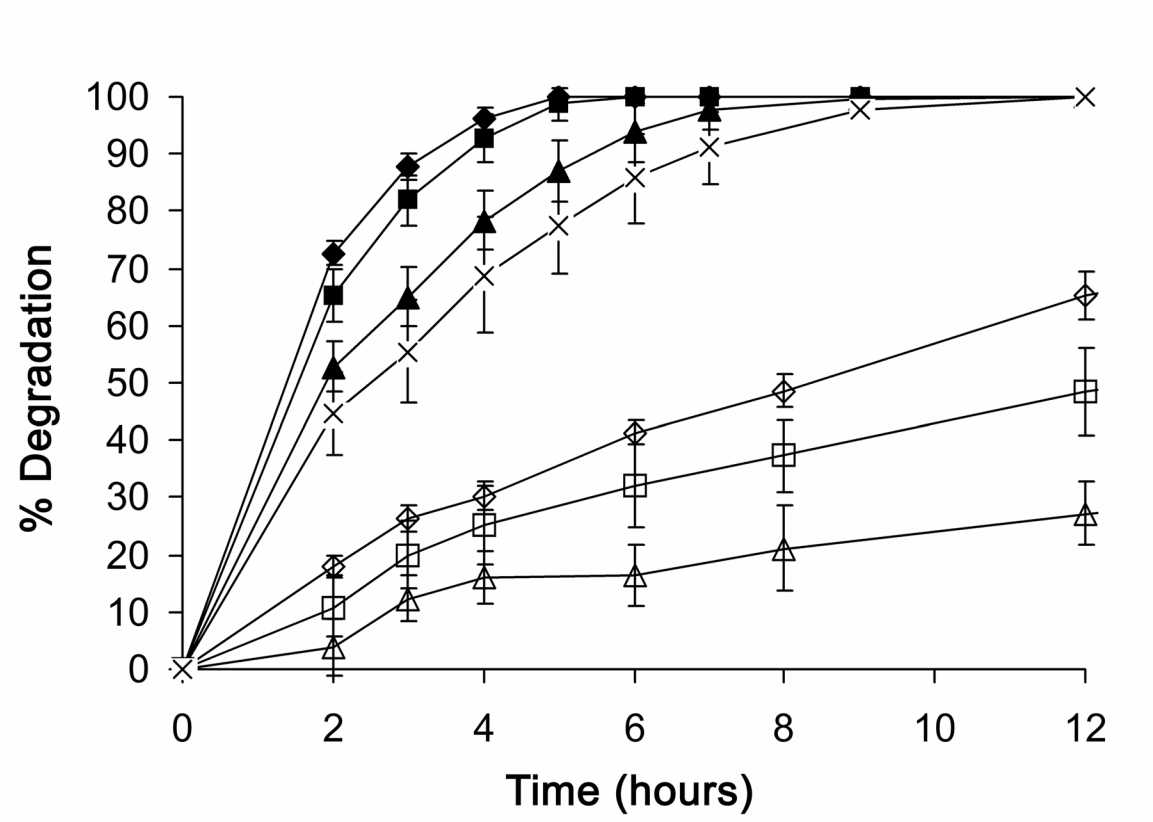

Figure 4.7. Degradation profiles of chemically crosslinked hydrogels treated with 500 U/mL hyaluronidase at 37°C in PBS. The degradation rate decreases with an increase in BDDE concentration. (♦) 10% w/v HA hydrogel crosslinked with 150 μL BDDE/g HA; (■) 10% HA, 250 μL/g; (▲) 10% HA, 350 μL/g; (**x**) 10% HA, 500 μL/g; (◊) 20% HA, 125 μL/g; (□) 20% HA, 250 μL/g; (Δ) 20% HA, 350 μL/g. Data points are the mean ± standard deviation of at least six measurements.

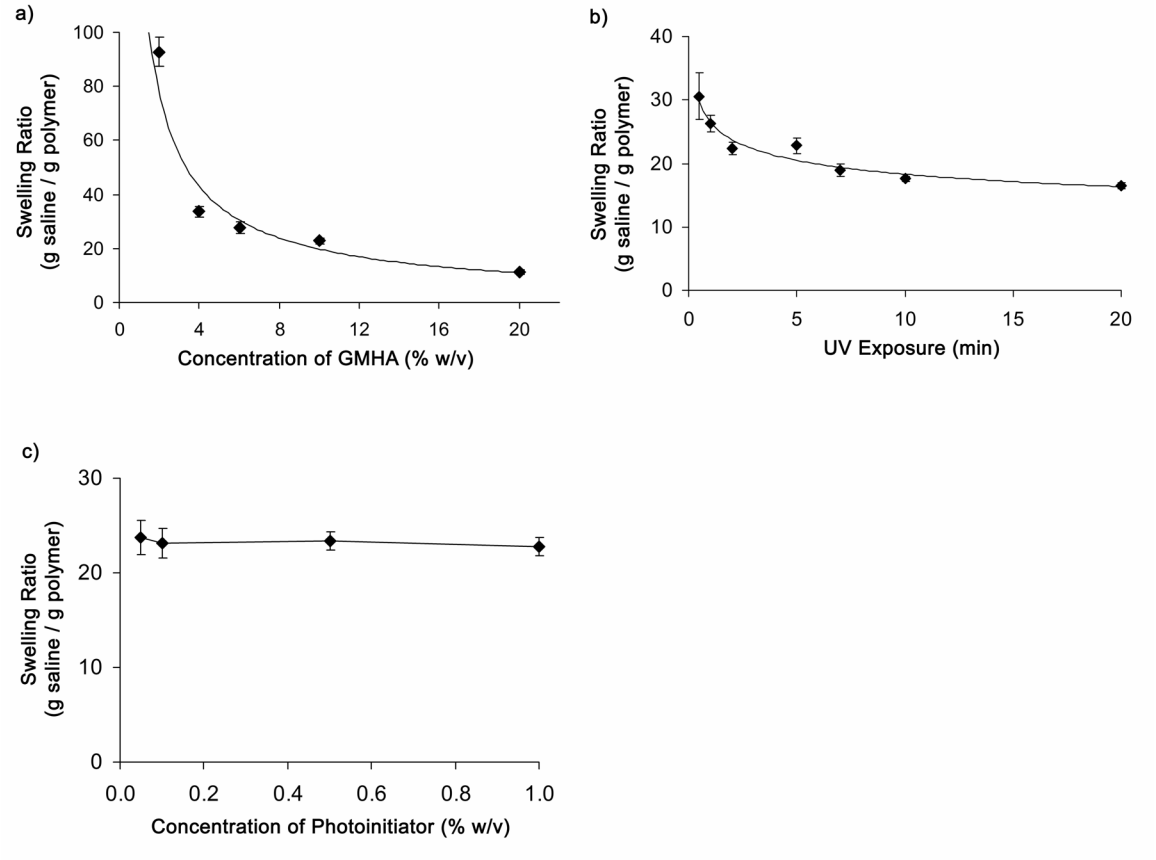

Figure 4.8 Optimization of photocrosslinking conditions. (**a**) Swelling ratio as a function of HA concentration. 5 minutes of UV exposure and 1% photoinitiator were held constant for these hydrogels. (**b**) Swelling ratio as a function of duration of UV exposure. An HA concentration of 10% w/v and 1% photoinitiator were held constant for these hydrogels. (**c**) Swelling ratio as a function of photoinitiator concentration. An HA concentration of 10% w/v and 5 minutes of UV exposure were held constant for these hydrogels. Data points are the mean ± standard deviation of at least seven measurements.

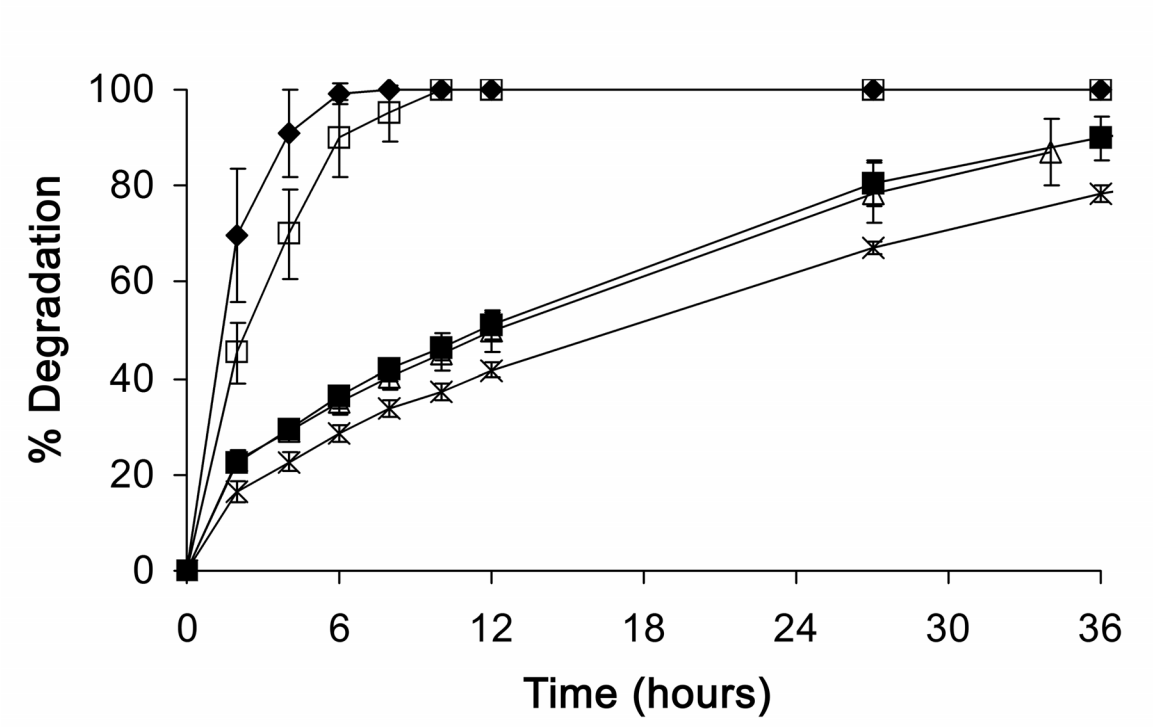

Figure 4.9 Degradation profiles of photocrosslinked hydrogels of 10% w/v HA. The crosslinking conditions that exhibited the fastest rate of degradation yielded the greatest swelling ratios. The crosslinking conditions with the slowest rate of degradation yielded the least swelling ratios. (♦) 1% photoinitiator (PI), 0.5 min UV, swelling ratio (SR) = 28; (□) 0.05% PI, 5 min UV, SR = 19; (■) 1% PI, 5 min UV, SR = 18; (Δ) 0.5% PI, 10 min UV, SR = 18; (**x**) 1% PI, 20 min UV, SR = 16. Data points are the mean ± standard deviation of at least seven measurements.

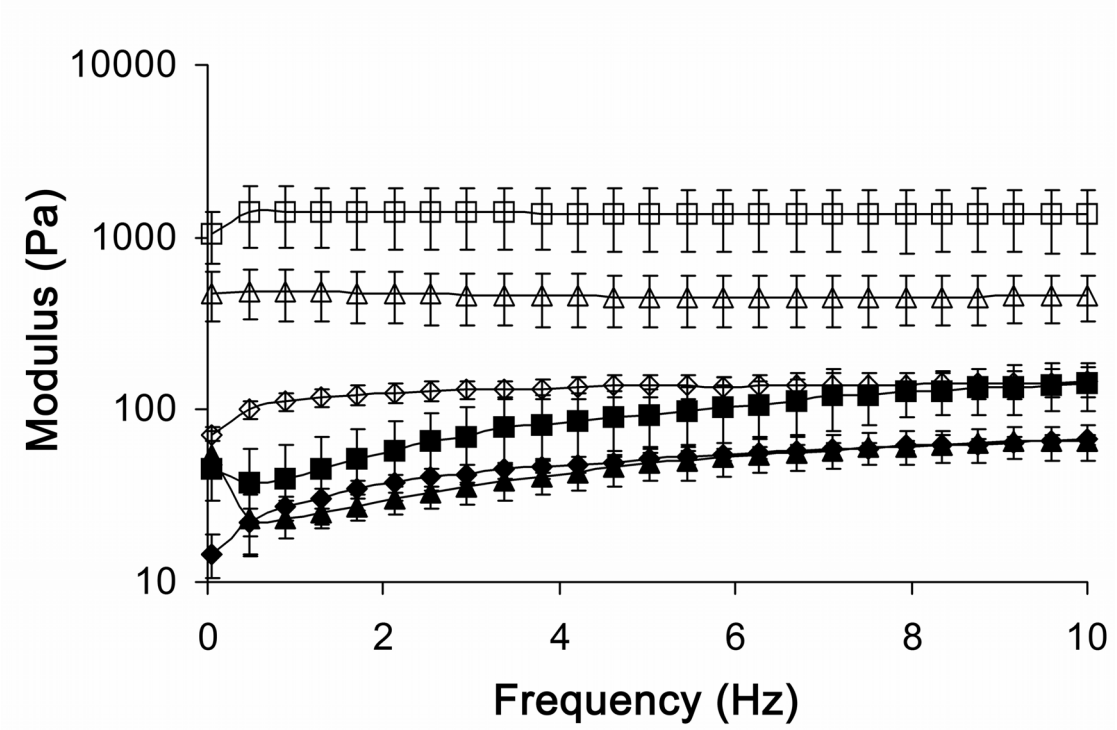

Figure 4.10 Effect of dual crosslinking on viscoelasticity of HA hydrogels. Storage (G′) and loss modulus (G″) as a function of frequency: (□) G′ (■) G″ of dual crosslinked hydrogel; (Δ) G′ (▲) G″ of chemically crosslinked hydrogel; (◊) G′ (♦) G″ of photocrosslinked hydrogel. Hydrogels with both photocrosslinks and chemical crosslinks had higher storage moduli throughout the frequency range than either type of crosslinking alone. The hydrogels were swollen in saline overnight and then measurements were taken at 25°C. Data points are the mean ± standard deviation of three measurements.

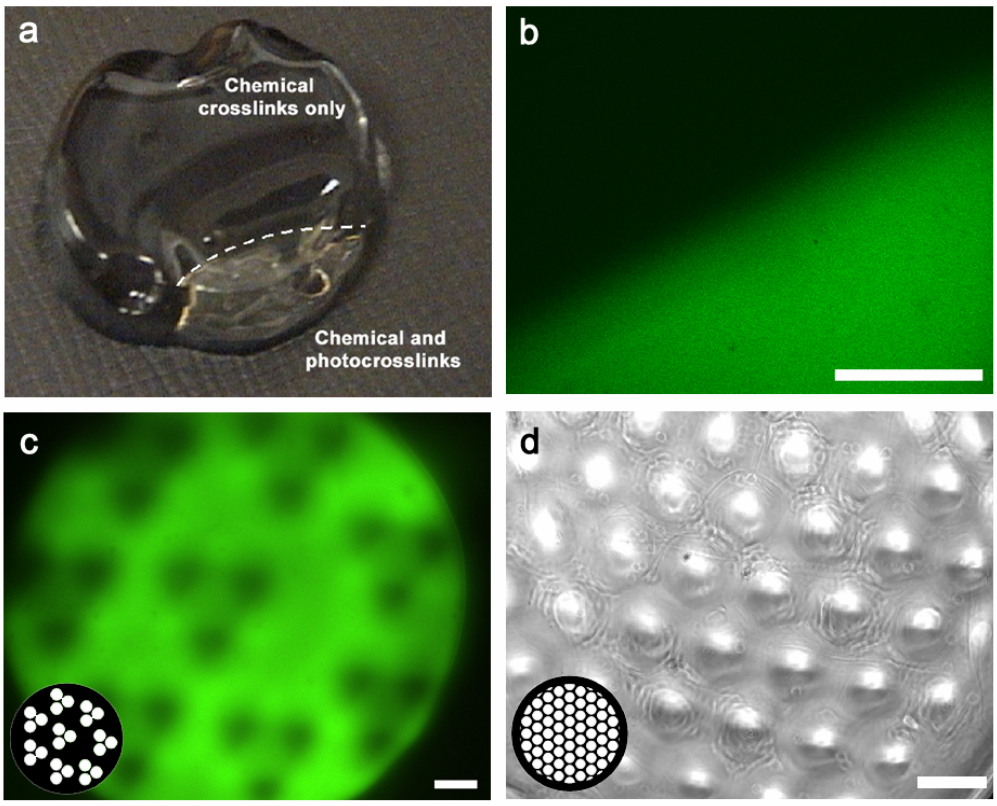

Figure 4.11 Patterned anisotropic dual-crosslinked hydrogels. (**a**) An anisotropically swelling hydrogel. Half was photocrosslinked by exposure to UV. The UV exposed (i.e., dual-crosslinked) region exhibited low swelling and the non-exposed (i.e., chemically-crosslinked) region exhibited high swelling. (**b**) This is a fluorescent image of the hydrogel in (a) depicting the interface between the two crosslinking regions. The photocrosslinked region incorporated fluorescein-acrylate during photopolymerization. (**c**) This hydrogel demonstrates micro-patterning of dual-crosslinked and chemically-crosslinked regions. The photomask used to pattern the photocrosslinks is shown in the bottom left corner. The fluorescent regions of the hydrogel correspond to dual-crosslinked regions that incorporated fluorescein-acrylate. (**d**) This dual-crosslinked hydrogel depicts micro-patterning with a hexagonal lattice photomask. The regions coinciding with the mask have a high crosslink density and low swelling. The regions coinciding with the interstices have a low crosslink density and high swelling. The result is a hydrogel surface with regular repeating bumps arising from anisotropic swelling.

Chapter 5: Dendritic Macroporous Hydrogels of Hyaluronic Acid Templated by *In Situ* Crystallization

Abstract

We have developed a novel crystal-templating technique to fabricate hydrogels with dendritic porous networks. Crystal-templating works by growing a crystal template within a solution of uncrosslinked polymer, crosslinking the polymer around the template, and removing the crystals by washing with water. The result is a macroporous hydrogel with a network of pores matching the intricate architecture of the crystal template at the micron and sub-micron levels. This technique addresses the challenge of fabricating polymeric materials with dendritic porosity which is not possible by current methods. Additional advantages of crystal-templating are that it is compatible with natural materials, is fast, can be scaled up, and does not require any expensive equipment or reagents. We have used crystalline urea templates to pattern photocrosslinked hyaluronic acid and calcium-crosslinked alginate hydrogels for use as implantable tissue engineered constructs. Control over the pore morphology is important because it influences cellular infiltration, scaffold remodeling, nutrient diffusion, vascular ingrowth, and functional integration with native tissues.

5.1 Introduction

The goal of tissue engineering is to create materials that can replace or repair injured tissue. To that end it is desirable to have tissue engineered constructs that mimic the microarchitecture of native tissues. Important structural features of many tissues are highly branched networks of vessels and ducts (**Figure 5.1**). Examples are the bronchioles, the microvasculature, lymphatic vessels, the ductal networks of salivary gland, mammary gland, and kidney, and the dendritic trees produced by neurons.[1-4] Such networks exhibit branching, multiple length scales, a directional orientation, and three-dimensionality. A tissue may contain multiple entwined networks; for example, bronchioles, arterial vessels, and venous vessels within the lungs. Although many techniques are available for creating porosity within tissue engineered constructs they fall short of faithfully reproducing the complexity of native tissues (**Figure 5.2**).[5]

Current techniques available for creating porosity are gas-foaming, lyophilization, thermally-induced phase separation and porogen leaching of salts and un-crosslinked polymer microspheres (**Table I**).[6-8] The advantages of these methods are that they are easy to implement and scale-up. The disadvantage is that they produce random pore morphology and compatibility with natural materials is limited. Soft replica molding can transfer branched patterns from etched silicon to polymers such as poly(lactide-co-glycolide); however, this is an inherently two-dimensional technique and stacked layering methods are a poor approximation of three-dimensional porosity.[9,10] Rapid prototyping techniques permit precise control over pore morphology through the use of computer-aided design systems.[11-13] Rapid prototyping is suitable for creation of

square and hexagonal lattices but not the complex three-dimensional dendritic patterns observed in native tissues. Although rapid prototyping techniques are compatible with synthetic polymers they are not as suitable for natural materials which are water soluble and viscous. A further limitation is that the resolution of such techniques is larger than the length scale of individual cells and neuronal processes. Scaffolds depicted in the literature typically have features hundreds of microns in length which are too large to precisely guide cellular infiltration. Fabrication of three-dimensional multilayer constructs can be impractical because each scaffold must be built layer by layer with costly equipment.

Hydrogel scaffolds are uniquely suited for tissue engineering applications because they more closely resemble natural tissues with respect to mechanical properties, porosity, and water content than do other materials.[14] In particular, polysaccharides, such as hyaluronic acid (HA) and sodium alginate (SA) are attractive materials because they are composed of the same chemical building blocks as native extracellular matrix components. They also exhibit excellent biocompatibility and non-immunogenicity. HA has found use as a dermal filler, adhesion barrier, intra-articular viscosupplement, vitreal substitute, drug delivery matrix and tissue engineering scaffold for cartilage, skin, adipose, and vocal cord.[15-21] Alginate has been used extensively for cell encapsulation, drug delivery, and tissue engineering of adipose and cartilage.[22-24]

Few of the techniques developed for synthetic polymers are applicable to these natural biomaterials. In comparison to synthetics, these polysaccharides are considerably more difficult to work with because they are high molecular weight, polydisperse,

insoluble in organic solvents, pH and temperature sensitive, and produce viscous solutions even at dilute concentrations. Thus, new techniques that are compatible with the unique properties of these biopolymers need to be developed. To address this challenge we have invented a crystal-templating technique that uses *in situ* crystallization to carve out pores within biopolymer hydrogels. Salts and small organic molecules can precipitate as crystalline branching networks under certain conditions. The similarity between such networks and the dendritic patterns of microvasculature and neuronal dendritic trees prompted us to use *in situ* crystallization to template biopolymer hydrogels with macroporous networks.

HA and SA are both linear, unbranched, anionic, high molecular weight polysaccharides (their chemical structures are depicted in Figure 5.3), however they are distinguished by their mode of crosslinking. HA can be crosslinked by derivatization with methacrylate side chains and exposure to UV light and photoinitiator.[25] Alginate can be crosslinked by addition of divalent cations which crosslink adjacent guluronic acid blocks.[24] We have confirmed that both modes of crosslinking are compatible with the crystal-templating technique. We chose urea as the crystallite because it has high water solubility and a propensity for extensive hydrogen bonding to permit interaction with biopolymer chains in solution.

5.2 Results

5.2.1 Characterization of crystal growth and hydrogel morphology. Our technique consists of five steps: solution casting, solvent evaporation, crystal growth,

crosslinking, and rinsing. These steps are depicted in **Figure 5.3**. Small droplets (2 μL) of biopolymer and urea were cast onto microscope slides. The droplets were evaporated at 50% relative humidity to produce thin hydrated films on microscope slides. Solvent evaporation is required to achieve the super-saturation conditions necessary for crystallization. Evaporation also greatly increases the biopolymer concentration and solution viscosity. The combination of high viscosity and hydrogen bonding supresses spontaneous urea crystallization and facilitates super-saturation which is the driving force for crystallization. Urea seed crystals were deposited on the tips of a fine pair of tweezers and applied to the centers of each HA/urea and SA/urea film. Crystal growth began immediately and produced long dendritic branches that radiated from the center to the edge of the film. Within seconds the entire volume of the hydrogel film was filled with urea crystals.

After crystallization was completed the films were crosslinked by either UV exposure (HA hydrogels) or calcium (SA hydrogels). Both methods of crosslinking are rapid and accurately preserved the configuration of the crystal template. After crosslinking the crystals were easily removed with water. The end products were hydrogels with dendritic macroporous networks. Crystal-templated HA hydrogels are depicted in **Figure 5.4**. These thin films were easily observable by phase contrast and polarized light microscopy. Droplets containing biopolymer and urea crystals (i.e., biopolymer-urea "composites") were highly birefringent when observed through crossed polarizers. These composite films exhibited a characteristic maltese cross pattern indicative of radial alignment. The colors of the composites in polarized light appeared to

correspond to film thickness; the films were thickest at the center and thinnest at the edges. After crosslinking and rinsing, the hydrogels lost most of their birefringence and exhibited only a faint white color when viewed through crossed polarizers. The hydrogel morphology consisted of aligned "fibrils" that were the inverse shape of the crystal template.

We captured images of urea crystal growth using video microscopy. The sequence of panels in **Figure 5.5** depict high magnification images of a growing urea crystal front. The crystals were thin, tightly packed needles that sprouted a high density of branches. As the urea branches approached neighboring branches the local concentration of urea became depleted and branch growth was terminated; therefore, the longest continuous branches were those that grew in the most radial direction away from the point of nucleation. Direct observation of crystal growth confirmed that the crystals grew continuously; therefore, we conclude that the porous network within the crystal-templated hydrogels is also continuous.

The micro-topography of a rinsed urea-templated HA hydrogel was observed by contact mode atomic force microscopy in air (**Figure 5.6a**). The surface of the hydrogel consisted of alternating parallel valleys and ridges that were carved out during crystal growth. During crystallization, the crystal front expels the biopolymer as an impurity. Thus, the biopolymer was compressed into the interstices between urea crystals and formed the radially aligned thin ridges. A profile of the hydrogel perpendicular to the length of the ridges is shown in **Figure 5.6b**. The dimensions of these ridges, less than 1

μm in height and spaced between 1 and 2 μm apart, demonstrate the fidelity of the crystal-templating technique on the micron and sub-micron length scales.

The hydrogels were rendered fluorescent by dissolving a small amount of TRITC-conjugated dextran into the GMHA solution prior to solvent casting. Like GMHA, the fluorescent dextran was phase separated from the urea crystal template permitting the hydogel phase to be imaged by confocal fluorescent microscopy. The non-fluorescent crystalline phase was easily distinguishable from the fluorescent hydrogel phase. Branch points within the porous network were observed throughout the hydrogel volume. A volume reconstruction of a series of confocal z-slices illustrates that the urea crystals grow throughout the entire volume of the hydrogel (**Figure 5.7a**). Scans of individual z-slices of samples with urea crystals and without urea crystals (imaged both in water and dry) demonstrate that the hydrogel preserves the macroporous network after template removal (**Figures 5.7b-d**).

Branches were not observed when urea crystals were grown in the absence of biopolymer which indicates the importance of viscosity to induction of dendritic growth. Such an effect has been observed by others who have examined crystal growth in the presence of polymers.[26,27] We found that both crystal growth rate and crystal morphology were dependent on the degree of super-saturation (i.e., the ratio of urea and HA concentrations). Super-saturation was adjusted by fixing the initial HA solution concentration at 10 mg/mL and varying the urea concentration from 2.5 to 180 mg/mL. Crystal growth could not be nucleated for a ratio of 0.25. For increasing ratios, the growth rate increased until reaching a rate of 1000 μm/sec for a ratio of 6 (**Figure 5.8**).

For ratios of 8 and greater, a viscous liquid was expelled from the crystals shortly after crystallization. This liquid was clearly visible under polarized light as dark liquid on the surface of the birefringent urea crystals. The liquid was likely rich in HA and photoinitiator which are impurities with respect to urea crystals. At higher ratios the urea crystals became increasingly more tightly packed, more needle-like and less branched. Bulk polyhedral urea crystals were observed on the surface of the needle crystals when the ratio was 18. We concluded that ratios of 6 and under were most effective at templating the biopolymer because higher concentrations produced urea crystals that were increasingly less branched and too tightly packed for effective templating.

Urea crystal growth can be nucleated by either spontaneous nucleation or by seed crystal application. Spontaneous nucleation occurs when the concentration of urea exceeds a critical super-saturation. Typically, spontaneous nucleation occurred on the edges of the hydrogels. Hydrogels never had more than one spontaneous nucleation event because crystal growth was very rapid. We found that applying a seed crystal to initiate urea crystal growth was a simple method for controlling the macro-morphology of the crystal template. To do this we used humid conditions that suppressed spontaneous nucleation. At equilibrium under 50% relative humidity the moist hydrogel films have a concentration of urea great enough to support crystal growth from a seed crystal but too low for spontaneous nucleation. Un-nucleated hydrogel films could be maintained for up to several days until the introduction of a seed crystal. This permitted us to select both the time and location of the nucleation. Individual seed crystals produced radial crystal growth. Films produced by the application of one seed in the center of the film are

depicted in **Figure 5.9a**. Simultaneous application of three seeds produced the three domain template in **Figure 5.9b**. A line of seeds produced parallel alignment throughout the hydrogel film (**Figure 5.9c**). Thus, seed nucleation is a simple method for engineering template morphology.

5.2.2 Degradation of templated hydrogel films. The droplets deposited on microscope slides formed thin films a few microns thick as estimated by electron microscopy. Crosslinked films could be released from the surfaces of the microscope slides by agitation and transferred to solution for storage if desired. These films remained intact and did not fall apart. Some hydrogel film samples were transferred to solutions containing the degradative enzyme, hyaluronidase. The mesh size of GMHA hydrogels is too small to permit ingress of the hyaluronidase enzyme into the bulk of the hydrogel; thus degradation was surface-mediated and exhibited three distinct phases. In the first phase, surface degradation of the dense fibrillar hydrogel resulted in partial dissociation of the fibers and a frayed morphology at the periphery of the hydrogel (**Figure 5.10a**). During this phase, the mechanical integrity of the bulk hydrogel became increasingly compromised as the surface-mediated degradation continued to dissociate hydrogel fibers. The second phase was characterized by catastrophic failure of the bulk hydrogel precipitated by mild mechanical stress from routine handling (**Figure 5.10b**). The third phase was the degradation of the remaining dissociated fibers. We infer that if urea-templated hydrogels were implanted *in vivo* they would also exhibit the three phases of slow surface degradation, bulk catastrophic mechanical failure, and slow degradation of dissociated fibers.

5.2.3 Scale-up of urea-templated hydrogels. Scale-up of the urea-templating procedure was accomplished for both HA and SA using a procedure similar to that used for the droplets. The scaled-up films were prepared by casting 2.6 mL of solution into 12-well plates with diameters of 2.2 cm. Three to four days were required to evaporate the solvent. Crystal growth could be nucleated both spontaneously and by seed crystal. Crystal-templated films were opaque white and had a fibrillar morphology observable even by eye (**Figure 5.11a**). In contrast, non-templated films of HA were transparent and featureless. Non-templated SA films were a light milky white and had a fine granular morphology when viewed under phase contrast microscopy. All templated and non-templated HA and SA films were durable, pliable and easy to handle in both dry and swollen conditions.

Scaled-up templated films were too thick for their features to be observed by transmittance light microscopy; therefore, the morphology of these films was investigated by scanning electron microscopy (SEM). Dehydration of swollen hydrogel specimens can easily create artifacts in the hydrogel structure particularly on the surface. To minimize such artifacts the SEM specimens were extensively soaked and rinsed with methanol rather than water to remove urea. Urea is highly soluble in methanol (~160 mg/mL) and the templated hydrogel swelled minimally. The urea crystals had been so tightly packed that the templated HA hydrogel had a fibrillar appearance. The hydrogel has a fibrillar rather than dendritic morphology because it is composed of a single continuous bulk that was molded among the interstices of the dendritic urea crystals. When observed from the top-down, a repeating “arrowhead” fibrillar morphology of the film was clearly revealed

(**Figure 5.11b**). A curled portion of the film viewed at an angle revealed the interior crevices among the fibers (**Figure 5.11c)**. Cross-sections of the film perpendicular and parallel to the fiber orientation are depicted in **Figures 5.11d and 5.11e**, respectively. These cross-sections demonstrate that the pore and fiber morphology were present throughout the thickness of the film and not confined to the surfaces; thus, confirming that the templates are three-dimensional.

Thermal gravimetric analysis was performed to assess whether water-rinsing was sufficient to remove urea from scaled-up, thick hydrogel films. Four samples were analyzed: (i) urea; (ii) uncrosslinked, non-templated GMHA hydrogel film; (iii) uncrosslinked, urea-templated GMHA hydrogel film containing 80% w/w urea before rinsing; and (iv) crosslinked, urea-templated GMHA hydrogel film after rinsing. Similarity among degradation profiles was assessed by comparing the temperatures corresponding to onset of weight loss. Before rinsing, the degradation profile of the urea-templated hydrogel film was similar to urea; both exhibited broad weight loss at 150°C (**Figure 5.12**). After rinsing, the degradation profile of the urea-templated hydrogel film was similar to non-templated GMHA; both exhibited sharp weight loss at 220°C and an absence of the 150°C weight loss characteristic of urea. These data demonstrate that water-rinsing was sufficient to wash out all urea; thus, scaled-up hydrogel films consist primarily of hyaluronic acid without detectable urea.

5.3 Discussion

Crystallization begins at a point of nucleation and then radiates outward filling the entire three dimensional volume. This process of growth ensures that the resulting

pores are interconnected and oriented. Importantly, the crystals were suspended within the viscous biopolymer solution permitting crystal growth in three dimensions. Scale-up was achieved because crystallization occured rapidly over large distances. We found that the crystallization of urea within HA and SA hydrogels was both reproducible and highly robust with respect to the concentrations of urea and biopolymer. This robustness to concentration permitted the hydrogels to be scaled from droplets to large films. The formation of the crystal templates was, however, sensitive to ambient humidity which affected the rate of solvent evaporation and the final water content of the evaporated, equilibrated hydrogel films. This sensitivity was circumvented through the use of controlled humidity conditions. Although crystal-templating lacks precise control over the final pore morphology this can be alleviated through temporal and spatial control of the nucleation event through the use of seed nucleation.

In addition to hyaluronic acid and alginate we have also confirmed that poly(ethylene glycol) acrylate hydrogels are patternable by urea crystallization (**Figure 5.13**). Exploration of other crystallites and crystal growth conditions will yield a range of template morphologies. For example, we have engineered potassium phosphate templates that possess dendritic structures that are much larger and thicker than the urea templates (Figure 5.13c). We are currently exploring a variety of growth conditions with the goal of engineering templates closely similar in shape and dimension to neuronal dendritic trees and microvasculature. Crystal engineering methods can tailor the supramolecular assembly of crystalline materials by manipulating crystal growth conditions. Important parameters are the concentrations and ratios of biopolymer and urea, solution viscosity,

pH, and temperature. Additives such as surfactants and chiral molecules can selectively adhere to crystal faces and thereby control the branching, size and chirality of the resulting crystal structures.[28] Such techniques may refine the crystal structures and produce a wide selection of crystal templates.

Our target application for crystal-templated hydrogels are macroporous tissue engineering scaffolds. Urea-templated hydrogels possess micro-architecture on a length scale suitable for infiltration and guidance of neuronal axons and dendrites. Although the macropores are very small the bulk hydrogel should permit oxygen and nutrient diffusion to the interior of the scaffold. Presently, we are working on creating larger branched structures, such as in Figure 5.13c, with length scales more suited for infiltration of cell bodies and micro-vessels. Additionally, crystal-templated hydrogels offer a unique platform for the creation of composite materials. We envision that polymerization reactions and biomineral growth within the pores can yield novel composites in which one component is distributed throughout the other in oriented branched micron-sized pores.

5.4 Materials and Methods

5.4.1 Materials. Sodium hyaluronate from *Streptococcus equi* of molecular weight 1.6×10^6 Da as indicated by the supplier, low viscosity alginic acid from brown algae, and bovine testicular hyaluronidase (1000 U/mg) were obtained from Sigma-Aldrich (St. Louis, MO). Tetra-functional poly(ethylene glycol) acrylate (PEG4A, MW = 10 kDa) was obtained from SunBio. Photoinitiator, Irgacure 2959, was obtained from

Ciba Specialty Chemicals (Basel, Switzerland). Photopolymerizations were initiated by a longwave UV lamp filtered around 365 nm and with an intensity of 22 mW/cm^2 (Blak-Ray B-100A, UVP, Upland, CA). Photocrosslinkable hyaluronic acid was prepared by our standard procedure of derivatization of HA with glycidyl methacrylate to yield GMHA (modifications to this protocol discussed in Chapter 4).[25]

5.4.2 Synthesis of Crystal Templated Hydrogels. Urea-templated GMHA films were prepared as depicted in Figure 5.3. An aqueous solution was prepared of 10 mg/mL GMHA with 40 mg/mL urea and 0.5 mg/mL Irgacure 2959 photoinitiator in distilled deionized water. Solutions also contained 0.1 mg/mL dextran-TRITC when hydrogels for confocal flourescent microscopy were prepared. Droplets of 2 μL were dispensed onto a glass microscope slide. The solvent was partially evaporated overnight at ambient conditions or in sealed containers with ~50% relative humidity maintained by saturated solutions of calcium nitrate. GMHA is very hygroscopic and retained residual moisture in equilibrium with the humid atmosphere. Thus, evaporation yielded viscous hydrogel films that were super-saturated with urea. After drying, urea seed crystals were deposited onto the tips of a fine pair of tweezers by scraping the tweezers against solid urea. Then the tweezers were carefully touched to the center of each droplet to nucleate crystallization. Similarly, a razor-blade scraped against urea was used to nucleate continuous straightlines. GMHA was crosslinked by 1 minute of exposure to UV. The hydrogels were rinsed in water to remove urea.

Templated alginate hydrogels were prepared as shown in Figure 5.3. Aqueous solutions of 10 mg/mL alginate with 40 mg/mL urea were dispensed onto microscope

slides and air-dried. After crystallization the hydrogels were crosslinked by incubating the droplet with 200 mg/mL calcium chloride solution for one minute. Rinsing with water removed excess calcium chloride and urea.

Templated PEG4A hydrogels (Figure 5.13c) were prepared from aqueous solutions of 60 mg/mL PEG4A, 40 mg/mL urea and 0.5 mg/mL Irgacure 2959. Potassium phosphate templated GMHA (Figure 5.13b) was prepared from a solution of 20 mg/mL GMHA, 10 mg/mL potassium dihydrogen phosphate and 0.5 mg/mL Irgacure 2959. These droplets were incubated in humid chambers equilibrated with saturated sodium chloride solutions (i.e., relative humidity ~75%) until crystal growth was complete. Alginate hydrogels templated with βCD were prepared from aqueous solutions of 30 mg/mL alginate and 15 mg/mL βCD. Droplets were dried and βCD crystals were grown at ambient temperature and humidity.

5.4.3 Enzymatic Degradation. Degradation was carried out in a solution of PBS containing 500 U/mL hyaluronidase. Microscope slides with urea-templated GMHA films were submerged in hyaluronidase solution and incubated at 37°C for 96 hours. The entire volume of hyaluronidase solution was replaced after 48 hours with freshly prepared.

5.4.4 Scale-up of Crystal Templated Hydrogels. Thick crystal-templated hydrogels were prepared under sterile conditions to prevent contamination during solvent evaporation. Aqueous solutions were prepared as described above, filter sterilized (0.22 μm PVDF, Millipore), and dispensed into sterile, non-tissue culture treated 12-well plates. Each well was 2.2 cm in diameter and a volume of 2.6 mL of sterile solution was

dispensed per well. The solvent was evaporated in a sterile horizontal flow hood in the dark for four days. During this time urea crystallization either nucleated spontaneously or was nucleated by the seed crystal technique. GMHA films were crosslinked by 1 minute of UV exposure, and rinsed extensively with exchanges of water over several days to remove urea. Alginate films were crosslinked by immersion in 200 mg/mL calcium chloride for twenty minutes and then rinsed extensively with water.

Plain GMHA films required an additional humidifying step after air-drying and before photocrosslinking. This step was required because the photocrosslinking reaction was moisture sensitive. It is likely necessary for water to be retained within the film to permit diffusion of photoinitiator and movement of GMHA chains during photoexposure. Therefore, air-dried films were placed in a sealed container at ~85% relative humidity which was achieved by equilibration with saturated potassium chloride solution. GMHA films were incubated under these conditions for four days and then photocrosslinked by exposure to UV for 1 minute.

Thermal gravimetry was performed with a Perkin Elmer TGA 7. The mass of each sample was between 6.4 and 7.2 mg. Samples were heated at 40°C/min from room temperature to 100°C and then heated at a rate of 10°C/min from 100°C to 400°C.

5.5 References

1. Larina, O. & Thorn, P. Ca^{2+} dynamics in salivary acinar cells: distinct morphology of the acinar lumen underlies near-synchronous global Ca^{2+} responses. *J. Cell Sci.* **118**, 4131-4139 (2005).

2. Brisken, C. & Rajaram, R.D. Alveolar and lactogenic differentiation. *J. Mammary Gland Biol. Neoplasia* **11**, 239-248 (2006).

3. Shah, M.M., Sampogna, R.V., Sakurai, H., Bush, K.T., Nigam, S.K. Branching morphogenesis and kidney disease. *Development* **131**, 1449-1462 (2004).

4. Bekkers, J.M. & Hausser, M. Targeted dendrotomy reveals active and passive contributions of the dendritic tree to synaptic integration and neuronal output. *P. Natl. Acad. Sci. USA* **104**, 11447-11452 (2007).

5. Khademhosseini, A., Langer, R., Borenstein, J., Vacanti, J.P. Microscale technologies for tissue engineering and biology. *P. Natl. Acad. Sci. USA* **103**, 2480-2487 (2006).

6. Mikos, A.G., Thorsen, A.J., Czerwonka, L.A., Bao, Y., Langer, R., Winslow, D.N., Vacanti, J.P. Preparation and characterization of poly(L-lactic acid) foams. *Polymer* **35**, 1068-1077 (1994).

7. Ma, P.X. & Choi, J.W. Biodegradable polymer scaffolds with well-defined interconnected spherical pore network. *Tissue Eng.* **7**, 23-33 (2001).

8. Chen, J., Park, H., Park, K. Synthesis of superporous hydrogels: hydrogels with fast swelling and superabsorbent properties. *J. Biomed. Mater. Res*. **44**, 53-62 (1999).

9. King, K.R., Wang, C.C.J., Kaazempur-Mofrad, M.R., Vacanti, J.P., Borenstein, J.T. Biodegradable microfluidics. *Adv. Mater.* **16**, 2007-2012 (2004).

10. Duffy, D.C., McDonald, J.C., Schueller, O.J.A., Whitesides, G.M. Rapid prototyping of microfluidic systems in poly(dimethylsiloxane). *Anal. Chem.* **70**, 4974-4984 (1998).

11. Yang, S.F., Leong, K.F., Du, Z., Chua, C.K. The design of scaffolds for use in tissue engineering. Part II. Rapid prototyping techniques. *Tissue Eng.* **8**, 1-11 (2002).

12. Lu, Y., Mapili, G., Suhali, G., Chen, S., Roy, K. A digital micro-mirror device-based system for the microfabrication of complex, spatially patterned tissue engineering scaffolds. *J. Biomed. Mater. Res.* **77A**, 396-405 (2006).

13. Tsang, V.L. *et al*. Fabrication of 3D hepatic tissue by additive photopatterning of cellular hydrogels. *FASEB J.* **21**, 790-801 (2007).

14. Peppas, N.A., Bures, P., Leobandung, W., Ichikawa, H. Hydrogels in pharmaceutical formulations. *Eur. J. Pharm. Biopharm.* **50**, 27-46 (2000).

15. Marshall, K.W. Intra-articular hyaluronan therapy. *Curr. Opin. Rheumatol.* **12**, 468-474 (2000).

16. Reijnen, M.M.P.J., Bleichrodt, R.P., van Goor, H. Pathophysiology of intra-abdominal adhesion and abscess formation, and the effect of hyaluronan. *Brit. J. Surg.* **90**, 533-541 (2003).

17. Monheit, G.D. & Coleman, K.M. Hyaluronic acid fillers. *Dermatol. Ther*. **19**, 141-150 (2006).

18. Chung, C. *et al*. Effects of auricular chondrocyte expansion on neocartilage formation in photocrosslinked hyaluronic acid networks. *Tissue Eng.* **12,** 2665-2673 (2006).

19. Park, S.N., Kim, J.K., Suh, H. Evaluation of antibiotic-loaded collagen-hyaluronic acid matrix as a skin substitute. *Biomaterials* **25**, 3689-3698 (2004).

20. Jia, X.Q. *et al*. Synthesis and characterization of in situ cross-linkable hyaluronic acid-based hydrogels with potential application for vocal fold regeneration. *Macromolecules* **37**, 3239-3248 (2004).

21. Hemmrich, K. *et al*. Implantation of preadipocyte-loaded hyaluronic acid-based scaffolds into nude mice to evaluate potential for soft tissue engineering. *Biomaterials* **26**, 7025-7037 (2005).

22. Uludag, H., de Vos, P., Trasco, P.A. Technology of mammalian cell encapsulation. *Adv. Drug Deliver. Rev*. **42**, 29-64 (2000).

23. George, M. & Abraham, T.E. Polyionic hydrocolloids for the intestinal delivery of protein drugs: alginate and chitosan – a review. *J. Control. Release* **114**, 1-14 (2006).

24. Augst, A.D., Kong, H.J., Mooney, D.J. Alginate hydrogels as biomaterials. *Macromol. Biosci.* **6**, 623-633 (2006).

25. Leach, J.B., Bivens, K.A., Patrick, C.W., Schmidt, C.E. Photocrosslinked hyaluronic acid hydrogels: natural, biodegradable tissue engineering scaffolds. *Biotechnol. Bioeng.* **82**, 578-589 (2003).

26. Oaki, Y. & Imai, H. Experimental demonstration for the morphological evolution of crystals grown in gel media. *Cryst. Growth Des.* **3,** 711-716 (2003).

27. Ulcinas, A., Butler, M.F., Heppenstall-Butler, M., Singleton, S., Miles, M.J. Direct observation of spherulitic growth stages of $CaCO_3$ in a poly(acrylic acid)-chitosan system: In situ SPM study. *J. Cryst. Growth* **307,** 378-85 (2007).

28. Xu, A., Ma, Y., Colfen, H. Biomimetic mineralization. *J. Mater. Chem.* **17**, 415-449 (2007).

29. Tawhai, M.H., Hunter, P., Tschirren, J., Reinhardt, J., McLennan, G., Hoffman, E.A. CT-based geometry analysis and finite element models of the human and ovine bronchial tree. *J. Appl. Physiol.,* **2004**, 97, 2310-2321.

30. Nordsletten, D.A., Blackett, S., Bentley, M.D., Ritman, E.L., Smith, N.P. Structural morphology of renal vasculature. *Am. J. Physiol. Heart Circ. Physiol.,* **2006**, 291, H296-H309.

31. Murphy, W.L., Dennis, R.G., Kileny, J.L., Mooney, D.J. Salt fusion: an approach to improve pore interconnectivity within tissue engineering scaffolds. *Tissue Eng.,* **2002**, 8, 43-52.

32. Zhang, J., Wu, L., Jing, D., Ding, J. A comparative study of porous scaffolds with cubic and spherical macropores. *Polymer,* **2005**, 46, 4979-4985.

33. Tsang, V.L., Bhatia, S.N. Three-dimensional tissue fabrication. *Adv. Drug. Deliver. Rev*., **2004**, 56, 1635-1647.

34. Mapili, G., Lu, Y., Chen, S., Roy, K. Laser-layered microfabrication of spatially patterned functionalized tissue-engineering scaffolds. *J. Biomed. Mater. Res*., **2005**, 75B, 414-424.

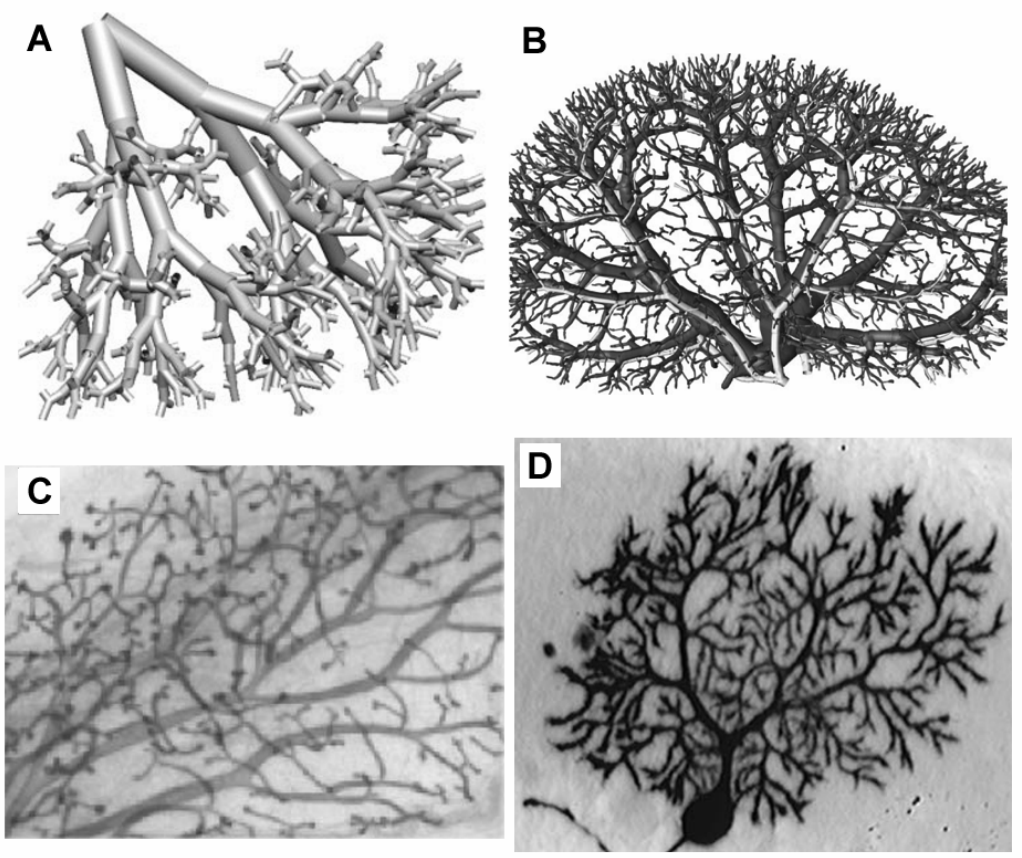

Figure 5.1 Branching morphologies are found throughout native tissues. **(A)** Computer generated model of branching bronchioles in the human lung [29]. **(B)** Reconstructed image generated from computed tomography of rat renal vasculature [30]. **(C)** Ductal system of mouse mammary gland [2]. **(D)** Rat cerebellar Purkinje neuron with dendritic tree [4].

Table I. Techniques for producing porous tissue engineered constructs.

Technique	Description	Compatible Materials	Pore Morphology	3D / 2D	References
Gas Foaming	Monomer is mixed with sodium bicarbonate salts in organic solvent. Acidification produces foaming of the effervescent salts and pores are produced by released CO_2 gas.	Synthetics (acrylates, acrylamides, methacrylates)	Random (Figure 5.2A)	3D	[8]
Porogen Leeching (Water Soluble)	Salts are dispersed in organic solvent along with organic soluble synthetic monomer. The monomer is polymerized around the salts which are subsequently rinsed out to leave behind pores.	Organic Soluble Polymers	Random (Figure 5.2B)	3D	[6, 31, 32]
Porogen Leeching (Organic soluble)	Polymer microspheres are suspended in water with polymer. After polymerization the porogens are washed out by methylene chloride, hexane or other suitable organic solvent.	Water Soluble Polymers	Inverse Opal (Figure 5.2C)	3D	[7]
Solid Free Form Fabrication	A collection of techniques that fabricates three-dimensional structures layer by layer using CAD design and automated machinery.	Synthetics (acrylates, acrylamides, methacrylates)	Arbitrary (Figure 5.2D)	3D	[12, 33, 34]
Soft Lithography	Arbitrary 2D patterns are etched into silicon. The patterns are then transferred by soft replica molding to disposable PDMS mold and then transferred to other biomaterials.	Synthetic and Natural Polymers	Arbitrary (Figure 5.2E)	2D	[9]

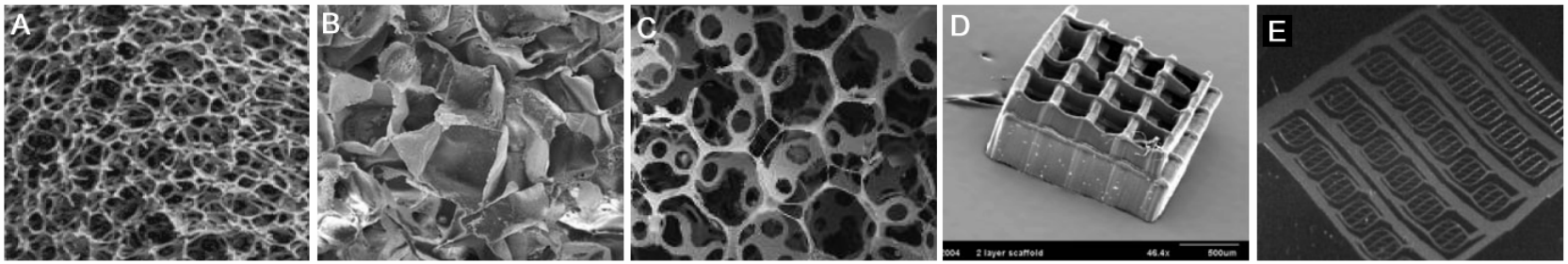

Figure 5.2 Representative images of porous structures created by the techniques listed in Table I. (**A**) Gas foamed poly(acrylamide-co-acrylic acid) [8] (**B**) PLGA leeched with cubic sodium chloride crystals [32]. (**C**) PLGA leeched with paraffin microspheres [7]. (**D**) Two layer scaffold constructed from poly(ethylene glycol) dimethacrylate using sterolithography [34]. (**E**) A PLGA microfluidic network created by soft lithography [9].

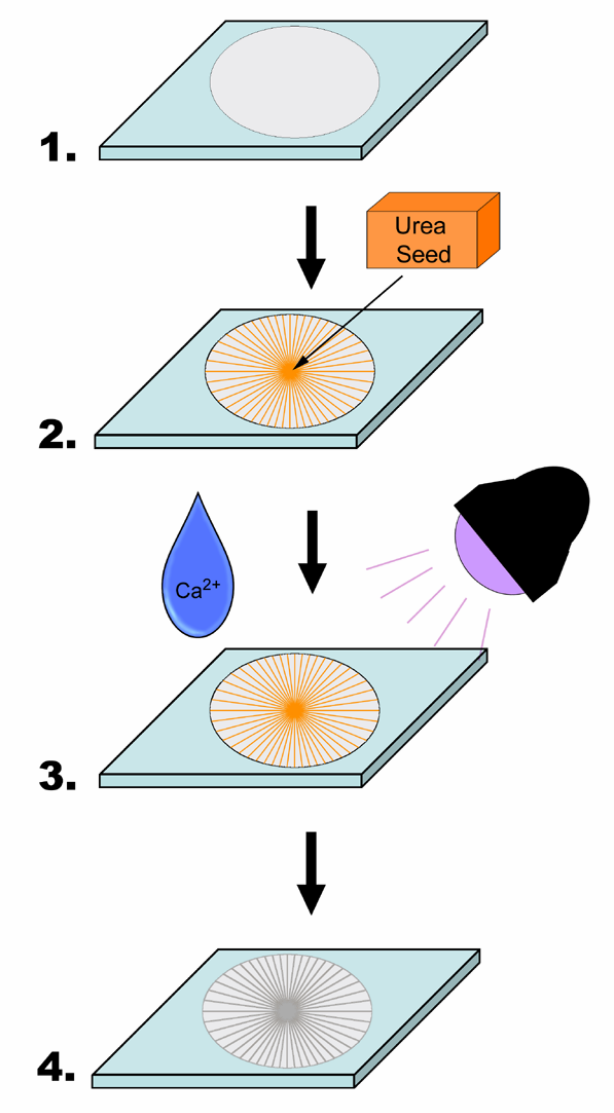

Figure 5.3 Schematic of the crystal-templating technique. **1.** A droplet of biopolymer-urea solution was deposited on a glass slide and the solvent was evaporated to achieve supersaturation concentrations of urea. **2.** Application of a seed crystal to the center of the film nucleated urea crystallization. **3.** The biopolymer was crosslinked by either UV or calcium. **4.** A rinse in water removed the urea crystals leaving behind a macroporous hydrogel templated with the pattern of the urea crystals.

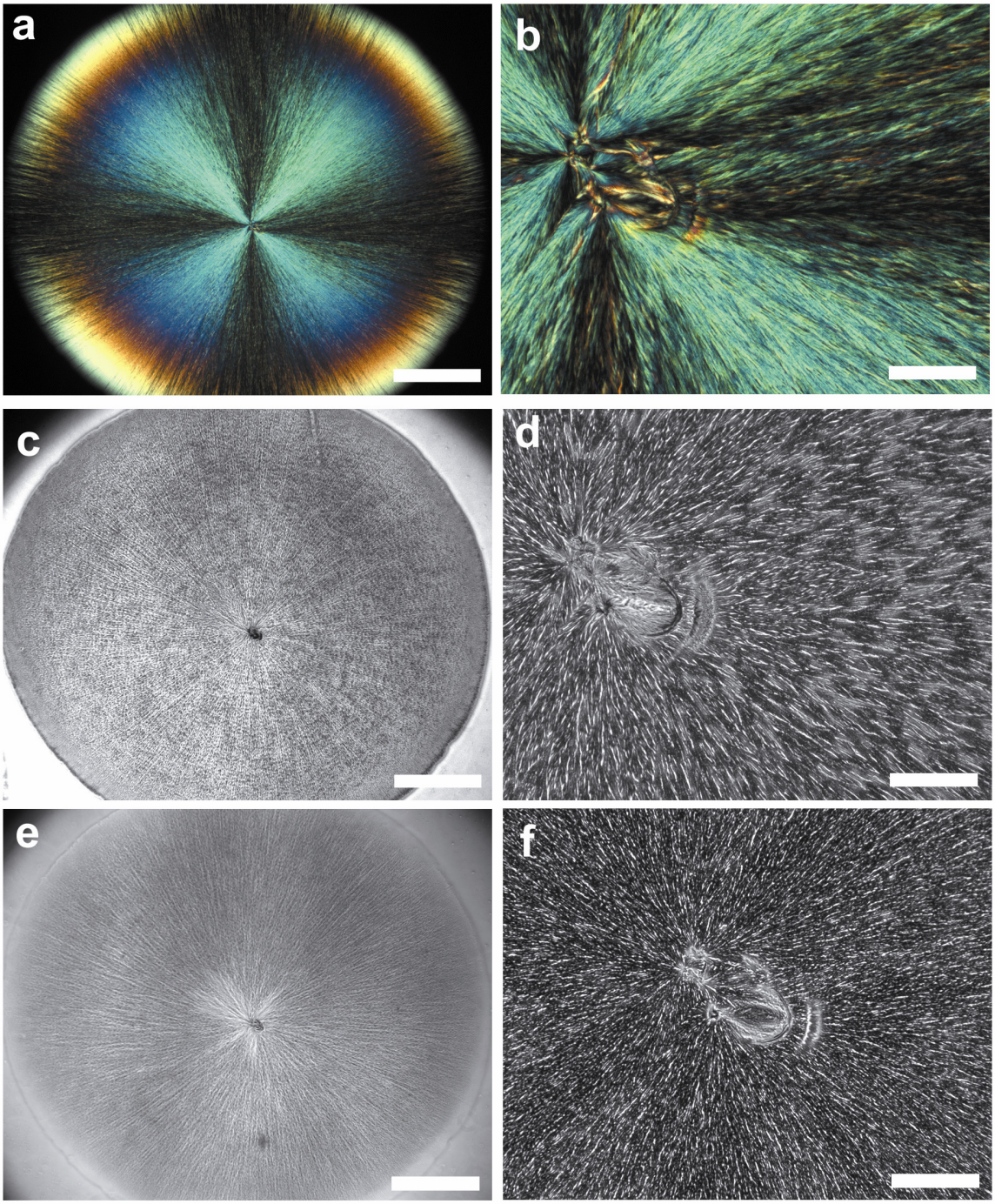

Figure 5.4 Polarized light (a, b) and phase contrast (c-f) microscopy images of a urea crystal templated hyaluronic acid hydrogel. Images depict the templated hydrogel before crystal removal (a-d) and after crystal removal (e, f). These images demonstrate that the hydrogel retained the crystal template pattern. Scale bars are 1000 μm (a, c, e) and 100 μm (b, d, f).

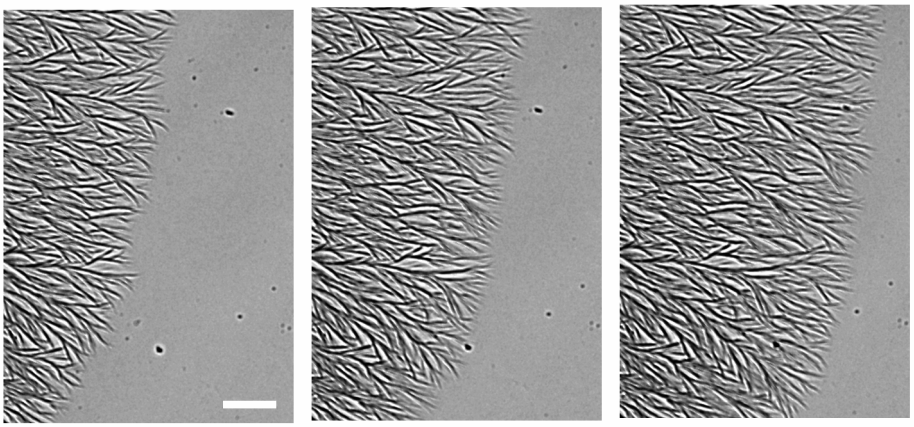

Figure 5.5 Time lapse series of the growing urea crystal front in hyaluronic acid captured with brightfield video microscopy. These images show that crystal growth was continuous and dendritic; therefore, pores created by the crystal templating technique are also continuous and dendritic. Images are five seconds apart. Scale bar is 20 μm.

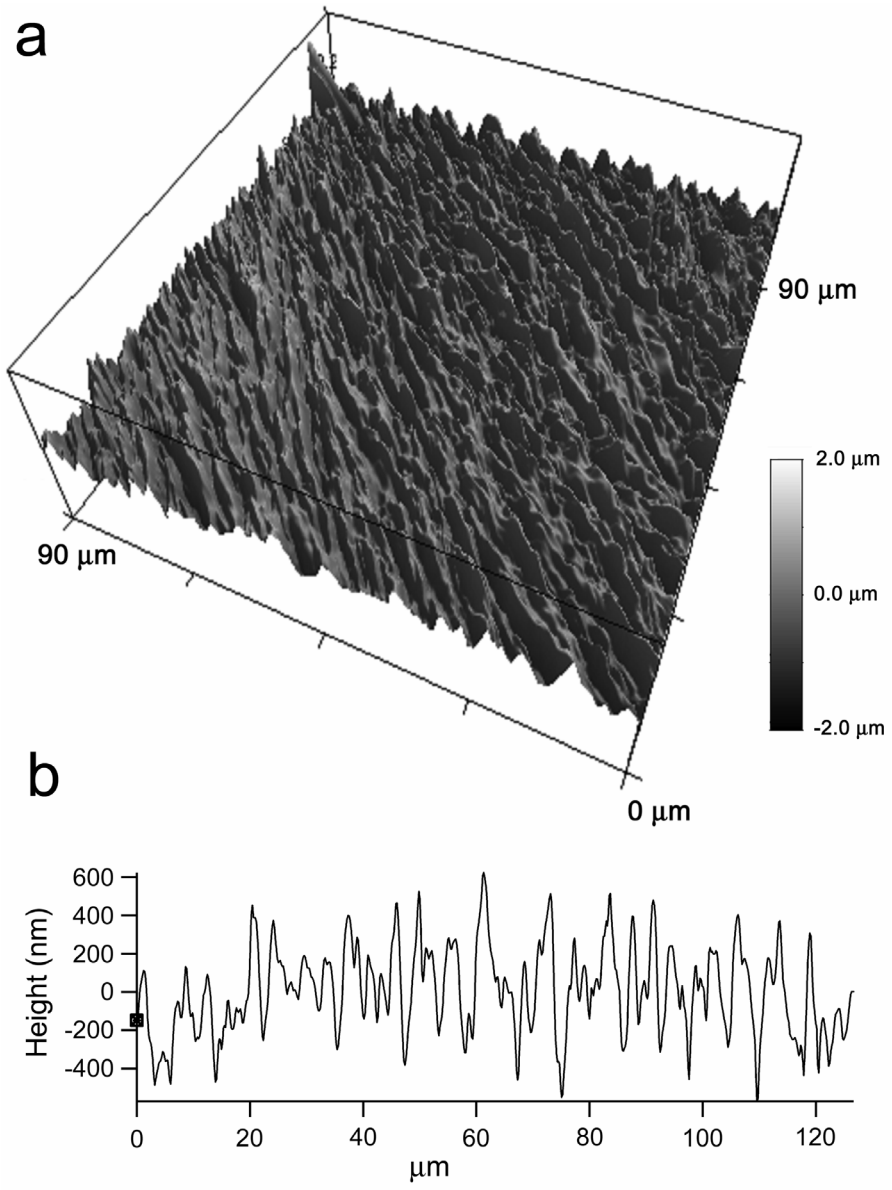

Figure 5.6 The surface topography of a templated hyaluronic acid hydrogel after crystal removal obtained by atomic force microscopy. (**a**) The grooves between the ridges had been carved by urea crystal growth. The ridges correspond to the hyaluronic acid which had been concentrated into the interstitial spaces between urea crystal. (**b**) A profile perpendicular to the direction of the ridges.

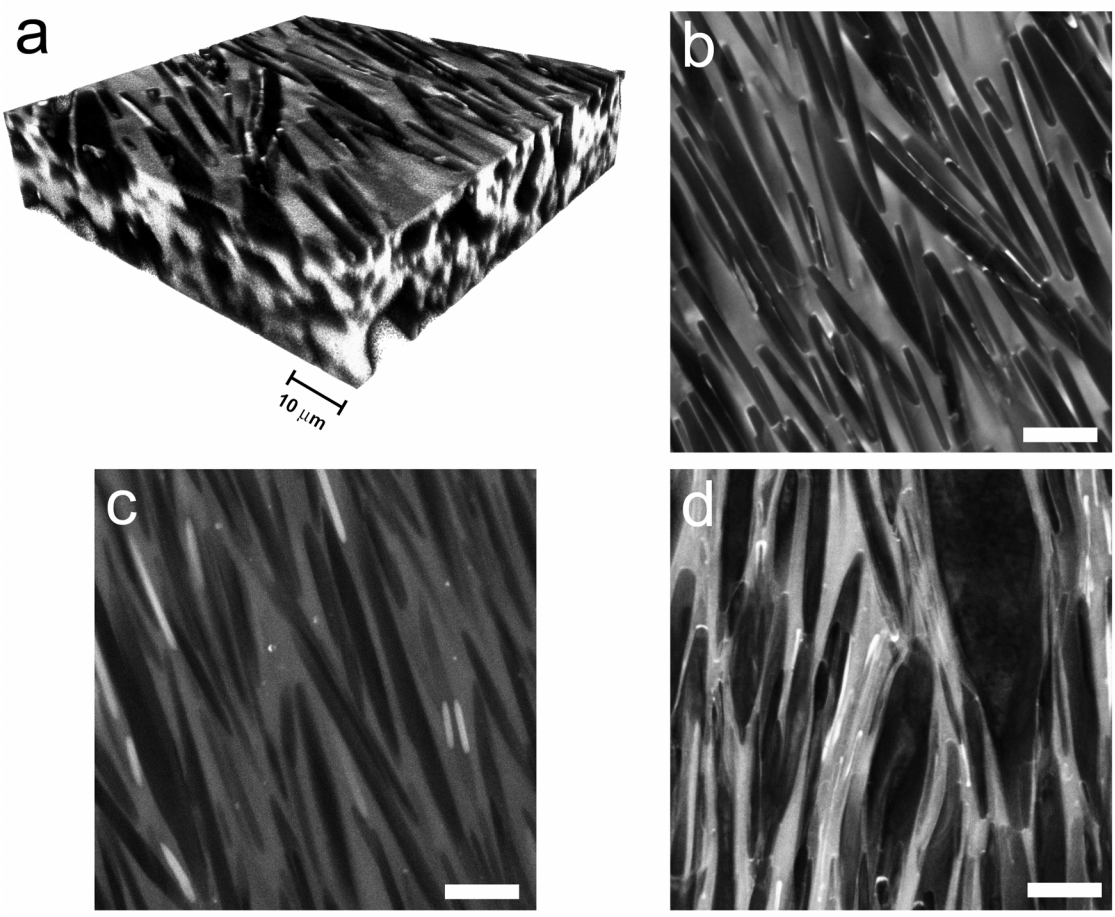

Figure 5.7 Confocal fluorescent microscopy of TRITC-labeled urea-templated GMHA hydrogels. Images demonstrate that the urea crystals grew throughout the volume of the hydrogel and that a macro-porous network was preserved after removal of the crystal template. (**a**) Volume reconstruction of a composite urea crystal-GMHA hydrogel. (**b**) Single z-slice of a composite urea crystal-GMHA hydrogel. (**c**) Single z-slice of a urea templated GMHA hydrogel swollen in water after crystal removal. (**d**) Single z-slice of a dried urea-templated GMHA hydrogel after crystal removal. All scale bars are 10 μm.

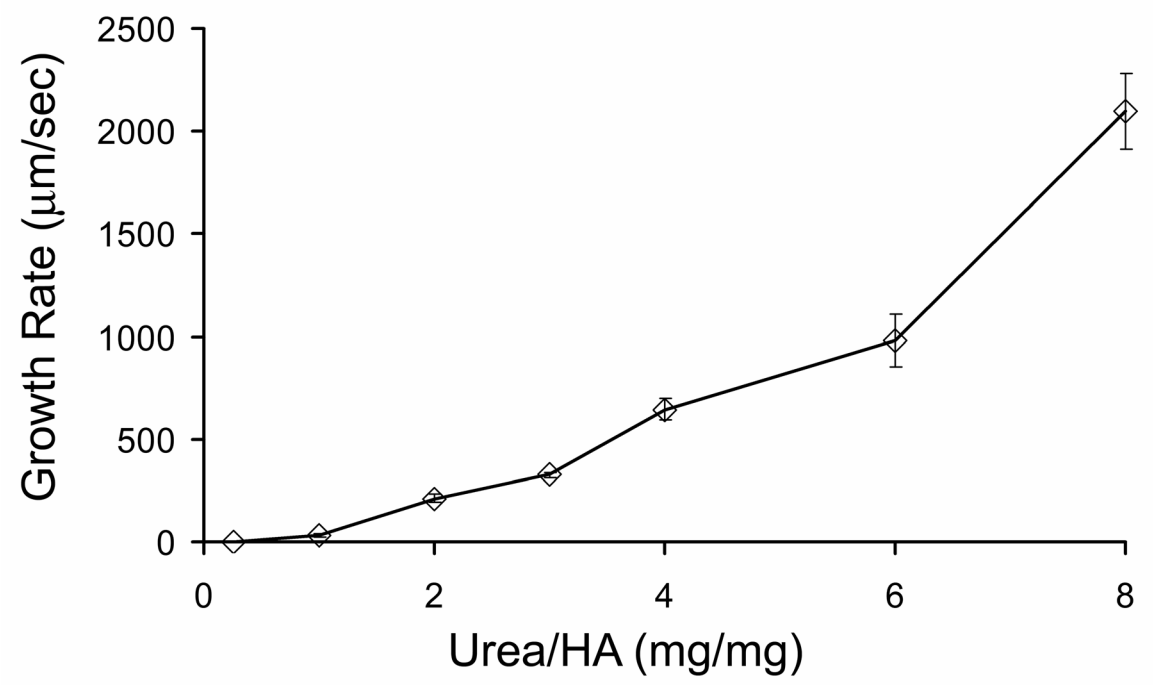

Figure 5.8 Crystal growth rate measured by video microscopy as a function of the ratio of urea/HA concentration (i.e., super-saturation). The concentration of HA was fixed at 10 mg/mL and the concentration of urea was varied from 2.5 mg/mL to 80 mg/mL. The urea crystal growth rate increased as the ratio of urea/HA increased (i.e., increasing the super-saturation of urea increased the crystal growth rate). Ratios greater than 8 produced growth rates too fast to accurately measure by video microscopy.

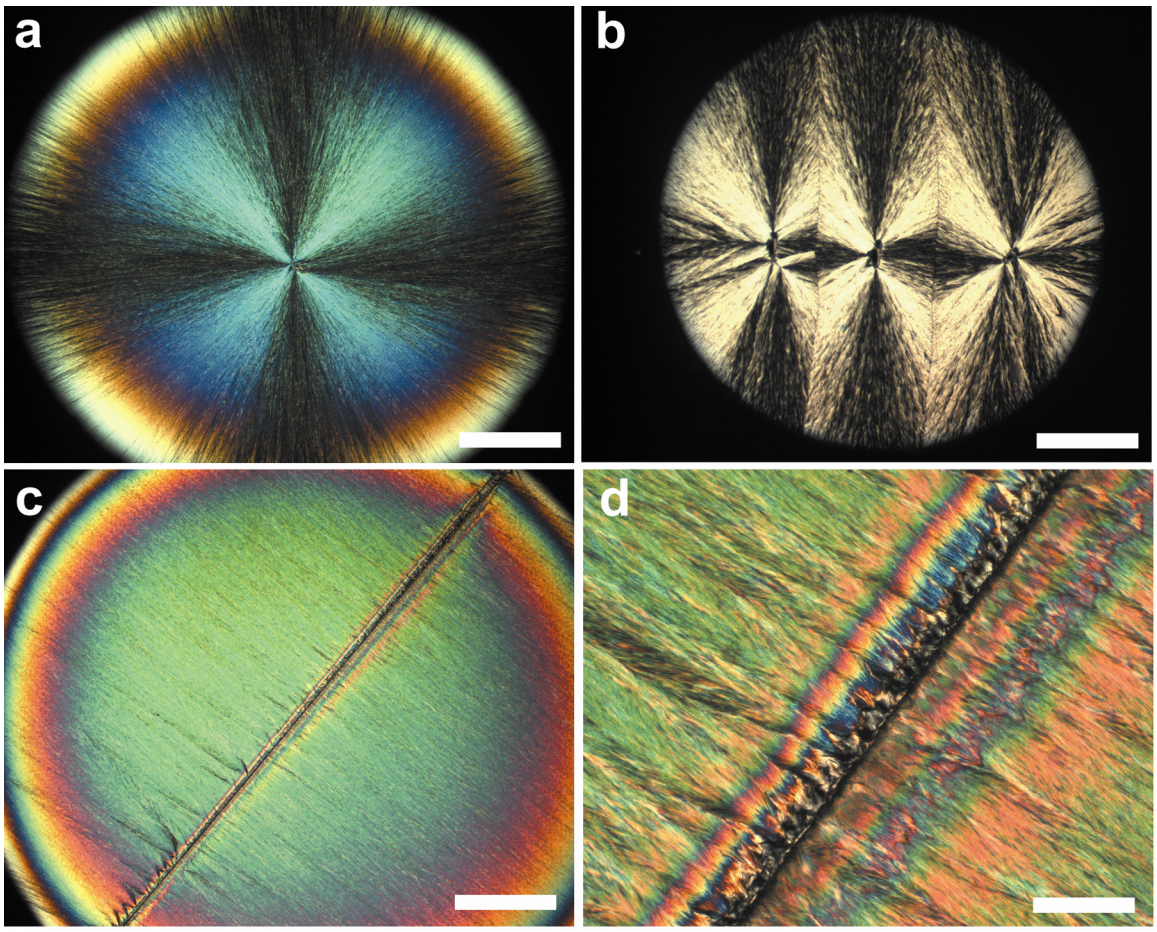

Figure 5.9 The urea seed crystal technique can be used to control the morphology of crystals and pores within HA hydrogels. (**a**) One nucleation point in the center of a hydrogel. (**b**) Three separate and simultaneous nucleation points produced a hydrogel with three radial patterns. (**c**) A line of nucleation points created using the edge of a razor blade produced a hydrogel with linear alignment of crystals. (**d**) A magnified image of c. Scale bars are 1000 μm (a-c) and 100 μm (d).

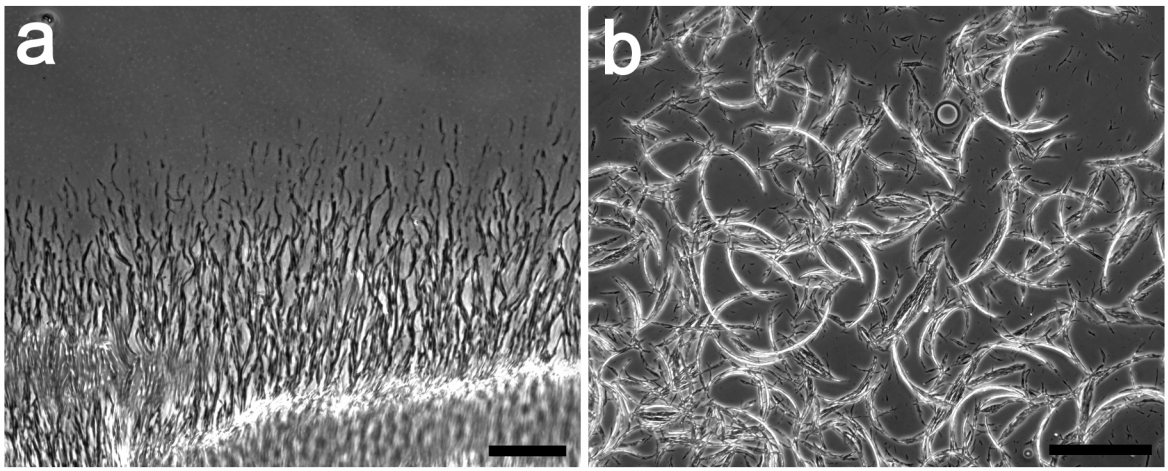

Figure 5.10 Enzymatic degradation of urea-templated GMHA films. Hydrogels were degraded at 37°C in a solution of PBS containing 500 U/mL hyaluronidase. (**a**) After 48 hours of degradation the edges of the films had begun to fray. Scale bar is 50 μm. (**b**) After 96 hours of degradation the hydrogels were very fragile and were reduced to individual fibers by mild mechanical shearing. Scale bar is 200 μm.

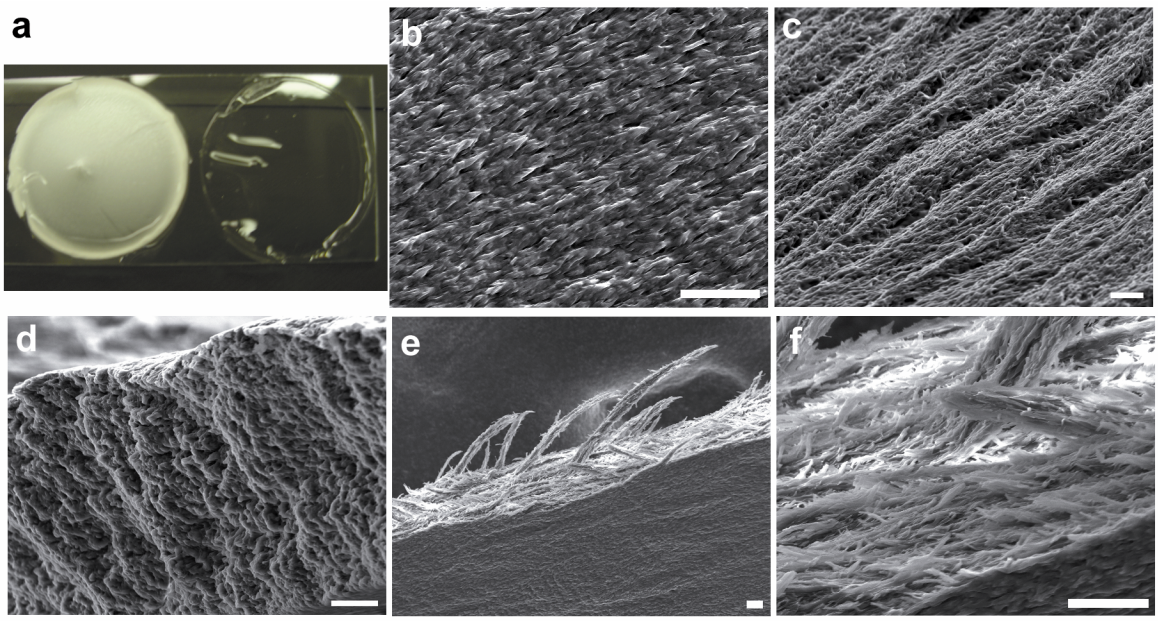

Figure 5.11 The process of urea-templating was scaled up from droplets to thick films. Scale bars are 10 μm. (**a**) Photograph of scaled-up freestanding hydrogels of urea-templated (left) and plain (right) hyaluronic acid. (**b-e**) SEM images of crystal templated hyaluronic acid after crosslinking and rinsing. (**b**) Top down view. HA hydrogel was sculpted into a "fibrous" morphology. (**c**) This portion of the film was curled back to expose the crevices in the hydrogel that had been created by urea crystals. (**d**) Cross-section of the hydrogel perpendicular to the pore orientation depicting that the pores are present throughout the thickness of the hydrogel. (**e**) Parallel cross-section depicting the fibrillar morphology. (**f**) Magnified view of e.

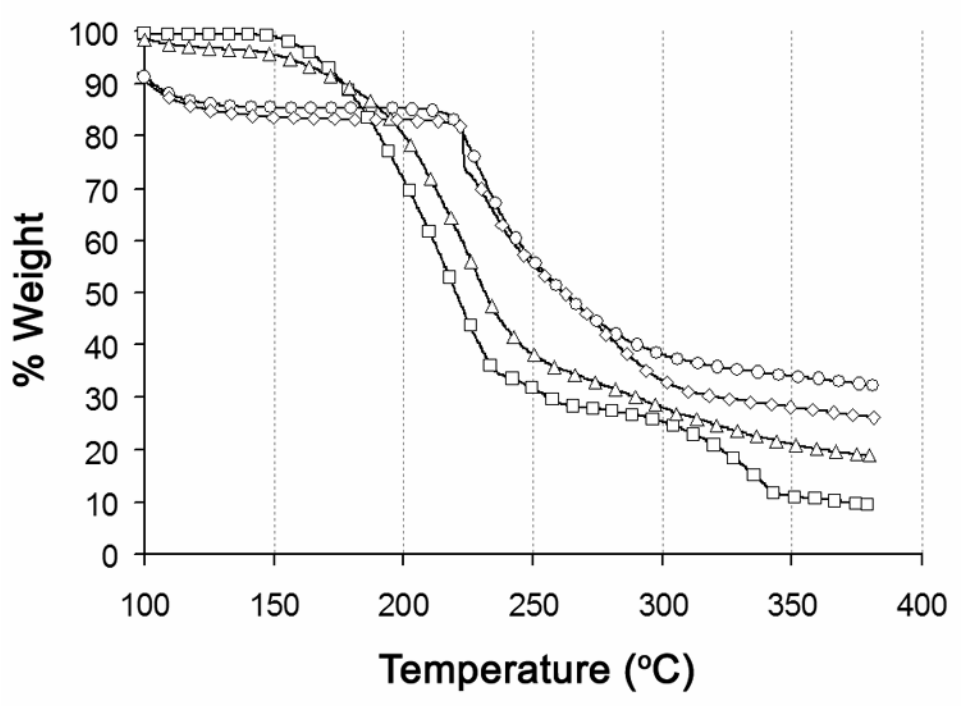

Figure 5.12 Thermal degradation of hydrogel samples obtained by thermal gravimetric analysis. The percent weight loss is plotted as a function of temperature. Scan rate was 10°C/min. Four samples were analyzed: urea (□); uncrosslinked, non-templated GMHA hydrogel film (○); uncrosslinked, urea-templated GMHA hydrogel film containing 80% w/w urea before rinsing (∆); and crosslinked, urea-templated GMHA hydrogel film after rinsing (◊). Unrinsed, templated GMHA films had degradation profiles similar to urea; however, after rinsing they had degradation profiles similar to non-templated GMHA. These data indicate that extensive water rinsing was sufficient to remove urea from scaled-up, thick, urea-templated GMHA films.

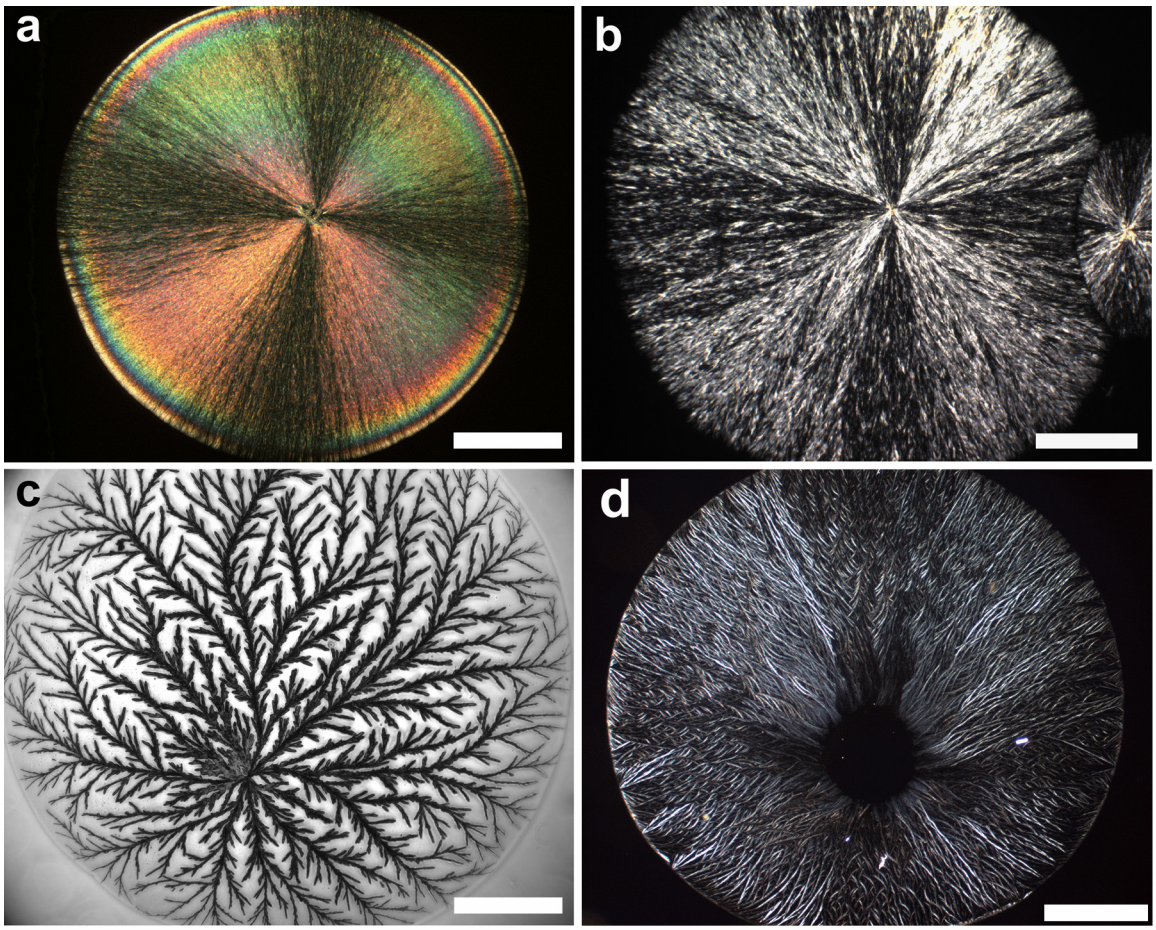

Figure 5.13 Polarized light (a, b, d) and phase contrast (c) microscopy images of hydrogel-crystal composites. (**a**) Urea crystal and alginate. (**b**) Urea crystal and 4-arm-PEG acrylate. (**c**) Potassium phosphate crystal and hyaluronic acid. (**d**) βCD crystal and alginate. Scale bars are 1000 μm.

Chapter 6: Patterned Hydrogel Meshes for Living Cell Microarrays

Abstract

Living cell microarray technology is expected to enable a number of cell-based assays and diagnostic tools that would be highly synergistic with existing DNA and RNA microarrays. Current methods for creating living cell microarrays rely on clean room equipment and lithographic techniques, but this requirement hampers the adoption of living cell microarray technology by many research groups that lack microfabrication expertise. This chapter describes a novel method for obtaining cell microarrays that circumvents the need for clean room labs and lithography. Here we show that an array of hydrogel compartments on glass and TCPS can be readily obtained by patterning with an inexpensive, off-the-shelf, polymer mesh. These hydrogel compartments can produce living cell microarrays by isolating individual cells and cell clusters. We have obtained patterned hydrogels compartments using photocrosslinked hyaluronic acid, calcium-crosslinked alginic acid, and pH-induced gelation of chitosan. The advantages of this technique are that it can cover wide areas, is compatible with both glass and TCPS, requires no clean room equipment, and does not require any highly specialized technical or chemical synthetic skills. This patterning technique answers the need for a simple, inexpensive method for obtaining living cell microarrays that can be easily disseminated to non-specialist research groups.

6.1 Introduction

The ability to precisely pattern living cells within a standardized array would have applications in medical diagnostics, cell-based sensors, and would be highly complementary with existing technology for DNA and RNA microarrays.[1-3] A DNA microarray consists of a substrate patterned with islands of immobilized DNA oligomers. These arrays are fabricated using either contact printing with robotic pins or non-contact printing with inkjet printers.[4] Methods for patterning cells and interfacing them with DNA microarrays is desired to fully exploit microarray technology. Current methods completely cover the DNA array with a continuous layer of cells to create a "cellular microarray" in which the DNA is patterned in islands but the cells are not.[2] Although this method of cell blanketing is easy to perform it permits the cells to migrate among DNA islands and sample multiple DNA sequences. A true cell microarray would confine the cells to particular islands of DNA sequences.

To create true cell microarrays DNA printing equipment can be modified to dispense cells. For example, a DNA microarray printing robot has been adapted to print libraries of yeast mutant strains onto microscope slides.[5] This method uses steel printing tips to transfer cell suspension to a substrate to yield 200 μm diameter spots spaced 410 μm apart. A similar approach which also used a DNA contact printing robot employed a deformable substrate that "cratered" when impacted by the printing pins.[6] The result was an array of *Escherichia coli* deposited in craters of 125 μm in diameter and separated by 375 μm. The large spacing between bacterial colonies resulted in a low spot density and it is unclear whether these printing methods are compatible with

mammalian cells. This method could be improved if there were a way to sequester a high density of cell colonies within identical microenvironments.

The primary hurdle to obtaining living cell microarrays is the difficulty of fabricating a substrate that can control cell adhesion.[7] The pre-dominant strategies use lithographic methods to pattern non-adhesive substrates with arrayed islands of cell-adhesive ligands.[8] Cells that are seeded upon these substrates cluster within the islands to form the cellular array. The converse of this strategy is to pattern an adhesive substrate with a non-adhesive hydrophilic polymer such as hyaluronic acid or poly(ethylene glycol).[9] Cells seeded upon this type of substrate adhere to regions that are not covered with the polymer and thus form the cellular array. Both strategies are compatible with the techniques of soft lithography and photolithography; however, reliance on lithography hampers the spread of cell microarray technology to biological research groups that do not have micro-fabrication expertise and access to specialized clean room labs. Therefore, we have developed a simple cell patterning method that can be easily disseminated to other labs.

A cell microarray should consist of patterned cells within a grid in which each cell cluster can be assigned a unique set of coordinates. Each compartment of the array should be about 50-100 μm in length to accommodate several cells. Smaller compartments can be used to isolate individual cells. The distance separating compartments should be minimized to increase the density of compartments within the array but without compromising the isolation of each compartment.

We recognized that the geometry of a woven polymer mesh is almost exactly the geometry that is required for cell microarrays. In particular, Nylon mesh screening is abundantly available, off-the-shelf, inexpensive, and can be produced with mesh openings as small as a few microns. The Nylon mesh used in this method is a plain weave in which the warp and weft threads pass over and under each other (**Figure 6.1**). The mesh openings ranged from 90 μm to 36 μm and the thread diameters ranged from 33 to 39 μm according to the manufacturer (**Table I**). There is no need for lithographic methods to create a grid pattern from scratch because the Nylon mesh is already in the grid pattern. Thus, one only needs to transfer the grid pattern from the Nylon mesh to a non-cell adhesive hydrogel on the surface of a cell-adhesive substrate to obtain an array of hydrogel compartments. A cell microarray can then be readily obtained by seeding cells within the compartments. Our objectives for this work were (i) develop a method for creating an array of hydrogel compartments from Nylon mesh and (ii) use the hydrogel compartments to create living cell microarrays.

6.2 Results

6.2.1 Synthesis of Hydrogel Meshes. The steps for obtaining cell microarrays from hydrogel meshes are schematically illustrated in **Figure 6.2**. First, a piece of Nylon mesh is coated with an aqueous solution of biopolymer and deposited on top of the substrate. The solvent is evaporated through the mesh openings. During evaporation the biopolymer solution recedes from the mesh openings and becomes concentrated between the substrate and the Nylon mesh. The process of drying can be easily followed under

the microscope (**Figure 6.3**). After the solution has evaporated the Nylon mesh is carefully removed and a viscous hydrogel solution in a mesh pattern is left remaining on the substrate. The hydrogel solution must then be crosslinked to stabilize the mesh against dissolution in water. Crosslinking can be accomplished by photocrosslinking of GMHA, ion-gelation of alginic acid, and pH-induced gelation of chitosan.

The size of the hydrogel compartment determines how many cells can fit within each element of the array and is determined by the Nylon mesh size; however, the hydrogel compartments are not exactly identical to the Nylon mesh openings. The width of each hydrogel compartment is about equal to the sum of the mesh opening and the thread diameter because the hydrogel walls formed during evaporation are much thinner than the Nylon threads (Figure 6.3b). For example, a Nylon mesh with 64 μm openings and 33 μm diameter threads yields hydrogel compartments with widths of 92 μm (Figure 6.3c). The Nylon mesh can be cut to any size and can cover very large areas. To illustrate this we patterned a 150 mm tissue culture dish with 70 μm hydrogel compartments. The result was a dish containing roughly 1.8 million hydrogel compartments (**Figure 6.4**).

The hydrogel mesh has a surprising morphology that is the result of the biopolymer solution closely adhering to the Nylon threads. The over-and-under weave of the threads results in “boat” shaped hydrogel curvature (**Figure 6.5**). A rough estimate based on the SEM images suggests that the hydrogel walls reach up to several microns high. This is a formidable barrier to cell migration among neighboring compartments. The non-adhesivity of the biopolymer hydrogel further impedes cell migration.

Complementary data was obtained by imaging with confocal fluorescence microscopy of chitosan mesh labeled with TRITC (**Figure 6.6**). Fluorescent labeling was easily accomplished by mixing chitosan with dextran-TRITC which became entangled in the hydrogel. The confocal images demonstrate two things: first, the height of the hydrogel compartments is roughly 3-4 μm; and second, the hydrogel meshes can be easily functionalized by adding macromolecules that become entangled in the gelled meshes.

Hydrogel patterning was found to be compatible with both glass and tissue culture polystyrene, the two most common substrates for cell studies. The meshes are not covalently attached to these substrates; therefore, they risk coming loose if sheared in solution. Qualitatively, we found that an increasing strength of adherence to the substrate was exhibited by hyaluronic acid, alginic acid, and chitosan in that order. GMHA meshes were particularly susceptible to floating off of the surface and adhered more strongly to TCPS than to glass. Alginic acid only sometimes floated free and chitosan adhered so strongly that even harsh scraping could not pull the mesh from the substrate. Unlike GMHA and alginic acid, chitosan is positively charged and is cast from an acidic solution which may facilitate adsorption to the substrate. An important factor to adherence is hydrogel swelling. The more the hydrogel swells in solution the more likely it is to float away from the substrate. GMHA hydrogels tend to swell more than either alginic acid or chitosan and probably explains the different adherence of these hydrogels.

6.2.2 Living cell microarrays. To determine whether the hydrogel meshes are effective at creating cellular microarrays two types of cells were seeded onto the hydrogel patterned substrates. Primary human dermal fibroblasts are a large cell type

that is known for robustly adhering to many substrates. Primary rat Schwann cells, on the other hand, are a smaller cell type that is less adherent than fibroblasts.

Clusters of fibroblasts were successfully cultured in a microarray within a hydrogel mesh of 90 μm wide compartments (**Figure 6.7**). Several fibroblasts were adhered within each compartments and calcein staining verified cell viability. Some fibroblasts were observed to have been trapped within the "boat" shaped curvature of the hydrogel mesh. When a small 70 μm wide hydrogel mesh was used only one fibroblast adhered per compartment. A separate microarray of fibroblasts were stained with the nuclear stain, DAPI, and the actin stain, phalloidin (**Figure 6.8**). The DAPI stain indicates that between one to three cells adhered per hydrogel compartment. The phalloidin stain indicates that the cells spread to fill the available area within each compartment.

A microarray of a second cell type, Schwann cells, was obtained within 70 μm hydrogel mesh. Unlike the fibroblasts, several Schwann cells fit within each compartment due to their smaller size. After five days of culture the GMHA hydrogel mesh was removed by rocking the cell culture media gently to shear the mesh and cause it to break free of the substrate. The cells were then stained with calcein and imaged (**Figure 6.9**). With the hydrogel mesh removed these cells would be able to proliferate and spread as normal.

6.3 Discussion

Nylon meshes are coated with biopolymer solution simply by dipping; therefore, the amount of biopolymer solution that is transferred to the substrate is inexact. If too little solution is transferred then the walls of the hydrogel compartments will have gaps. If too much solution is transferred then the evaporated solution will become so viscous that a thin layer of hydrogel becomes deposited across the surface of each compartment. This is particularly problematic because the thin hydrogel layer will prevent cells from adhering to the underlying glass or TCPS. Therefore, some trial and error experience is required by users to judge qualitatively how much solution should be placed onto the substrate for drying. Future work should revise the hydrogel patterning protocol to eliminate the need for trial and error by unexperienced users.

The technique described here is similar to micro-contact stamping in which a solution is transferred from a stamp to a substrate; however, transfer of ink occurs primarily by adsorption to substrate which results in a thin nanometer scale layer of ink patterned on the substrate's surface. Our method uses evaporation through the mesh openings to obtain a viscous solution of hydrogel between the Nylon and the substrate. Thus, we obtain a micron scale layer of hydrogel on the substrate that is easily observed even by the naked eye. This hydrogel wall is a highly effective barrier to cell migration.

The cell studies indicate the feasibility of using the hydrogel meshes to obtain cellular microarrays. There are many attractive features of this technology in addition to the ease, inexpensiveness, and simplicity of the technique. Other patterning techniques that do not have physical barriers separating the adhesive islands must separate each

island by a wide distance to prevent cells from bridging multiple islands. In our technique a hydrogel wall that is thinner than the size of a cell isolates each compartment; thus, the density of compartments that can be fit into a given area is very high. Additionally, the porous hydrogel walls provide space to entrap biomolecules that can be delivered to the cells within the compartments, and the hydrogel walls can contain sensing elements that monitor and capture cytokines secreted by the arrayed cells. Furthermore, hyaluronic acid and alginic acid possess carboxyls and hydroxyls and chitosan possesses amines that can be used to attach further chemical functionalities after patterning.

Another attractive feature of the patterning is that it can be reversible. GMHA hydrogel mesh can be removed by agitation of the solution and alginate mesh can be removed by a brief treatment with the calcium chelator, EDTA. We believe that this can be a useful feature to obtain patterned co-cultures as others have demonstrated with related lithographic based patterning methods.[10] In another respect, however, this feature can be regarded as a limitation because the hydrogel meshes are not covalently attached to the substrate. The hydrogel meshes must be handled carefully to prevent them from accidentally separating from the substrate which would permit cells to grow outside the confines of the array. Chitosan hydrogels adhere very strongly to glass and never separate from the substrate even under extreme agitation but chitosan microarrays are not reversible.

In conclusion, hydrogel meshes are an effective means for obtaining cellular microarrays that is superior to other techniques with respect to cost, equipment

requirements and simplicity. With this method many research groups can create cellular microarrays without needing to learn lithographic techniques and finding access to clean room labs. The cellular microarrays obtained by this method are applicable to a wide variety of cell-based sensors and medical diagnostics that are of general interest to the biomedical community.

6.4 Materials and Methods

6.4.1 Materials. Sodium hyaluronate from *Streptococcus equi* of molecular weight $1.6x10^6$ Da as indicated by the supplier and low viscosity alginic acid from brown algae were obtained from Sigma-Aldrich (St. Louis, MO). Photoinitiator, Irgacure 2959, was obtained from Ciba Specialty Chemicals (Basel, Switzerland). Nylon 6/6 screening mesh was obtained from Small Parts Inc. (Miramar, FL). Photopolymerizations were initiated by a longwave UV lamp filtered around 365 nm and with an intensity of 22 mW/cm^2 (Blak-Ray B-100A, UVP, Upland, CA). Photocrosslinkable hyaluronic acid was prepared by our standard procedure of derivatization of HA with glycidyl methacrylate to yield GMHA (modifications to this protocol discussed in Chapter 2).[11]

6.4.2 Synthesis of Hydrogel Meshes. 1% w/v aqueous biopolymer solutions were prepared. Cut sections of nylon mesh were dipped into the solutions and then removed and excess liquid was wicked away. The solution-coated mesh was then placed onto a either a glass or TCPS substrate and either air-dried or dessicated as necessary. The nylon was removed with tweezers and left behind a hydrogel mesh adherent to the

substrate. GMHA hydrogel meshes were crosslinked with 1 minute of UV exposure. Alginate hydrogel meshes were crosslinked by soaking in a solution of 20% w/v calcium chloride for 3 minutes. Chitosan was dissolved at a concentration of 1% in 1 M acetic acid and the meshes were gelled by soaking in 10 M sodium hydroxide for 3 minutes.

6.4.3 Scanning Electron Microscopy. Samples were dessicated and sputter coated with 15 nm of platinum/palladium. Images were brightness and contrast enhanced.

6.4.4 Seeding of Cell Microarrays. Normal human dermal fibroblasts were obtained from Lonza (Basel, Switzerland) and cultured in DMEM supplemented with 10% fetal bovine serum. Fibroblasts were cultured in standard TCPS flasks, 37°C, 5% CO_2, passaged with 0.025% TRED, and not used past passage 10.

Primary rat Schwann cells were obtained from ScienCell (San Diego, CA) and cultured in DMEM with 10% fetal bovine serum. Schwann cells were cultured in poly-L-lysine coated TCPS dishes at 37°C, 5% CO_2, passaged with 0.25% TRED, and not used past passage 10.

6.4.5 Fixing and staining of cell microarrays. Fibroblast microarrays were fixed after 12 hours of culture. Cells were treated with 4% paraformaldehyde in PBS and 4% sucrose for 20 minutes at 37°C. Cells were permeabilized for 5 minutes with 0.1% Triton X-100 for 5 minutes and blocked for 30 minutes at room temperature with 3% fetal bovine serum in PBS. Cells were stained for actin by treatment with Alexa-Fluor 488 phalloidin (1:400) for 60 minutes. Cell nuclei were stained by DAPI (1:1000) for five minutes at room temperature. Fixed cells were then coverslipped and imaged by confocal fluorescence microscopy.

6.5 References

1. Kim, H., Cohen, R.E., Hammond, P.T., Irvine, D.J. Live lymphocyte arrays for biosensing. *Adv. Funct. Mater.,* **16**, 1313-1323 (2006).
2. Ziauddin, J., Sabatini, D.M. Microarrays of cells expressing defined cDNAs. *Nature*, **411**, 107-110 (2001).
3. Wheeler, D.B., Carpenter, A.E., Sabatini, D.M. Cell microarrays and RNA interference chip away at gene function. *Nature Genetics*, **37**, S25-S30 (2005).
4. Dufva, M. Fabrication of high quality microarrays *Biomol. Eng.,* **22**, 173-184 (2005).
5. Narayanaswamy, R., Niu, W., Scouras, A.D., Hart, G.T., Davies, J., Ellington, A.D., Iyer, V.R., Marcotte, E.M. Systematic profiling of cellular phenotypes with spotted cell microarrays reveals mating-pheromone response genes. *Genome Biol.,* **7**:R6 (2006).
6. Xu, C.W. High-density cell microarrays for parallel functional determinations. *Genome Res.,* **12**, 482-486 (2002).
7. Falconnet, D., Csucs, G., Grandin, H.M., Textor, M. Surface engineering approaches to micropattern surfaces for cell-based assays. *Biomaterials*, **27**, 3044-3063 (2006).
8. Lee, J.Y., Shah, S.S., Zimmer, C.C., Liu, G., Revzin, A. Use of photolithography to encode cell adhesive domains into protein microarrays. *Langmuir* **24**, 2232-2239 (2008).

9. Revzin, A., Tompkins, R.G., Toner, M. Surface engineering with poly(ethylene glycol) photolithography to create high-density cell arrays on glass. *Langmuir* **19**, 9855-9862 (2003).

10. Fukuda, J., Khademhosseini, A., Yeh, J., Eng, G., Cheng, J.J., Farokhzad, O.C., Langer, R. Micropatterned cell co-cultures using layer-by-layer deposition of extracellular matrix components. *Biomaterials*, **27**, 1479-1486 (2006).

11. Leach, J.B., Bivens, K.A., Patrick, C.W., Schmidt, C.E. Photocrosslinked hyaluronic acid hydrogels: natural, biodegradable tissue engineering scaffolds. *Biotechnol. Bioeng.,* **82**, 578-589 (2003).

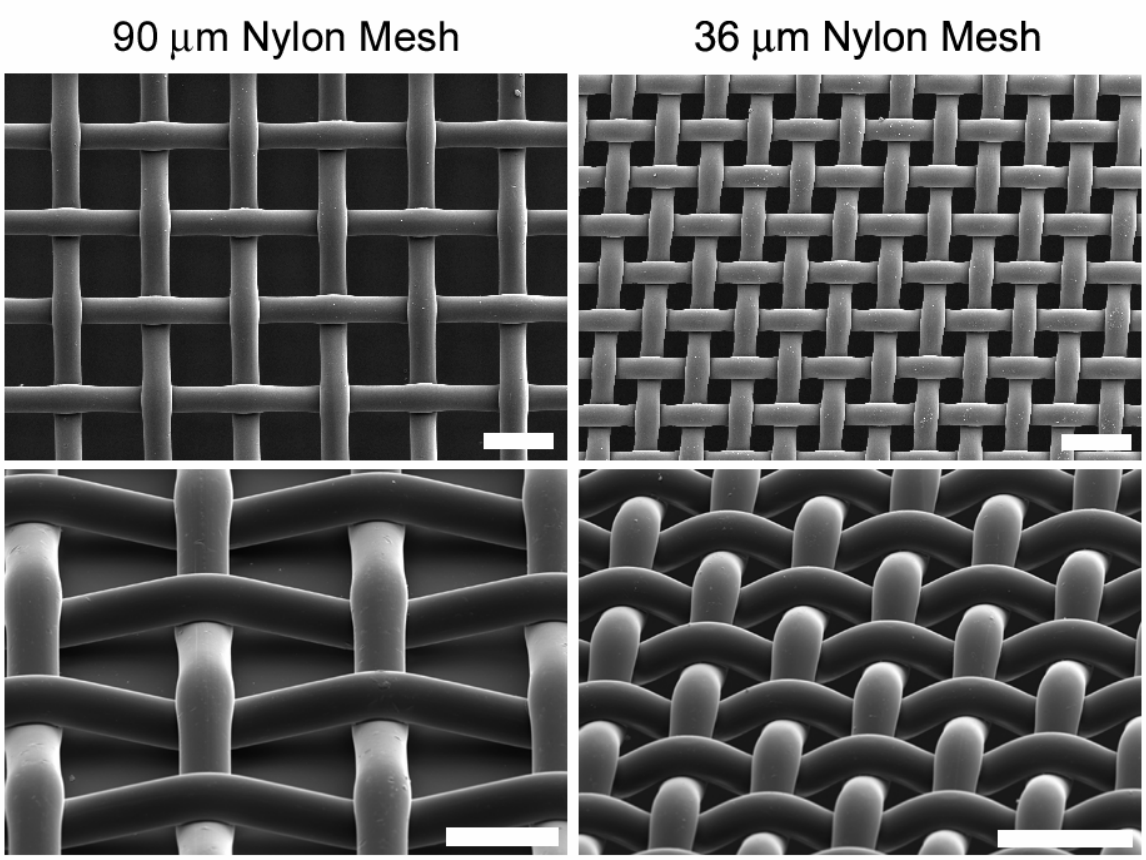

Figure 6.1 Scanning electron micrographs of Nylon polymer mesh with 90 μm and 36 μm mesh openings. Top row images are a top-down view. Bottom row images are an angled view. Scale bars are 100 μm.

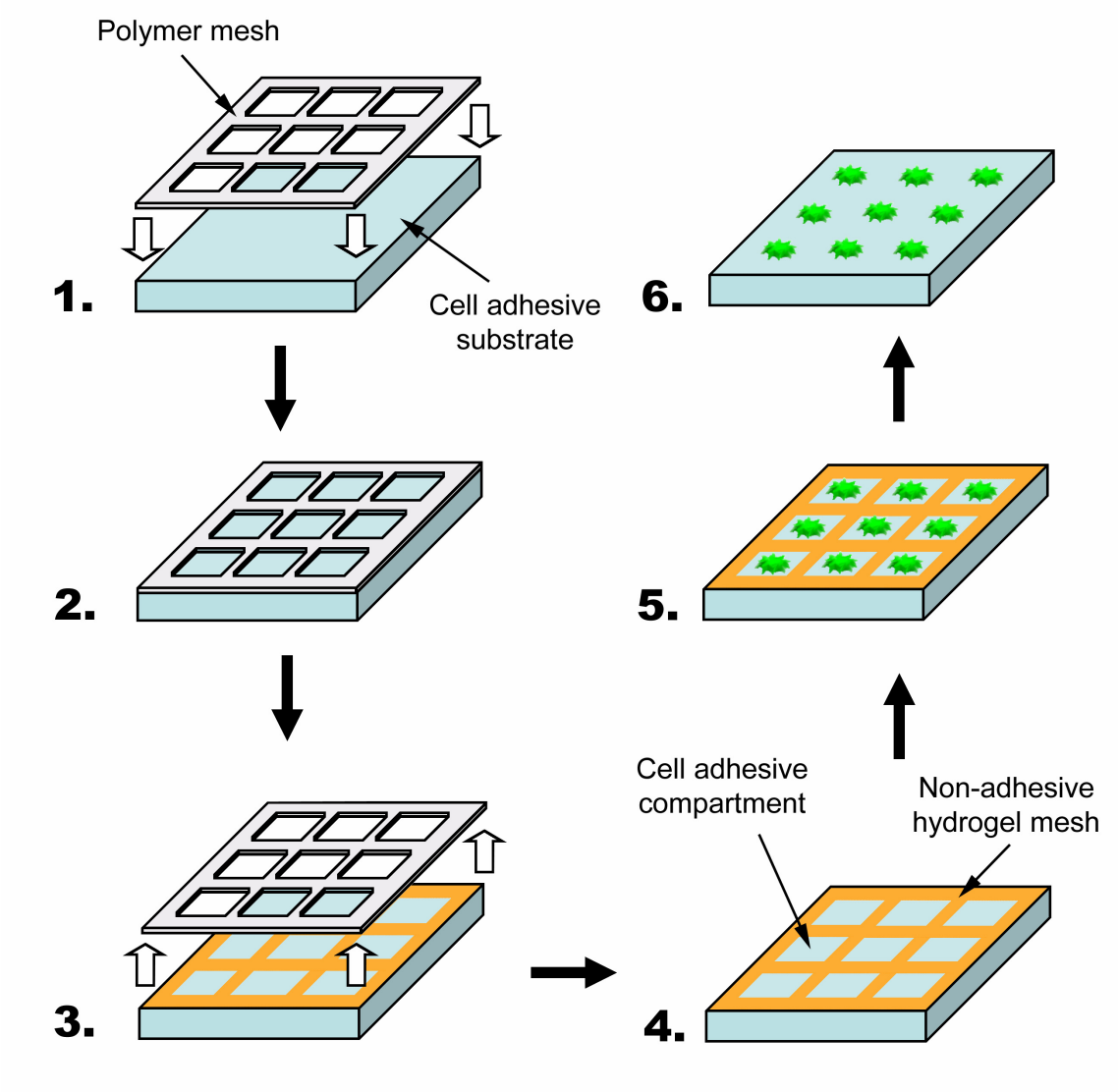

Figure 6.2 Steps for obtaining hydrogel meshes from Nylon polymer mesh. **1.** A polymer mesh is dipped into a solution of biopolymer and then laid flat on a cell adhesive substrate. **2.** The water evaporates through the holes in the mesh and the biopolymer recedes into the space between the mesh and the substrate. **3.** The polymer mesh is removed and a hydrogel mesh adheres to the substrate. **4.** The non-adhesive hydrogel delineates a microarray of cell adhesive compartments. The hydrogel mesh can be crosslinked by a method such as ion-gelation or photocrosslinking which stabilizes the hydrogel against dissolution. **5.** Cells are seeded onto the substrate and adhere within the cell adhesive compartments. The patterned cells and hydrogel together constitute the cell microarray. **6.** An optional step is to remove the mesh and release the cells from the compartments.

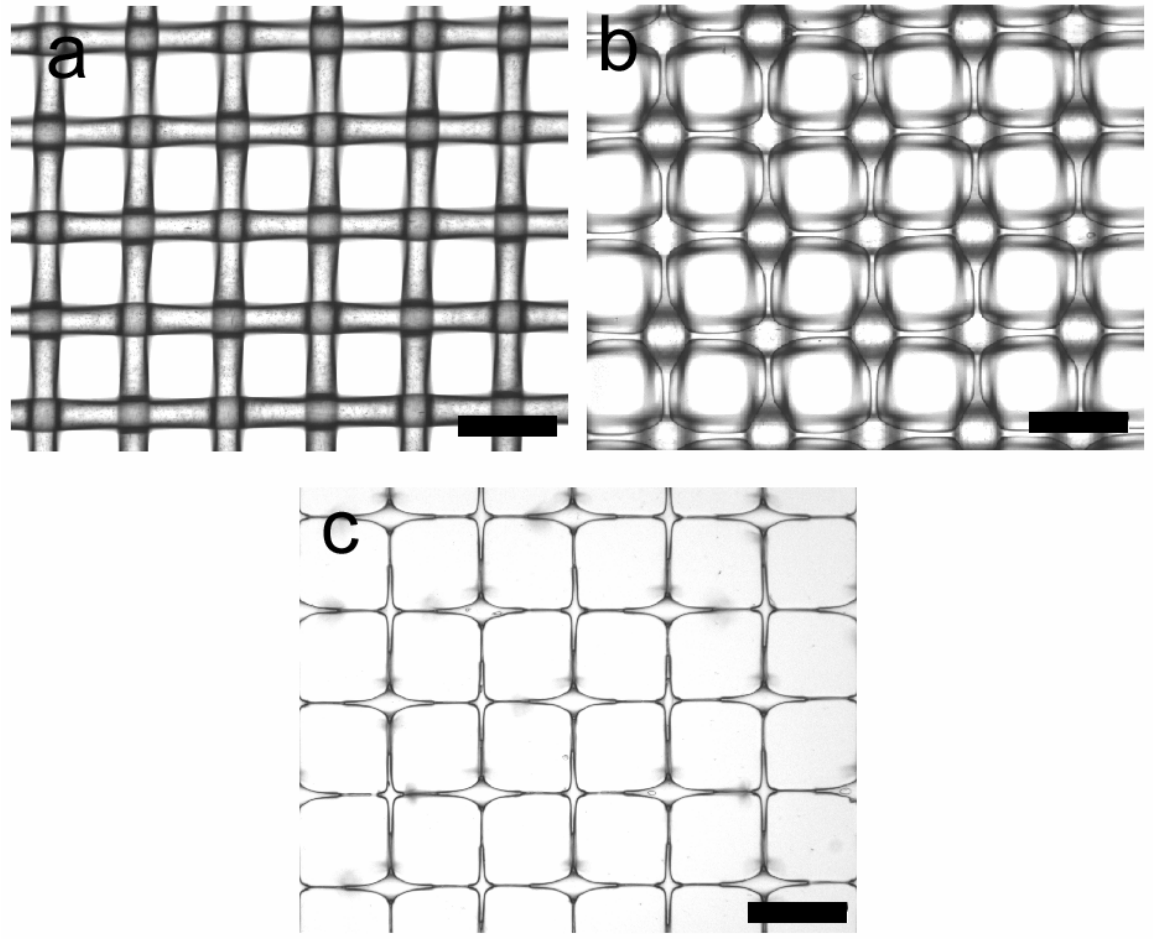

Figure 6.3 Brightfield microscopy images demonstrating the patterning of hydrogel by evaporation through a polymer mesh. (**a**) Nylon 6/6 polymer mesh with 64 μm mesh opening. (**b**) Polymer mesh with a biopolymer solution that has partially dried. The viscous polymer solution concentrates in the space between the polymer mesh and the glass substrate. (**c**) A GMHA hydrogel mesh after removal of the nylon polymer. Scale bars are 100 μm.

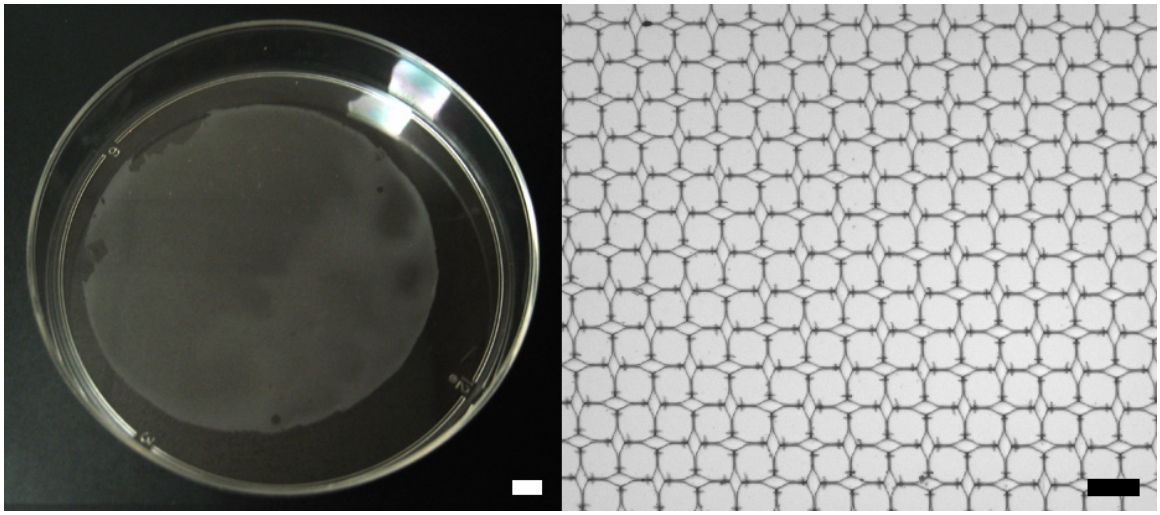

Figure 6.4 Photograph of a 150 mm polystyrene tissue culture plate patterned with a hydrogel mesh. This dish contains ~1.8 million identical hydrogel compartments and demonstrates the large areas that can be patterned by this technique. Scale bars are 1 cm (left) and 100 μm (right).

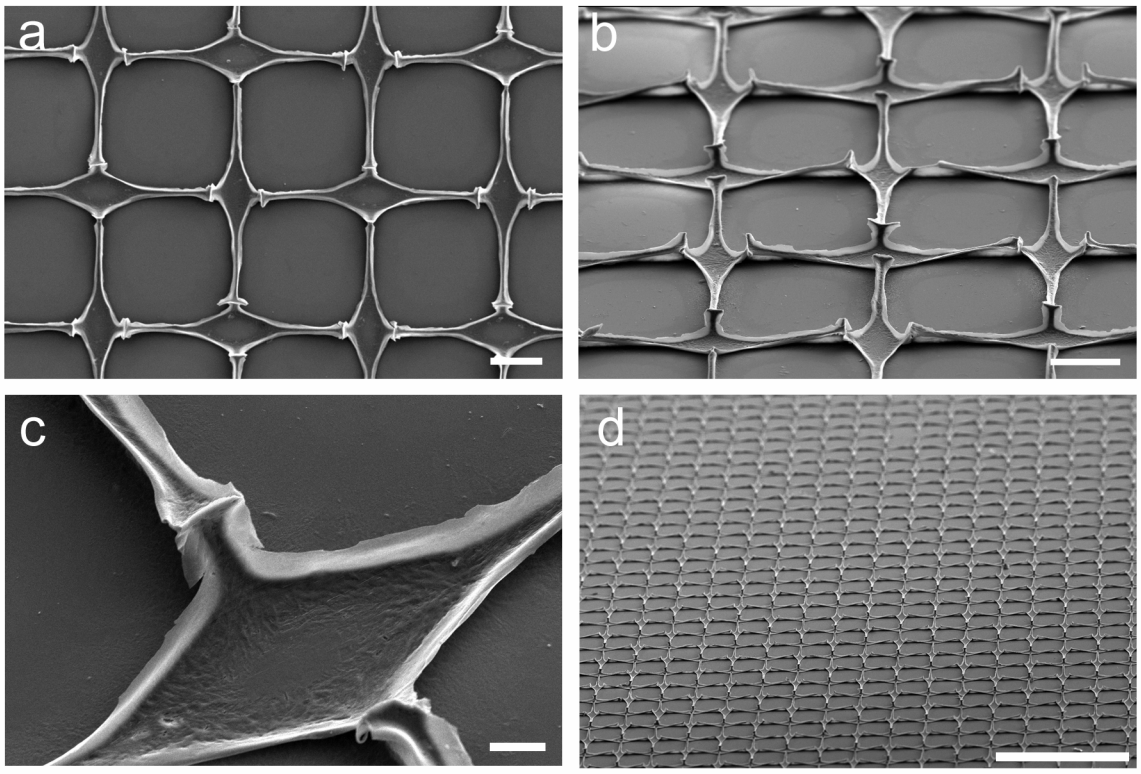

Figure 6.5 SEM micrographs of an alginate hydrogel mesh. This mesh was patterned with a nylon mesh containing a 90 μm mesh opening. Each hydrogel compartment is about 110 μm wide. This hydrogel mesh has a distinctive "boat" shaped appearance due to the over-and-under weave of the nylon fibers by which the hydrogel was patterned. The scale bars are (a) 50 μm; (b) 50 μm; (c) 10 μm; and (d) 500 μm.

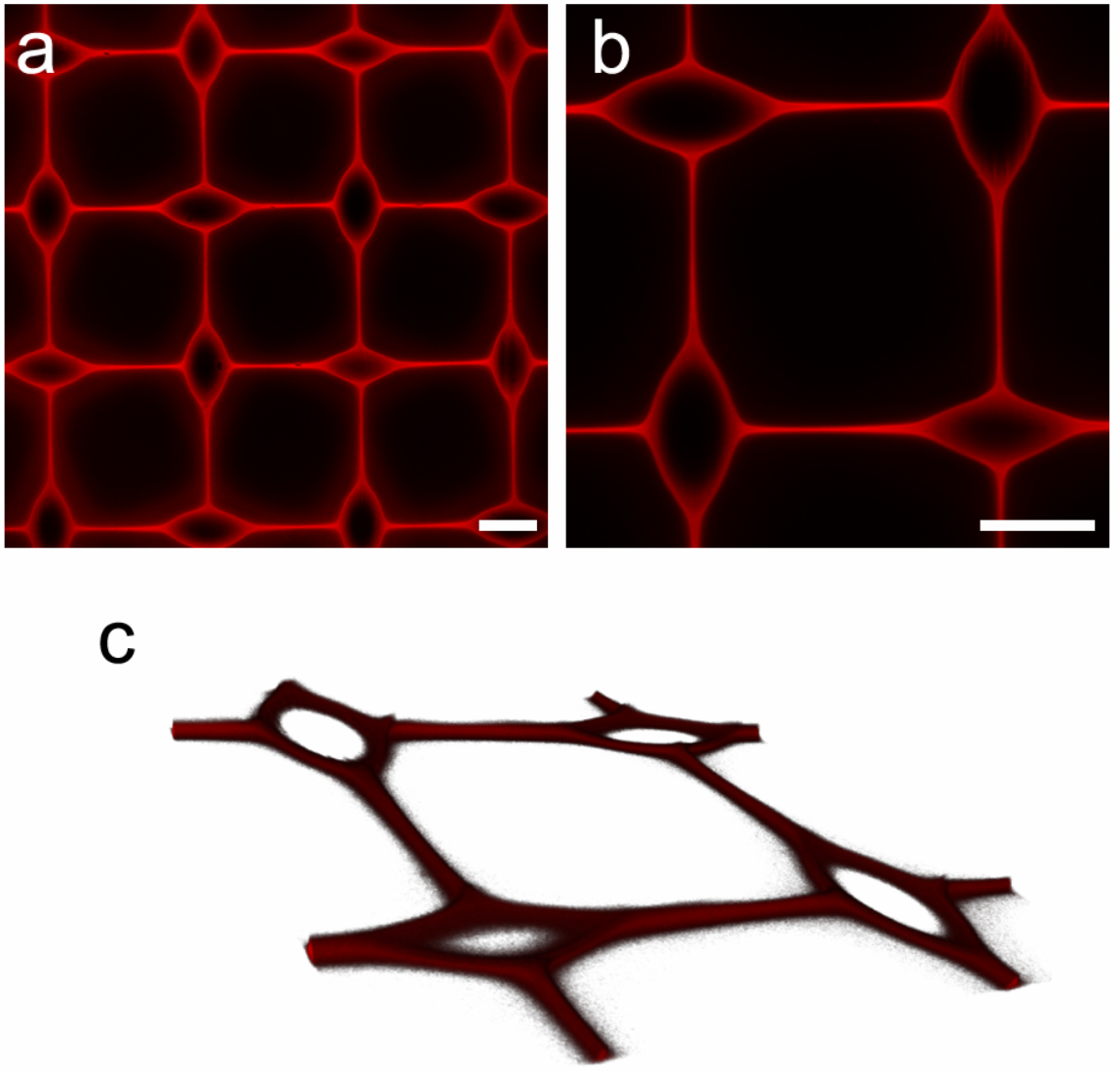

Figure 6.6 Confocal fluorescent microscopy of chitosan hydrogel compartments labeled with dextran-TRITC. (**a,b**) These single scans demonstrate that the hydrogel meshes can incorporate macromolecules including fluorescent labels. Scale bars are 25 μm. (**c**) Three-dimensional volume projection of a series of confocal z-slices showing the height of the hydrogel compartments.

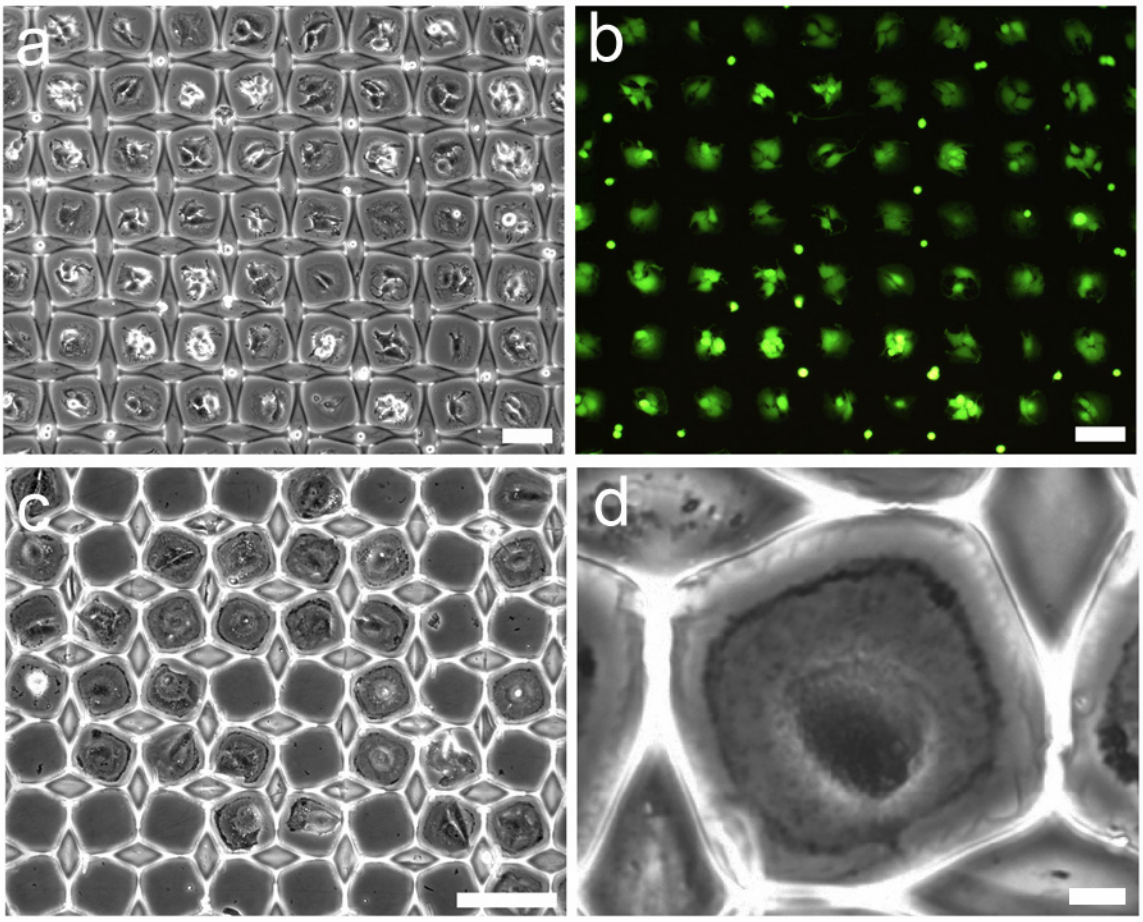

Figure 6.7 Phase contrast and fluorescence images of living cell microarrays patterned by hydrogel meshes. The cell source is normal human dermal fibroblasts. Large meshes yield microarrays of cell clusters (top row). Small meshes yield microarrays of individual cells (bottom row). (**a**) Clusters of fibroblasts are adhered in each compartment. (**b**) Calcein labeled fibroblasts indicating cell viability. (**c**) Individual fibroblasts are adhered within the compartments. (**d**) A magnified image of a single fibroblast within the hydrogel microarray. Scale bars are 100 μm (a-c) and 10 μm (d).

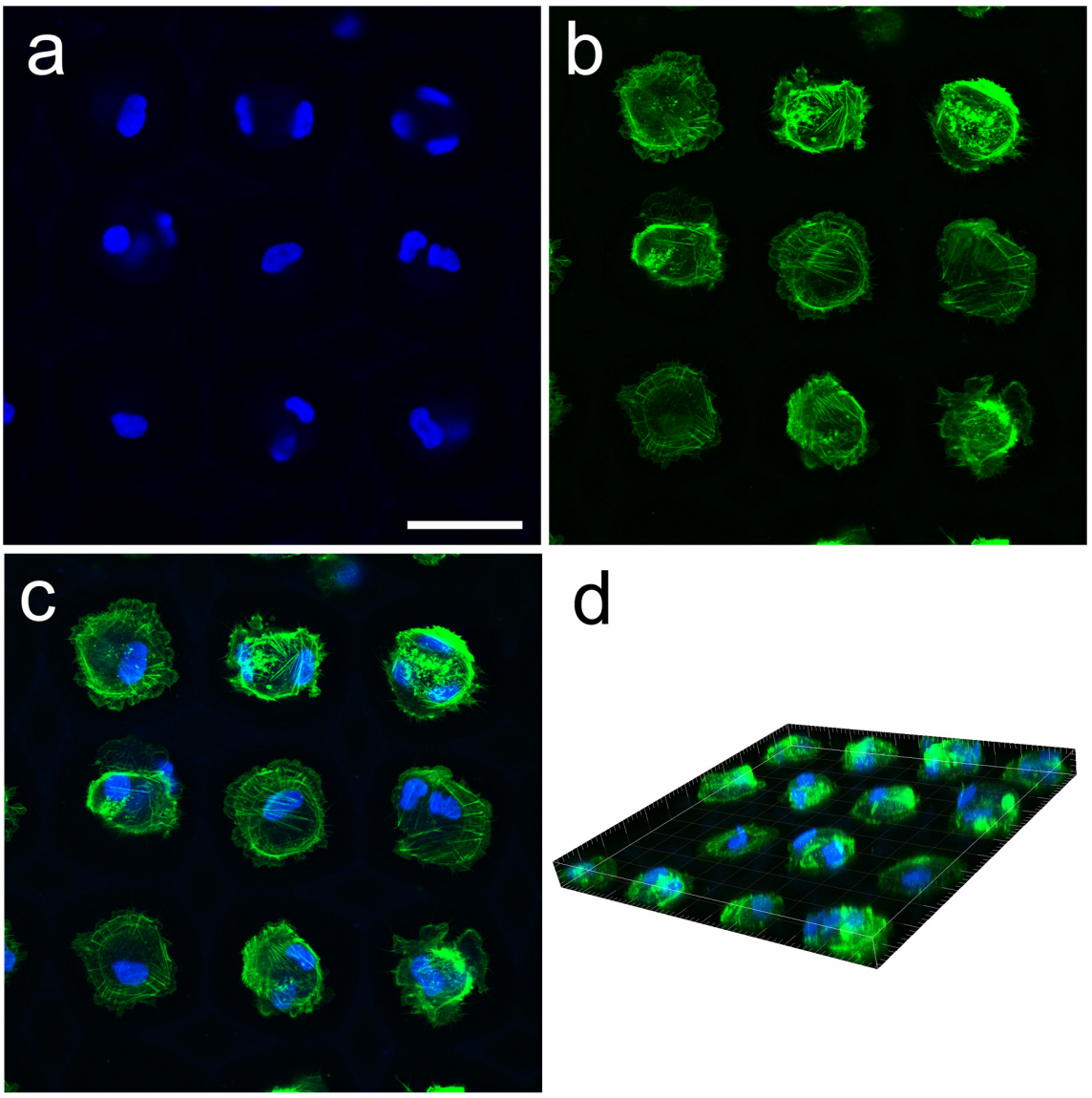

Figure 6.8 Microarray of human dermal fibroblasts imaged by confocal fluorescence microscopy. These cells were seeded within a chitosan mesh, cultured for 12 hours, fixed and stained with DAPI nuclear stain (blue) and phalloidin actin stain (green). (**a**) DAPI staining shows that one to three cells adhered per compartment. Scale bar is 50 μm. (**b**) Phalloidin staining shows that the fibroblasts spread to fill up the available area within each hydrogel compartment. (**c**) Overlay of DAPI and phalloidin images. (**d**) Volume projection depicting a cell microarray in three dimensions.

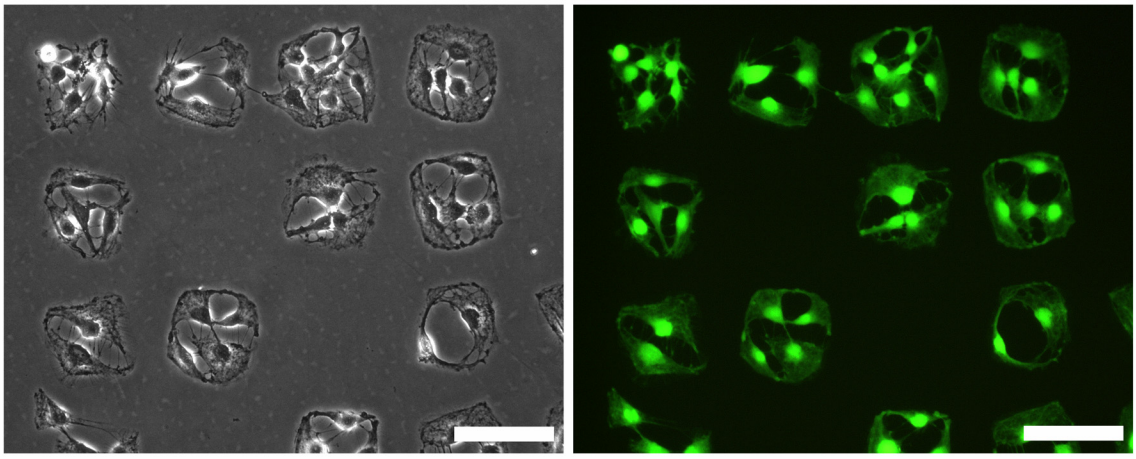

Figure 6.9 Microarray of primary rat Schwann cells. The cells were cultured within GMHA hydrogel meshes for 5 days. The hydrogel was removed by gentle agitation of the dish and the cells were immediately imaged. Without the hydrogel barrier the cells are free to proliferate and spread as normal if given adequate time. Green cells are fluorescently labeled with calcein which indicates cell viability. Scale bars are 100 μm.

Table I. Dimensions of Nylon mesh.

Mesh Opening (μm)	Thread Diameter (μm)	Mesh Count per cm^2
90	39	6,009
64	33	10,628
48	38	13,521
36	33	21,004

Chapter 7: Conclusions

7.1 Historical perspective on HA biomaterials. HA-based materials with four kinds of novel properties were described in this dissertation: drug-binding, anisotropic swelling, dendritic porosity, and microarray morphology. To put this dissertation's research into perspective the historical development of HA-based materials for biomedical applications is briefly summarized here. HA was first isolated in 1934 from the vitreous fluid of bovine eyeballs.[1] The vitreous fluid, primarily composed of HA and collagen II, is an acellular space-filler between the retina and lens that stabilizes eyeball and absorbs shock.[2] The vitreous fluid is susceptible to a number of pathologies such as shrinkage, haemorrhage, and detachment.[2] It is not surprising that E.A. Balazs, an opthalmologist studying the composition of the vitreous at Harvard Medical School, was inspired to create an HA-based material that could replace the vitreous in patients afflicted with these pathologies. Thus, Balazs developed and patented the first method for obtaining purified medical grade HA from rooster comb.[3] This source of HA became the basis of Healon® a 1% solution of HA in PBS used to supplement the vitreous during opthalmological surgeries.[4]

HA solutions were soon adapted to function as visco-supplements of the intra-articular joint (i.e., Synvisc®) and as injectable dermal fillers.[5,6] To obtain the necessary visco-elastic properties of these HA solutions, crosslinking technologies using divinyl sulfone, aldehydes, and epoxides were developed.[7] The modern fields of tissue engineering and drug delivery, however, require materials with complex properties that

cannot be obtained from these lightly crosslinked HA solutions. Therefore, engineering HA-based materials with novel properties and structural features is an ongoing area of research. Fortunately, relatively inexpensive HA that is obtained from bacteria is widely available for engineers to use in designing the next generation of HA-based materials.[8,9]

The original applications of HA to the vitreous, joint fluid, and skin were relatively simple because all that was required was an injectable, biocompatible, viscous polymer solution. Above and beyond these basic properties, this work describes methods for engineering HA materials with a variety of complex and useful properties. An important enabling technology for this research that was developed by several labs, including previous work in Schmidt lab, is the grafting of methacryloyl and acryloyl functionalities to HA to render it photocrosslinkable.[10-12] The benefits of this photocrosslinking technology for HA hydrogels are that it works at room temperature and neutral pH, the reaction is rapid, and can be easily controlled by manipulation of UV intensity and duration. Furthermore, UV exposure can be spatially patterned using photomasks and lasers. The research in this dissertation uses photocrosslinkable hyaluronic acid (GMHA) as the basis for novel HA-based materials that span a wide range of applications from tissue engineering to drug delivery and microarrays.

7.2 Drug-binding HA hydrogels. HA hydrogels are attractive for drug delivery because they are biocompatible and non-immunogenic. These properties arise because the hydrogels consist predominantly of water. Therefore, HA hydrogels are suited for delivery of water-soluble proteins but not the many classes of poorly water soluble drugs. In Chapter 3 we addressed this problem by designing hydrogels of HA functionalized

with a methacryloyl β-cyclodextrin monomer. The β-cyclodextrin monomer is able to bind poorly water soluble drugs and conferred this property to the HA hydrogels. Drug binding was verified by contrasting the hydrocortisone uptake of hydrogels with α-cyclodextrin and β-cyclodextrin. Further evidence of drug binding was obtained by inhibiting the hydrogels with adamantane carboxylic acid which completely prevented drug binding. Therefore, we concluded that HA hydrogels functionalized with βCD do indeed bind hydrocortisone through inclusion complexation and that this ability permits the functionalized hydrogels to uptake and deliver more hydrocortisone that un-functionalized hydrogels. This is a useful finding because it is a method for combining the biocompatible, hydrophilic HA hydrogel with a poorly water soluble drug. HA hydrogels that complex hydrophobic drugs have not been previously described.

7.3 Dual-crosslinked HA hydrogels. By definition hydrogels swell in mass and volume when placed in aqueous solution. Our goal in Chapter 4 was to design a novel HA hydrogel that would exhibit anisotropic swelling. Our design strategy used two modes of crosslinking. We synthesized a super-swelling chemically crosslinked hydrogel and then, before swelling, we added photopatterned crosslinks. When placed in solution the super-swelling regions swelled to a great extent whereas the regions that contained photopatterned crosslinks swelled less. The result was a hydrogel that swelled anisotropically that may have applications as an implantable tissue engineering scaffold that slowly changes shape as it swells. Hydrogels with photopatterned anisotropic swelling have not been previously described.

7.4 HA hydrogels with dendritic porosity. Many methods have been developed

for creating polymer scaffolds with biomimetic porosity; however, no method is able to engineer networks of fine branched pores which is a highly desirable feature for tissue engineered scaffolds. Dendritic porosity would be able to guide cellular infiltration, microvessel invasion, and axon pathfinding in a way that random, open porous scaffolds cannot. In Chapter 5, we invented a "crystal templating" strategy for obtaining dendritic porosity based on the insight that crystals can form large branched structures. By crosslinking biopolymer hydrogels around such crystals we obtained unique dendritic networks. This crystal templating method for obtaining branched pores has not been previously described.

7.5 HA hydrogel meshes for cell microarrays. Finally, in Chapter 6 we created hydrogel meshes of photocrosslinked hyaluronic acid. Due to the non-cell adhesive nature of the hyaluronic acid we found that the meshes could be used to pattern cells within microarrays. This is an extremely useful invention because it addresses the fundamental hurdle of inventing a simple method for obtaining cellular microarrays that does not require expertise in microfabrication. With this method the use of cellular microarrays can be more readily adopted by biological research labs. A further feature of these hydrogel meshes is that they can be removed to release cells from hydrogel confinement. This method for using Nylon polymer meshes to create microarrays without the need for microfabrication has not been previously described.

7.6 Applicability of these methods to other polymers. The work in this dissertation was based upon hyaluronic acid but is generalizable to other polymers. Our methods for demonstrating inclusion complexation by GMHA-βCD hydrogels can be

used to evaluate cyclodextrin functionalization of any kind of hydrogel. The dual-crosslinking method for obtaining anisotropic swelling is readily generalizable; all that is required are two orthogonal modes of crosslinking in which at least one mode can be photopatterned. The crystal templating technique has been verified with alginic acid, chitosan, and poly(ethylene glycol) diacrylate as well as hyaluronic acid. The essential requirement for crystal templating is a rapid method of crosslinking that can preserve the morphology of the crystals. Furthermore, we have found that changing the crystallizable material from urea to βCD and potassium phosphate produces very different porous morphologies. Lastly, microarrays of hydrogel compartments can be obtained from hyaluronic acid, alginic acid, and chitosan each of which have their own combination of advantages and limitations.

7.7 Recommendations and Future Work. The two aspects of this dissertation with the most potential for future development are the crystal templating method for obtaining dendritic porosity and the hydrogel mesh method for obtaining cellular microarrays. Only by supporting cellular infiltration will the crystal templated hydrogels be applicable as tissue engineered scaffolds. Future work will need to functionalize them with cell adhesive proteins that can permit cell adhesion and invasion. Future avenues of research should investigate methods for creating novel composite materials using the templated hydrogels. For example, polymerization reactions and biomineral growth within the pores would yield novel composites in which a biomineral or synthetic polymer phase is closely entwined with the hydrogel phase.

A number of applications for the hydrogel mesh microarrays are readily

conceivable. Many assays are commercially available that detect cell viability, proliferation, protein synthesis, cytotoxicity, and other aspects of cellular function. These assays should be adapted so that they can be applied to the local microenvironments of each hydrogel compartment and thereby permit individual clusters of cells to be monitored. This is achievable by entrapping the assay reagents within the hydrogel mesh and/or covalently attaching them to the hydrogel's surface.

In conclusion, the novel methods and materials in this dissertation are a significant contribution to the engineering of HA-based materials. These novel HA hydrogel possess unique properties that have not been previously reported. Crystal templating and hydrogel meshes are particularly applicable to the fields of tissue engineering and microarrays and address fundamental hurdles in these fields. Future work should be aimed at further developing crystal templated HA scaffolds and hydrogel meshes.

7.8 References

1. Meyer, K., Palmer, J.W. The polysaccharide of vitreous humor *J. Biol. Chem.,* **107**, 629-634 (1934).
2. Chirila, T.V., Hong, Y., Dalton, P.D., Constable, I.J., Refojo, M.F. The use of hydrophilic polymers as artificial vitreous *Prog. Polym. Sci.,* **23**, 475-508 (1998).
3. Balazs, E.A. Ultrapure hyaluronic acid and the use thereof. US Patent No 4,141,973 (1979).
4. Arshinoff, S.A. Dispersive-cohesive viscoelastic soft shell technique. *J. Cataract*

Refract. Surg., **25**, 167-173 (1999).

5. Brockmeier, S.F., Shaffer, B.S. Viscosupplementation therapy for osteoarthritis. *Sports Med. Arhtrosc. Rev.* **14**, 155-162 (2006).

6. Monheit, G.D., Coleman, K.M. Hyaluronic acid fillers. *Dermatol. Ther.,* **19**, 141-150 (2006).

7. Balazs, E.A. Cross-linked gels of hyaluronic acid and products containing such gels. US Patent No. 4,636,524 (1987).

8. Agerup, B., Berg, P., Akermark, C. Non-animal stabilized hyaluronic acid. *BioDrugs,* **19**, 23-30 (2005).

9. Shiedlin, A., Bigelow, R., Christopher, W., Arbabi, S., Yang, L., Maier, R.V., Wainwright, N., Childs, A., Miller, R.J. Evaluation of hyaluronan from different sources: streptococcus zooepidemicus, rooster comb, bovine vitreous, and human umbilical cord. *Biomacromolecules,* **5**, 2122-2127 (2004).

10. Leach, J.B., Bivens, K.A., Patrick, C.W., Schmidt, C.E. Photocrosslinked hyaluronic acid hydrogels: natural, biodegradable tissue engineering scaffolds. *Biotechnol. Bioeng.,* **82**, 578-589 (2003).

11. Park, Y.D., Tirelli, N., Hubbell, J.A. Photopolymerized hyaluronic acid-based hydrogels and interpenetrating networks. *Biomaterials,* **24**, 893-900 (2003)

12. Smeds, K.A., Pfister-Serres, A., Hatchell, D.L., Grinstaff, M.W. Synthesis of a novel polysaccharide hydrogel. *J.M.S. Pure Appl. Chem.,* **A36**, 981-989 (1999).

Appendix: Experimental Protocols

A.1 Synthesis of methacryloyl hyaluronic acid

Purpose: Modify hyaluronic acid with glycidyl methacrylate to yield photocrosslinkable product.

Materials

Hyaluronic acid (HA)	Aldrich 53747
Glycidyl methacrylate (GM)	Aldrich 151238
Triethylamine (TEA)	Aldrich 471283
Acetone	Sigma A18
Deuterated water	Cambridge Isotope Laboratories DLM-4-25
Irgacure 2959	Ciba Specialty Chemicals
UV lamp (365 nm)	Blak-Ray Model B-100A

Procedure

Dissolve 0.5 g HA in 50 mL of water. Mix overnight.
Then add 3.6 mL triethylamine. Mix thoroughly.
Add 3.6 mL glycidyl methacrylate. Mix thoroughly.
Mix at room temperature in a sealed flask for 24 hours.
Precipitate the GMHA in acetone (one part GMHA solution to 20 parts acetone).
Pour acetone into a beaker. Slowly add GMHA solution while stirring acetone with a glass rod or pipet.
The GMHA will precipitate as a cottony white solid and collect on the glass stirrer.
Stop precipitation and replace acetone if it becomes very cloudy.
Transfer the precipitate to a dish and rinse with acetone.
Dissolve the precipitate in 50 ml dI overnight.
Reprecipitate the GMHA in acetone.
Rinse in acetone and dissolve in 50 ml dI overnight.
Freeze the solution and lyophilize for 48-72 hours.
Store with dessicant at -20°C.

This procedure produces GMHA with a degree of substitution of ~11% (11 out of 100 disaccharides bear a methacrylate group). Decreasing the amount of triethylamine and glycidyl methacrylate decreases the degree of substitution. Adding acetone to the reaction mixture increases the degree of substitution. The amount of reactants for 5% substituted GMHA are in 6-fold molar excess relative to HA disaccharides. The amount of reactants for 7% substituted are 10-fold molar excess. The other conditions use reactants that are 20-fold molar excess.

Table I. Conditions for producing 0.5 g of GMHA with different degrees of substitution.

Degree of Substitution (%)	Solvent	Triethylamine (mL)	Glycidyl Methacrylate (mL)
5	water	1.1	1.1
7	water	1.8	1.8
11	water	3.6	3.6
23	30% acetone	3.6	3.6
32	50% acetone	3.6	3.6

NMR

Purpose: verify methacrylation NMR.
Prepare 0.5% GMHA in D_2O.

Compare peak heights per proton of HA methyl peaks (1.93 ppm) and methacrylate peaks (5.6 and 6.1 ppm).

Photocrosslinking

Make a 1% solution of Irgacure 2959 in ddI water. Sonicate for 30-40 minutes to dissolve.
Store at room temperature in the dark for up to one month.
Make a 0.5-2.0% GMHA solution in I2959 solution.
Transfer the GMHA solution to rubber molds and expose to UV light for 0.5-5 minutes to produce a solid gel.

Notes

2959 concentrations greater than 0.1% are cytotoxic.
GMHA solutions of up to 1.5% can be filter sterilized through 0.2 μm syringe filters with a 0.8 μm pore size prefilter (0.8/0.2 μm Pall Gelman Supor Acrodisc PF syringe filter).

	HA	TEA	GM
MW	402	101.2	142
density (g/cm^3)		0.728	1.07

References – Photoinitiator Cytocompatibility

Bryant, S.J., Nuttelman, C.R., Anseth, K.S. Cytocompatibility of UV and visible light photoinitiating systems on cultured NIH/3T3 fibroblasts in vitro. *J. Biomater. Sci. Polym. Ed.,* **11**, 439-57, (2000).

Williams, C.G., Malik, A.N., Kim, T.K., Manson, P.N., Elisseeff, J.H. Variable cytocompatibility of six cell lines with photoinitiators used for polymerizing hydrogels and cell encapsulation. *Biomaterials*, **26**, 1211-8 (2005).

References – Photocrosslinked Hyaluronic Acid Hydrogels

Burdick, J.A., Chung, C., Jia, X., Randolph, M.A., Langer, R. Controlled degradation and mechanical behavior of photopolymerized hyaluronic Acid networks. *Biomacromolecules*, **6**, 386-91 (2005).

Jia, X., Burdick, J.A., Kobler, J., Clifton, R.J., Rosowski, J.J., Zeitels, S.M., Langer, R. Synthesis and characterization of in situ cross-linkable hyaluronic acid-based hydrogels with potential application for vocal fold regeneration. *Macromolecules,* **37**, 3239-3248 (2004).

Leach, J.B., Bivens, K.A., Patrick, C.W., Schmidt, C.E. Photocrosslinked hyaluronic acid hydrogels: natural, biodegradable tissue engineering scaffolds. *Biotechnol. Bioeng.,* **82**, 578-89 (2003).

Leach, J.B., Bivens, K.A., Collins, C.N., Schmidt, C.E. Development of photocrosslinkable hyaluronic acid-polyethylene glycol-peptide composite hydrogels for soft tissue engineering. *J. Biomed. Mater. Res.,* **70A**, 74-82 (2004).

Leach, J.B., Schmidt, C.E. Characterization of protein release from photocrosslinkable hyaluronic acid-polyethylene glycol hydrogel tissue engineering scaffolds. *Biomaterials,* **26**, 25-35 (2005).

Park, Y.D., Tirelli, N., Hubbell, J.A. Photopolymerized hyaluronic acid-based hydrogels and interpenetrating networks. *Biomaterials,* **24**, 893-900 (2003)

Smeds, K.A., Pfister-Serres, A., Hatchell, D.L., Grinstaff, M.W. Synthesis of a novel polysaccharide hydrogel. *J. Appl. Chem.,* **A36**, 981-989 (1999).

Smeds, K.A., Pfister-Serres, A., Miki, D., Dastgheib, K., Inoue, M., Hatchell, D.L., Grinstaff, M.W. Photocrosslinkable polysaccharides for in situ hydrogel formation. *J. Biomed. Mater. Res.,* **54**, 115-21 (2001).

Trudel, J., Massia, S.P. Assessment of the cytotoxicity of photocrosslinked dextran and hyaluronan-based hydrogels to vascular smooth muscle cells. *Biomaterials,* **23**, 3299-307 (2002).

A.2 Synthesis of methacryloyl cyclodextrin

Purpose: Graft cyclodextrin with methacryloyl groups to yield photocrosslinkable cyclodextrin monomer.

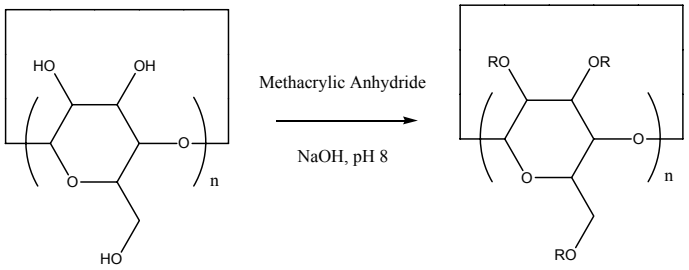

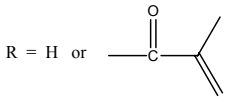

n = 6, α–cyclodextrin
n = 7, β–cyclodextrin

Materials

β-cyclodextrin	Fluka 28707
α-cyclodextrin	Sigma C4642
Methacrylic anhdyride	Aldrich 27668-5
Sodium hydroxide	
Dialysis Tubing (cellulose ester 500 MWCO)	Spectrum Labs 131057

Procedure

Dissolve 1 g cyclodextrin in 60 mL ddI water (0.85 g anhydrous βCD, 0.96 g anhydrous αCD).
Add methacrylic anhydride in chemical fume hood (see Table).
Adjust pH to ~8 with 10 M NaOH. Continue to monitor pH and adjust accordingly.
Add a total molar quantity of NaOH up to 110% of moles of methacrylic anhydride until pH stabilizes (~4 hours).
Dialyze for 48 hours in 500 MWCO membrane.
Freeze solution in liquid nitrogen and lyophilize at –50 C for 48 hours.

Reactants per 1 g of cyclodextrin

CD	Equivalents MA	MA (μL)	NaOH (μL 10 M)	DS
β	4.7	525	388	3.1
β	7.1	790	582	4.2
β	10.6	1185	875	5.2
α	4.2	610	450	2.6
α	6.4	920	680	3.3
α	9.6	1380	1018	4.8

Notes

β-cyclodextrin:	MW = 1134	Aqueous solubility = 1.85%	stock is 15% water weight
α-cyclodextrin:	MW = 972	Aqueous solubility = 14.5%	stock is 6% water weight

Methacrylic anhydride: MW = 154.16 Density = 1.035 g/ml

References – Methacrylated Cyclodextrins

Bowen, R.L., Farahani, M., Dickens, S.H., Guttman, C.M. MALDI-TOF MS analysis of a library of polymerizable cyclodextrin derivatives. *J. Dent. Res.,* **79**, 905-911 (2000).

Buchanan, C.M., Alderson, S.R., Cleven, C.D., Dixon, D.W., Ivanyi, R., Lambert, J.L., Lowman, D.W., Offerman, R.J., Szejtli, J., Szente, L. Synthesis and characterization of water-soluble hydroxybutenyl cyclomaltooligosaccharides (cyclodextrins). *Carbohydr. Res.,* **337**, 493-507 (2002)

Janus, L. et al. New sorbents containing β-cyclodextrin. Synthesis, characterization, and sorption properties. *React. Funct. Polym.,* 42, 173-180 (1999).

Liu, Y., Fan, X., Gao, L. Synthesis and characterization of β-cyclodextrin based functional monomers and its copolymers with N-isopropylacrylamide. *Macromol. Biosci.,* **3**, 715-719 (2003).

Saito, R., Yamaguchi, K. Synthesis of biomodal methacrylic acid oligomers by template polymerization *Macromolecules*, **36**, 9005-9013 (2003).

References – Methacrylic Anhydride and Hyaluronic Acid

Burdick, J.A., Chung, C., Jia, X., Randolph, M.A., Langer, R. Controlled degradation and mechanical behavior of photopolymerized hyaluronic acid networks. *Biomacromolecules,* **6**, 386-91 (2005).

Smeds, K.A., Pfister-Serres, A., Hatchell, D.L., Grinstaff, M.W. Synthesis of a novel polysaccharide hydrogel. *J. Appl. Chem.,* **A36**, 981-9 (1999).

A.3 HPLC purification of methacryloyl-cyclodextrin

Purpose: Purify methacryloyl-cyclodextrin of methacryloyl oligomers.

Materials
Acetonitrile
Water
200 mM Ammonium Bicarbonate
AKTA Purifier instrument ((Amersham Pharmacia Biotech)
Source 5RPC ST 4.6/150 column (Amersham Pharmacia Biotech) (Location: MBB)

Procedure

1. Dissolve crude MAβCD in water. Mix overnight. Remove solid particulates with syringe filtration (0.22 μm cellulose acetate filter). Crude MAβCD solutions greater than about 45 mg/mL will precipitate if left for 48 hours or longer.

2. Conditions for HPLC
   Column: C18
   Gradient Elution: 98/2 to 45/55
   Eluent A: Water
   Eluent B: Acetonitrile
   Flowrate: 0.8 ml/min
   Injection Volume: 1 mL
   Empty Loop with 1.5 mL
   Length of Gradient: 12 CV
   Program: CDMix1

3. Start HPLC and measure absorbance at wavelengths 230, 235 or 240 nm.

4. At end of run collect fractions 8-22. Lyophilize.

Note 1: Do not use TFA in buffer. 0.1% TFA causes oxidation of cyclodextrins. If column was previously run with TFA in buffer then first neutralize the column by washing with 200 mM ammonium bicarbonate (15.8 mg/ml) prior to run. After fractionation check the pH of the eluted fractions with pH paper (pH should be > 6). Adjust the pH to 7 with 200 mM ammonium bicarbonate if necessary.

Note 2: Can use same procedure for purifying MAαCD. At end of run collect fractions 7-22.

A.4 Phase solubility of hydrocortisone in cyclodextrin solutions

Purpose: Construct phase solubility diagram of hydrocortisone in aqueous cyclodextrin solutions.

Materials

Cyclodextrin	
Syringe Filters (0.22 μm PVDF)	Millipore
Hydrocortisone	Sigma H4001
Quartz microcuvette	

Procedure

Prepare 300 μL of cyclodextrin solutions of each concentration: 0, 1, 3, 5, 8, 10 and 15 mM in ddI water. Prepare the solutions in triplicate in 0.65 mL tubes.

Add several mg of hydrocortisone to each tube.

Sonicate tubes for 5 minutes.

Incubate tubes at room temperature for 6 days while rotating end over end.

At end of 6 days measure the concentration of hydrocortisone dissolved in solution spectrophotometrically.

Prepare a standard curve of hydrocortisone absorbance (248 nm) of 100, 50, 40, and 25 mM in ddI water.

Syringe filter the cyclodextrin solutions to remove undissolved hydrocortisone. Dilute the filtered solutions with ddI water 20-80 fold to get absorbance in range of standard curve.

Construct a phase solubility diagram by plotting concentration of hydrocortisone (mM) against concentration of cyclodextrin (mM).

Fit a line through the linear portion of the diagram and calculate the slope. Calculate the association constant by the following equation where K_a [mM^{-1}] is the association constant, C_0 [mM] is the solubility of hydrocortisone in water.

$$K_a = \frac{slope}{(1 - slope)C_0}$$

Reference: Higuchi, T.; Connors, K.A.; *Adva. Anal. Chem. Instr.* **1965**, 4, 117.

A.5 Hydrocortisone uptake by GMHA hydrogels

Purpose: Measure the uptake of hydrocortisone from solution by GMHA hydrogels with and without cyclodextrin functionalization.

Materials

Methacryloyl-hyaluronic acid (GMHA)	
Methacryloyl-β-cyclodextrin (MAβCD4)	
Methacryloyl-α-cyclodextrin (MAαCD6)	
Irgacure 2959	Ciba Specialty Chemicals
Adamantane carboxylic acid (ACA)	Fluka 01823
Hydrocortisone (HC)	Sigma H4001
Phosphate buffered saline (pH = 7.4, 10 mM)	
12-well tissue culture plates (24)	
1.5 mL tubes (256)	
2 dram vials (13)	

Solutions

Prepare 200 mL of PBS with 70 mg ACA. Stir 72 hours. Filter undissolved ACA.

Prepare 450 mL of PBS with 200 mg of HC. Stir for 72 hours. Filter undissolved HC. Store in refrigerator until needed.

Prepare 1% w/v Irgacure 2959 in PBS (20 mL PBS + 200 mg I2959).

Prepare a stock solution of 6 mL PBS (with 1% I2959) and 90 mg MAβCD4 (15 mg/mL).

Prepare a stock solution of 3 mL PBS (with 1% I2959) and 45 mg MAαCD6 (15 mg/mL).

Prepare photopolymerization solutions of GMHA with MAβCD4 and MAαCD6. Weigh out GMHA into a 2 dram vial. Add the appropriate amounts of PBS and PBS with MAβCD4 and MAαCD6. Stir overnight.

Measure out 150 mL saturated HC solution and add 50 mg ACA. Stir for 48 hours. Filter undissolved ACA.

Procedure

Photopolymerize gels of GMHA-MAβCD4 with 3, 6, 9, 12, 15 mg/mL MAβCD4 (n=8, total gels = 40). Put gels in 12-well plates with 3 mL of PBS. Exchange PBS after 4 hours, 8 hours and 24 hours. At 48 hours transfer gels to 3 ml of PBS saturated with ACA. Incubate at RT for 48 hours on orbital platform. Then transfer gels to 3 ml of PBS saturated with both ACA and HC. Incubate at RT for 7 days on orbital platform.

Photopolymerize gels of GMHA-MAβCD4 with 0, 3, 6, 9, 12, 15 mg/mL MAβCD4 (n=8, total gels = 48). Put gels in 12-well plates with 3 mL of PBS. Exchange PBS after 4 hours, 8 hours and 24 hours. At 48 hours transfer gels to 3 ml of PBS saturated with HC. Incubate at RT for 7 days on orbital platform.

Photopolymerize gels of GMHA-MAαCD6 with 3, 6, 9, 12, 15 mg/mL MAαCD6 (n=8, total gels = 40). Put gels in 12-well plates with 3 mL of PBS. Exchange PBS after 4 hours, 8 hours and 24 hours. At 48 hours transfer gels to 3 ml of PBS saturated with HC. Incubate at RT for 7 days on orbital platform.

Transfer all gels to fresh 12-well plates with 3 mL of PBS. Incubate at RT on orbital platform.

At 24 hours remove 0.5 mL of media from each well and transfer to a 1.5 mL tube. Replace with fresh 0.5 mL of PBS. Repeat at 48 hours.

Analyze samples with spectrophotometer. Read absorbance at 248 nm.

If necessary collect another sample at 72 hours.

A.6 Hydrocortisone release by GMHA hydrogels

Materials

Methacryloyl hyaluronic acid (GMHA)
Methacryloyl-β-cyclodextrin (M4βCD)
Hydrocortisone (HC) Sigma H4001
Phosphate buffered saline (pH = 7.4, 10 mM)
15 mL tubes
1.5 mL tubes
2 dram vials

Solutions

Prepare 120 mL of PBS with 53 mg of HC. Stir for 72 hours. Filter undissolved HC. Store in refrigerator until needed.

Prepare 1% I2959 in PBS (10 mL PBS + 100 mg I2959).

Prepare a stock solution of 2 mL PBS (with 1% I2959) and 30 mg MAβCD4 (15 mg/mL).

Prepare photopolymerization solutions of GMHA with MAβCD4. Weigh out GMHA into a 2 dram vial. Add the appropriate amounts of PBS and PBS with MAβCD4. Stir overnight.

Dilutions

Conc (mg/mL)	PI Soln (mL)	Stock Soln (mL)
0	1.000	0.000
5	0.666	0.333
10	0.333	0.666
15	0.000	1.000

Procedure

Photopolymerize gels of GMHA-MAβCD4 with 0, 5, 10, 15 mg/mL MAβCD4 (n=8, total gels = 32). Put gels in 12-well plates with 3 mL of PBS. Exchange PBS after 4 hours, 8 hours and 24 hours. At 48 hours transfer gels to 3 ml of PBS saturated with HC. Incubate at RT for 7 days on orbital platform.

Transfer all gels to 15 mL centrifuge tubes with 15 mL of PBS. Place on rotating apparatus at 37 °C in oven upstairs.

At 1, 2, 3, 4, 6, 8, 10, 12, 24, and 48 hours remove 0.5 mL of buffer from each tube and transfer to a 1.5 mL tube. Replace with fresh 0.5 mL of PBS.

Analyze samples with analytical HPLC.

A.7 Synthesis of chemically crosslinked HA hydrogels

Purpose: Synthesize super-swelling hydrogels of HA crosslinked with BDDE.

Materials

0.1 mL rubber perfusion molds	Grace Bio-Labs JTR8R-2.5
microscope slides	
syringe and 25 5/8 gauge needle	
0.2 M NaOH	
Butanediol diglycidyl ether (BDDE)	Aldrich 220892
Hyaluronic acid	Aldrich 53747
Medium binder clips	

Procedure

Push a rubber mold onto a microscope slide so that it adheres.
Weigh out 10 mg of HA into the mold.
Cover the mold with a second microscope slide and clip with two binder clips.
Prepare a solution of 950 μL 0.2 M NaOH + 50 μL BDDE.
Inject solution into each well until all air is replaced with solution. Avoid bubbles.
Place gels in oven at 40°C for 8-24 hours.
Remove gels from oven.
Place gels in large excess of saline (0.9% NaCl) for 24 hours to reach equilibrium swelling.

A.8 Hyaluronidase degradation of HA-BDDE hydrogels

Materials
Bovine testicular hyaluronidase (999 U/mg) Sigma H3506
Saline (0.9% sodium chloride)

Procedure
Swell hydrogels to equilibrium in saline after synthesis. Exchange buffer several times to rinse out sodium hydroxide solution.
Prepare 500 U/mL hyaluronidase in saline.
Weigh hydrogels for initial time point.
Transfer each gel to 10 mL of hyaluronidase and place in incubator at 37°C.
Remove hydrogels from solution, weigh, and return to solution at timepoints.
Calculate percent degradation by

$$\%Degradation = \frac{W_0 - W_t}{W_0} \times 100\%$$

where W_0 [mg] is the initial wet weight of the hydrogel and W_t [mg] is the wet weight of the hydrogel at time t.

A.9 Preparation of photocured GMHA films

Materials
Methacryloyl hyaluronic acid (GMHA)
Irgacure 2959 Ciba Specialty Chemicals
UV lamp (365 nm, 22 mW/cm^2)
0.2 μm syringe filter
non-TC treated 12-well plate

Important: Maintain the sterility of the GMHA films. Contaminated films turn white and opaque and can not be used for experiment.

Procedure

Prepare a stock solution of 1% w/v Irgacure 2959 in ddI water. Sonicate 30-45 minutes to dissolve. Do not oversonicate.

Weigh out 150 mg of GMHA into a 20 mL vial.

Add 14.25 mL of ddI water and 0.75 mL stock Irgacure solution to the vial. The final concentration of I2959 is 0.05% w/v. The final concentration of GMHA is 1% w/v.

Mix GMHA solution overnight.

Use a sterile non-TC treated 12-well plate for a mold. Area of one well is 3.8 cm^2.

Filter sterilize the GMHA solution with a 0.2 μm syringe filter directly into the 12 well plate. Use 2.6 mL per well.

Let the solution evaporate (~4 days at ambient conditions) in a sterile tissue culture flow hood in the dark.

After drying carefully remove the film from the mold with an exacto knife and tweezers. Use scissors to trim the edge of the film is necessary.

Transfer the film to a small sterile petri dish. Crosslink films by exposing to UV lamp for 1 minute.

Note: If ambient humidity is too low then the films will be too dry to crosslink. In this case place the films in a sterile air-tight container equilibrated with a saturated salt solution. Saturated KCl is equivalent to 84-86% relative humidity. Protect films from light. Equilibrate for 3-4 days before crosslinking.

A.10 Preparation of urea-templated hydrogels

Purpose: Create small droplet-sized hydrogels on microscope slide patterned with urea crystals.

Materials

Methacryloyl-hyaluronic acid (GMHA)	
Irgacure 2959	Ciba Specialty Chemicals
Sodium alginate	Sigma A2158
Chitosan	Aldrich 448877
Tetra-functional poly(ethylene glycol) acrylate (MW 10,000)	Sunbio
Urea	EM Science UX0065
Fish skin gelatin	Sigma G7041
Dextran-TRITC	Sigma T1162
Bovine serum albumin-FITC	Sigma A9771

Procedure for preparing urea-templated hyaluronic acid hydrogels

Prepare a 1% solution of GMHA in ddI water with 0.05% w/v Irgacure 2959 and 4% w/v urea. Stir overnight.

Dispense a small droplet (10-40 μL) onto a glass microscope slide.

Let droplet dry at ambient humidity and temperature. This can take up to 1-2 hours but is typically rapid. Protect from light and dust. The dried viscous droplet should attain a long-lasting metastable state of saturated urea solution.

Scrape the tips of a pair of fine needle forceps against solid urea crystals. Touch the tips of the forceps to the dried droplet to nucleate crystallization.

Photocrosslink the hydrogel with 1 minute of UV exposure. Rinse hydrogel in water to remove urea.

Procedure for low ambient humidity

It is recommended to perform the drying step at ambient conditions if possible for ease only. If ambient humidity is too low (during cold outdoor temperatures) then the urea will spontaneously nucleate.

In this case dry the droplet in a sealed container with a saturated solution of sodium chloride (relative humidity = 75-78%) or calcium nitrate (relative humidity = 47-56%). The droplets should be incubated overnight.

Open the container only when ready to nucleate crystallization.

After crystalliation keep hydrogel-crystals in container until immediately prior to UV exposure to prevent hydrogels from drying out.

Procedure for urea-templated hydrogels of other polymers

Alginate solutions should be prepared with 1% alginate and 4% urea. After drying the droplet the crosslinking can be accomplished by covering the droplets with a small volume of 20% w/v calcium chloride for 2 minutes.

Chitosan solutions should be prepared at 1% w/v in 0.1 M acetic acid. The droplets can be gelled by covering the droplets with a small volume of 10 M sodium hydroxide for 2 minutes.

Tetra-functional PEG-acrylate solutions should be prepared at 1% w/v with 0.05% Irgacure 2959. Crosslink the droplets with 1 minute of UV exposure.

Procedure for functionalization of hydrogels

The hydrogels can be fluorescently functionalized by addition of fluorescently conjugated macromolecules. Both BSA-FITC and dextran-TRITC can be used; however, dextran-TRITC is preferable because BSA exhibits foaming and aggregation. These fluorescently tagged molecules should be added to the biopolymer solutions at concentrations of 1-2% w/w with respect to the biopolymer concentration.

Fish skin gelatin can be added to render the hydrogels cell adhesive. Use a concentration of 2% w/v in the biopolymer solutions. However, this protein alters the viscosity of the droplets and crystal morphology. If alginate is used then the droplets can be dessicated to obtain the typical urea-template morphology, otherwise larger more florid crystal morphology will be obtained.

A.11 Preparation of urea-templated photocured GMHA and alginate films

Purpose: Create large free-standing thick films of hydrogel templated with urea-crystals

Materials

Methacryloyl hyaluronic acid (GMHA)	
Irgacure 2959	Ciba Specialty Chemicals
Sodium alginate	Sigma A2158
UV lamp (365 nm, 22 mW/cm^2)	
0.2 μm syringe filter	
non-TC treated 12-well plate	

Important: Maintain the sterility of the GMHA films.

Procedure

Prepare a stock solution of 1% w/v Irgacure 2959 in ddI water. Sonicate 30-45 minutes to dissolve. Do not oversonicate.

Weigh out 150 mg of GMHA and 600 mg of urea into a 20 mL vial.

Add 14.25 mL of ddI water and 0.75 mL stock Irgacure solution to the vial. The final concentration of I2959 is 0.05% w/v. The final concentration of GMHA is 1% w/v. (Note: Alginate solutions should be prepared with same concentrations but without photoinitiator).

Mix GMHA solution overnight.

Use a sterile non-TC treated 12-well plate for a mold. Area of one well is 3.8 cm^2.

Filter sterilize the GMHA solution with a 0.2 μm syringe filter directly into the 12 well plate. Use 2.6 mL per well.

Let the solution evaporate (~4 days at ambient conditions) in a sterile tissue culture flow hood in the dark.

Scrape the tips of a pair of fine needle forceps against solid urea crystals. Touch the tips of the forceps to the dried films to nucleate crystallization.

Carefully remove the film from the mold with an exacto knife and tweezers. Use scissors to trim the edge of the film if necessary.

Transfer the film to a small sterile petri dish.

Crosslink GMHA films by exposure to UV lamp for 1 minute. Crosslink alginate films by immersion in 15 mL of 20% calcium chloride for twenty minutes. Rinse extensively with water to remove urea.

A.12 Preparation of hydrogel mesh microarray

Purpose: Pattern a substrate with a microarray of hydrogel compartments.

Materials

Methacryloyl hyaluronic acid (GMHA)	
Irgacure 2959	Ciba Specialty Chemicals
Sodium alginate	Sigma A2158
Chitosan	Aldrich 448877
UV lamp (365 nm, 22 mW/cm^2)	Blak-Ray Model B-100A
Tissue culture treated polystyrene	
Glass microscope slides or coverslips	
Nylon 6/6 Mesh	Small Parts Inc.

Procedure

Prepare a solution of 1% w/v GMHA with 0.05% w/v Irgacure 2959. Stir overnight.

Cut out a small piece of Nylon mesh. Coat the Nylon mesh with GMHA solution by dipping.

Wick excess solution from the Nylon mesh if necessary.

Place the Nylon mesh flat onto a suitable substrate (glass or TCPS).

Dry in tissue culture hood. Time required is about 20-40 minutes.

Remove Nylon mesh with tweezers. Hydrogel mesh should remain adhered to substrate.

Crosslink mesh with 1 minute of UV exposure and rinse in water to remove photoinitiator.

Notes

Alginate mesh can be prepared by using a 1% w/v solution of alginate. Crosslink by immersion in 20% calcium chloride for two minutes.

Chitosan mesh can be prepared by using a 1% w/v solution of chitosan in 0.1 M acetic acid. Crosslink by immersion in 10 M sodium hydroxide for two minutes. Rinse to neutralize pH.

Dextran-TRITC can be added to render the hydrogel mesh fluorescent. Add dextran-TRITC at a concentration of 1-2% w/w with respect to biopolymer.

Troubleshooting

If hydrogel compartments are completely coated with hydrogel then wick off more solution before placing coated Nylon mesh onto substrate.

Adherence of hydrogel mesh to substrate rather than Nylon is sensitive to ambient humidity. If hydrogel mesh is not adhering to substrate then place Nylon mesh and substrate in a dessicator for ~10-20 minutes prior to remove Nylon. However, complete dessication will also cause the hydrogels to stick to Nylon.

A.13 Preparation of living cell microarray

Materials

Substrate patterned with hydrogel mesh	
Polycarbonate well	
PDMS spacer	
Electrical tape	
Normal human dermal fibroblasts	Lonza
Primary rat Schwann cells	ScienCell
Dulbeccos Modified Eagle's Medium (DMEM)	Sigma D5648
Fetal bovine serum (FBS)	Hyclone SH30071.03
Phosphate buffered saline (PBS, pH 7.4, 10 mM)	
Trypsin-EDTA solution (TRED 0.25%)	Sigma T4049
Pennicillin-Streptomycin antibiotic solution (PennStrep)	Sigma A5955
Live/Dead Cell Viability/Cytotoxicity Kit	Invitrogen L3224

Cell Culture

Fibroblasts should be cultured in TCPS 75 cm^2 flasks with DMEM supplemented with 10% FBS at 37°C and 5% CO_2. Passage fibroblasts using TRED diluted 10x in PBS.

Schwann cells should be plated in TCPS 10 cm plates coated with poly-L-lysine. Culture Schwann cells with DMEM supplemented with 10% FBS at 37°C and 5% CO_2. Passage Schwann cells using TRED.

Preparation of substrates with assembly of cell wells

Use polycarbonate cell wells with 1 cm^2 area for cell growth. Prepare thin (2-4 mm) spacers of PDMS from resin and curing agent. Cut spacers to same size as polycarbonate cell well. Sterilize polycarbonate and PDMS by soaking in 70% ethanol.

UV sterilize hydrogel patterned substrates for 30 minutes in vertical tissue culture flow hood.

Place a PDMS spacer onto substrate. Place a polycarbonate well on top of the spacer and secure pieces tightly with electrical tape.

Place substrates with assembled wells in sterile 10 cm TCPS dishes and wrap with ParaFilm. Store substrates at 4°C until use.

Preparation of living cell microarray

Prepare 10 mL of DMEM with 10% FBS and 1:100 dilution of PennStrep.

Passage cells, centrifuge, and resuspend in above media. Determine cell concentration by counting cells with hemocytometer. Dilute cells to about 50,000 per mL. Add 700 μL of cell suspension to each well.

Incubate cells for 15 minutes then gently rock well to distribute poorly adhered cells across substrate.

Incubate and rock for 1 hour. Then aspirate media and unadhered cells. Replenish media with fresh.

If desired treat cells with calcein (2 μL stock 4 mM calcein diluted in 10 mL PBS) for 45 minutes to assess cell viability.

Reference: Revzin, A., Tompkins, R.G., Toner, M. Surface engineering with poly(ethylene glycol) photolithography to create high-density cell arrays on glass. *Langmuir* **19**, 9855-9862 (2003).

A.14 Fixing and staining of living cell microarray

Purpose: Stain array of fibroblasts with DAPI and Phalloidin

Materials

Alexa-Fluor 488-Phalloidin	Invitrogen A12379
4'6-diamidino-2-phenyl-indole dihydrochloride (DAPI)	Invitrogen D1306
Paraformaldehyde	Sigma P6148
Triton X-100	Fluka 93426
Phosphate buffered saline (PBS, pH 7.4, 10 mM)	
Fetal bovine serum	Hyclone SH30071.03

Procedure

Prepare fixative solution of 4% paraformaldehyde and 4% sucrose in PBS.
Prepare a stock of sterile PBS for rinsing.
Prepare a stock of blocking solution (3% FBS in PBS).

Rinse cells twice with PBS to remove serum proteins.

Fix cells by incubating with fixative solutoin for 20 minutes at 37°C.

Rinse cells twice with PBS.

Permeabilize cells by incubation with 0.1% Triton X-100 in PBS for 5 minutes at room temperature.

Rinse cells twices with PBS.

Block cells with 3% FBS/PBS for 30 minutes at room temperature.

Prepare a solution of Phalloidin-Alexa 488 (1:400 dilution in blocking solution).

Incubate cells with Phalloidin for 60 minutes at room temperature.

Rinse cells once with PBS. Then rinse cells twice with PBS for 3 minutes.

Incubate cells with DAPI (1:1000 dilution in PBS) for 5 minutes at room temperature.

Rinse cells once with PBS. Then rinse cells twice with PBS for 3 minutes.

Check quality of fluorescent staining by epifluorescence.

Carefully disassemble cell well without disturbing cells. Place a small volume of PBS on cells. Cover cells with a No. 1 coverslip and seal with nail polish.

Image cells by confocal fluorescence microscopy (located in MBB 1.426). Capture single scans at 2048x2048 resolution and z-series at 512x512 resolution. DAPI stains heavier than Phalloidin by this protocol so make sure that DAPI fluorescence does not bleed into Phalloidin images which will cause cells to look uniformly blue-green. After imaging, use Imaris workstation in MBB to assemble 3-dimensional projections of confocal z-series.

Bibliography

Agerup, B. Polysaccharide gel composition. US Patent 5,827,937, 1998.

Agerup, B., Berg, P., Akermark, C. Non-animal stabilized hyaluronic acid. *BioDrugs,* **19**, 23-30 (2005).

Albrecht, D.R., Tsang, V.L., Sah, R.L., Bhatia, S.N. Photo- and electropatterning of hydrogel-encapsulated living cell arrays. *Lab Chip* **5**, 111-118 (2005).

Almarza, A.J., Athanasiou, K.A. Design characteristics for the tissue engineering of cartilaginous tissues. *Ann. Biomed. Eng.* **32**, 2-17 (2004).

Anniko, M., Arnold, W. Hyaluronic acid as a molecular filter and friction-reducing lubricant in the human inner ear. *ORL J. Otorhinolaryngol. Relat. Spec.* **57**, 82-86 (1995).

Arshinoff, S.A. Dispersive-cohesive viscoelastic soft shell technique. *J. Cataract Refract. Surg.,* **25**, 167-173 (1999).

Augst, A.D., Kong, H.J., Mooney, D.J. Alginate hydrogels as biomaterials. *Macromol. Biosci.* **6**, 623-633 (2006).

Balazs, E.A. Ultrapure hyaluronic acid and the use thereof. US Patent No 4,141,973 (1979).

Balazs, E.A., Leshchiner, A. Cross-linked gels of hyaluronic acid and products containing such gels. US Patent 4,582,865 (1986).

Bartsch, H., Konig, W.A., Strassner, M., Hintze, U. Quantitative determination of native and methylated cyclodextrins by matrix-assisted laser desorption/ionization time-of-flight mass spectrometry. *Carbohyd. Res.* **286**, 41-53 (1996).

Bekkers, J.M. & Hausser, M. Targeted dendrotomy reveals active and passive contributions of the dendritic tree to synaptic integration and neuronal output. *P. Natl. Acad. Sci. USA* **104**, 11447-11452 (2007).

Bencherif, S.A., Srinivasan, A., Horkay, F., Hollinger, J.O., Matyjaszewski, K., Washburn, N.R. Influence of the degree of methacrylation on hyaluronic acid hydrogels properties. *Biomaterials* **29**, 1739-1749 (2008).

Bishop, P.N. Structural macromolecules and supramolecular organization of the vitreous gel. *Prog. Retin. Eye Res.,* **19**, 323-344 (2000).

Brisken, C. & Rajaram, R.D. Alveolar and lactogenic differentiation. *J. Mammary Gland Biol. Neoplasia* **11**, 239-248 (2006).

Brockmeier, S.F., Shaffer, B.S. Viscosupplementation therapy for osteoarthritis. *Sports Med. Arthrosc. Rev.* **14**, 155-162 (2006).

Brondsted, H., Andersen, C., Hovgaard, L. Crosslinked dextran - a new capsule material for colon targeting of drugs. *J. Control Release* **53**, 7-13 (1998).

Bryant, S.J., Nuttelman, C.R., Anseth, K.S. Cytocompatibility of UV and visible light photoinitiating systems on cultured NIH/3T3 fibroblasts in vitro. *J. Biomater. Sci. Polym. Ed.* **11**, 439-457 (2000).

Burdick, J.A., Chung, C., Jia, X.Q., Randolph, M.A., Langer, R. Controlled degradation and mechanical behavior of photopolymerized hyaluronic acid networks. *Biomacromolecules*, **6**, 386-391 (2005).

Buvari-Barcza, A., Barcza, L. Influence of the guests, the type and degree of substitution on inclusion complex formation of subsituted β-cyclodextrins. *Talanta* **49**, 577-585 (1999).

Challa, R., Ahuja, A., Ali, J., Khar, R.K. Cyclodextrins in drug delivery: An updated review. *AAPS PharmSciTech* **6**, 329-357 (2005).

Chankvetadze B, Endresz G, Blaschke G, Juza M, Jakubetz H, Schurig V. Analysis of charged cyclomalto-oligosaccharides (cyclodextrin) derivatives by ion-spray, matrix-assisted laser-desorption/ionization time-of-flight and fast-atom bombardment mass spectrometry, and by capillary electrophoresis. *Carbohyd. Res.* **287**, 139-155 (1996).

Chen, J., Park, H., Park, K. Synthesis of superporous hydrogels: hydrogels with fast swelling and superabsorbent properties. *J. Biomed. Mater. Res*. **44**, 53-62 (1999).

Chen, W.Y., Abatangelo, G. Functions of hyaluronan in wound repair. *Wound Repair Regen.,* **7**, 79-89 (1999).

Chirila, T.V., Hong, Y., Dalton, P.D., Constable, I.J., Refojo, M.F. The use of hydrophilic polymers as artificial vitreous *Prog. Polym. Sci.,* **23**, 475-508 (1998).

Cho, C.H, Eliason, J.F., Matthew, H.W.T. Application of porous glycosaminoglycan-based scaffolds for expansion of human cord blood stem cells in perfusion culture. *J. Biomed. Mater. Res.,* **86**, 98-107 (2008).

Chung, C., Mesa, J., Miller, G.J., Randolph, M.A., Gill, T.J., Burdick, J.A. Effects of auricular chondrocyte expansion on neocartilage formation in photocrosslinked hyaluronic acid networks. *Tissue Eng.* **12**, 2665-2673 (2006).

Collins, M.N., Birkinshaw, C. Comparison of the effectiveness of four different crosslinking agents with hyaluronic acid hydrogel films for tissue-culture applications. *J. Appl. Polym. Sci.,* **104**, 3183-3191 (2007).

Crescenzi, V., Francescangeli, A., Taglienti, A., Capitani, D., Mannina, L. Synthesis and partial characterization of hydrogels obtained via glutaraldehyde crosslinking of acetylated chitosan and of hyaluronan derivatives. *Biomacromolecules* **4**, 1045-1054 (2003).

Cromwell, W.C., Bystrom, K., Eftink, M.R. Cyclodextrin adamantanecarboxylate inclusion complexes – Studies of the variation in cavity size. *J. Phys. Chem.* **89**, 326-332 (1985).

Davies, N.M., Wang, G., Tucker, I.G. Evaluation of a hydrocortisone/hydroxypropyl-beta-cyclodextrin solution for ocular drug delivery. *Int. J. Pharm.* **156**, 201-209 (1997).

Drury, J.L., Mooney, D.J. Hydrogels for tissue engineering: scaffold design variables and applications. *Biomaterials* **24**, 4337-4351 (2003).

Duffy, D.C., McDonald, J.C., Schueller, O.J.A., Whitesides, G.M. Rapid prototyping of microfluidic systems in poly(dimethylsiloxane). *Anal. Chem.* **70**, 4974-4984 (1998).

Dufva, M. Fabrication of high quality microarrays. *Biomol. Eng.,* **22**, 173-184 (2005).

Estes, J.M., Adzick, N.S., Harrison, M.R., Longaker, M.T., Stern, R. Hyaluronate metabolism undergoes an ontogenic transition during fetal development: implications for scar-free wound healing. *J. Pediatr. Surg.,* **28**, 1227-31 (1993).

Falconnet, D., Csucs, G., Grandin, H.M., Textor, M. Surface engineering approaches to micropattern surfaces for cell-based assays. *Biomaterials*, **27**, 3044-3063 (2006).

Fraser, J.R.E., Laurent, T.C., Laurent, U.B.G. Hyaluronan: It's nature, distribution, functions and turnover. *J. Intern. Med.* **242**, 27-33 (1997).

Fukuda, J., Khademhosseini, A., Yeh, J., Eng, G., Cheng, J.J., Farokhzad, O.C., Langer, R. Micropatterned cell co-cultures using layer-by-layer deposition of extracellular matrix components. *Biomaterials*, **27**, 1479-1486 (2006).

George, M. & Abraham, T.E. Polyionic hydrocolloids for the intestinal delivery of protein drugs: alginate and chitosan – a review. *J. Control. Release* **114**, 1-14 (2006).

Hahn, M.S., Miller, J.S., West, J.L. Three-dimensional biochemical and biomechanical patterning of hydrogels for guiding cell behavior. *Adv. Mater.,* **18**, 2679-2684 (2006).

Hahn, S.K., Jelacic, S., Maeir, R.V., Stayton, P.S., Hoffman, A.S. Anti-inflammatory drug delivery from hyaluronic acid hydrogels. *J. Biomat. Sci. Polym. E.* **15**: 1111-1119 (2004).

Hansell, P., Gorranson, V., Odlind, C., Gerdin, B., Hallgren, R. Hyaluronan content in the kidney in different states of body hydration. *Kidney Int.* **58**, 2061-2068 (2000).

Hedges, A.R. Industrial applications of cyclodextrins. *Chem. Rev.* **98**, 2035-2044 (1998).

Hemmrich, K., von Heimburg, D., Rendchen, R., Bartolo, C.D., Milella, E., Pallua, N. Implantation of preadipocyte-loaded hyaluronic acid-based scaffolds into nude mice to evaluate potential for soft tissue engineering. *Biomaterials* **26**, 7025-7037 (2005).

Higuchi, T., Connors, K.A. Phase solubility techniques. *Adv. Anal. Chem. Instru.* **4**, 117 (1965).

Hoare, T.R., Kohane, D.S. Hydrogels in drug delivery: progress and challenges. *Polymer*, **49**, 1993-2007 (2008).

Hongyan, H., Guan, J., Lee, J.L. An oral delivery device based on self-folding hydrogels. *J. Control Release* **110**, 339-346 (2006).

Hu, M., Sabelman, E.E., Cao, Y., Chang, J., Hentz, V.R. Three-dimensional hyaluronic acid grafts promote healing and reduce scar formation in skin incision wounds. *J. Biomed. Mater. Res. B Appl. Biomater.* **67**, 586-592 (2003).

Huang, X., Brazel, C.S. On the importance and mechanisms of burst release in matrix-controlled drug delivery systems. *J. Control Release* **73**, 121-136 (2001).

Huber, M., Trattnig, S., Lintner, F. Anatomy, biochemistry, and physiology of articular cartilage. *Invest. Radiol.,* **35**, 574-580 (2000).

Itano, N., Kimata, K. Mammalian hyaluronan synthases. *IUBMB Life* **54**, 195-199 (2002).

Ito, T., Fraser, I.P., Yeo, Y., Highley, C.B., Bellas, E., Kohane, D.S. Anti-inflammatory function of an in situ cross-linkable conjugate hydrogel of hyaluronic acid and dexamethasone. *Biomaterials* **28**, 1778-1786 (2007).

Jacquet, R., Favetta, P., Elfakir, C., Lafosse, M. Characterization of a new methylated beta-cyclodextrin with a low degree of substitution by matrix-assisted laser desorption/ionization mass spectrometry and liquid chromatography using evaporative light scattering detection. *J. Chromatogr. A* **1083**, 106-112 (2005).

Jia, X.Q. *et al*. Synthesis and characterization of in situ cross-linkable hyaluronic acid-based hydrogels with potential application for vocal fold regeneration. *Macromolecules* **37**, 3239-3248 (2004).

Jia, X., Yeo, Y., Clifton, R.J., Jiao, T., Kohane, D.S., Kobler, J.B., Zeitels, S.M., Langer, R. Hyaluronic acid-based microgels and microgel networks for vocal fold regeneration. *Biomacromolecules* **7**, 3336-3344 (2006).

Johl, S.S., Burgett, R.A. Dermal filler agents: a practical review. *Curr. Opin. Ophthalmol.,* **17**, 471-479 (2006).

Khademhosseini, A., Langer, R., Borenstein, J., Vacanti, J.P. Microscale technologies for tissue engineering and biology. *P. Natl. Acad. Sci. USA* **103**, 2480-2487 (2006).

Kim, H., Cohen, R.E., Hammond, P.T., Irvine, D.J. Live lymphocyte arrays for biosensing *Adv. Funct. Mater.,* **16**, 1313-1323 (2006).

Kim, S.W., Bae, Y.H., Okano, T. Hydrogels – Swelling, drug loading, and release. *Pharm. Res.* **9**, 283-290 (1992).

King, K.R., Wang, C.C.J., Kaazempur-Mofrad, M.R., Vacanti, J.P., Borenstein, J.T. Biodegradable microfluidics. *Adv. Mater.* **16**, 2007-2012 (2004).

Kirchner, M., Marshall, R.N. A double-blind randomized controlled trial comparing alternate forms of high molecular weight hyaluronan for the treatment of osteoarthritis of the knee. *Osteoarthritis Cartilage,* **14**, 154-162 (2006).

Larina, O. & Thorn, P. Ca^{2+} dynamics in salivary acinar cells: distinct morphology of the acinar lumen underlies near-synchronous global Ca^{2+} responses. *J. Cell Sci.* **118**, 4131-4139 (2005).

Leach, J.B., Bivens, K.A., Patrick, C.W., Schmidt, C.E. Photocrosslinked hyaluronic acid hydrogels: natural, biodegradable tissue engineering scaffolds. *Biotechnol. Bioeng.,* **82**, 578-589 (2003).

Leach, J.B., Bivens, K.A., Collins, C.N., Schmidt, C.E. Development of photocrosslinkable hyaluronic acid-polyethylene glycol-peptide composite hydrogels for soft tissue engineering. *J. Biomed. Mater. Res.,* **70**, 74-82 (2004).

Leach, J.B., Schmidt, C.E. Characterization of protein release from photocrosslinkable hyaluronic acid-polyethylene glycol hydrogel tissue engineering scaffolds. *Biomaterials,* **26**, 125-135 (2005).

Lee, J.Y., Shah, S.S., Zimmer, C.C., Liu, G., Revzin, A. Use of photolithography to encode cell adhesive domains into protein microarrays. *Langmuir* **24**, 2232-2239 (2008).

Liu, F.Y., Kildsig, D.O., Mitra, A.K. Beta-cyclodextrin steroid complexation – Effect of steroid structure on association equilibria. *Pharm. Res.* **7**, 869-873 (1990).

Loftsson, T., Frioriksdottir, H., Sigurdardottir, A.M., Ueda, H. The effect of water-soluble polymers on drug-cyclodextrin complexation. *Int. J. Pharm.* **110**, 169-177 (1994).

Lu, Y., Mapili, G., Suhali, G., Chen, S., Roy, K. A digital micro-mirror device-based system for the microfabrication of complex, spatially patterned tissue engineering scaffolds. *J. Biomed. Mater. Res.,* **77A**, 396-405 (2006).

Luo, Y., Shoichet, M.S. A photolabile hydrogel for guided three-dimensional cell growth and migration. *Nat. Mater.* **3**, 249-253 (2004).

Ma, P.X., Choi, J.W. Biodegradable polymer scaffolds with well-defined interconnected spherical pore network. *Tissue Eng.,* **7**, 23-33 (2001).

Malson, T., Lindqvist, B.L. Gel of crosslinked hyaluronic acid for use as a vitreous humor substitute. US Patent 4,716,154, 1987.

Mapili, G., Lu, Y., Chen, S.C., Roy, K. Laser-layered microfabrication of spatially patterned functionalized tissue engineering scaffolds. *J. Biomed. Mater. Res.* **75B**, 414-424 (2005).

Marshall, K.W. Intra-articular hyaluronan therapy. *Curr. Opin. Rheumatol.* **12**, 468-474 (2000).

Metcalfe, A.D., Ferguson, M.W.J. Tissue engineering of replacement skin: the crossroads of biomaterials, wound healing, embryonic development, stem cells and regeneration. *J. R. Soc. Interface,* **4**, 413-437 (2007).

Meyer, K., Palmer, J.W. The polysaccharide of vitreous humor *J. Biol. Chem.,* **107**, 629-634 (1934).

Mikos, A.G., Thorsen, A.J., Czerwonka, L.A., Bao, Y., Langer, R., Winslow, D.N., Vacanti, J.P. Preparation and characterization of poly(L-lactic acid) foams. *Polymer,* **35**, 1068-1077 (1994).

Monheit, G.D., Coleman, K.M. Hyaluronic acid fillers. *Dermatol. Ther.,* **19**, 141-150 (2006).

Murphy, W.L., Dennis, R.G., Kileny, J.L., Mooney, D.J. Salt fusion: an approach to improve pore interconnectivity within tissue engineering scaffolds. *Tissue Eng.,* **8**, 43-52 (2002).

Narayanaswamy, R., Niu, W., Scouras, A.D., Hart, G.T., Davies, J., Ellington, A.D., Iyer, V.R., Marcotte, E.M. Systematic profiling of cellular phenotypes with spotted cell microarrays reveals mating-pheromone response genes. *Genome Biol.,* **7**:R6 (2006).

Nettles, D.L., Vail, T.P., Morgan, M.T., Grinstaff, M.W., Setton, L.A. Photocrosslinkable hyaluronan as a scaffold for articular cartilage repair. *Ann. Biomed. Eng.* **32**, 391-397 (2004).

Nordsletten, D.A., Blackett, S., Bentley, M.D., Ritman, E.L., Smith, N.P. Structural morphology of renal vasculature. *Am. J. Physiol. Heart Circ. Physiol.,* **2006**, 291, H296-H309.

Oaki, Y. & Imai, H. Experimental demonstration for the morphological evolution of crystals grown in gel media. *Cryst. Growth Des.* **3,** 711-716 (2003).

Omidian, H., Rocca, J.G., Park, K. Advances in superporous hydrogels. *J. Control. Release* **102**, 3-12 (2005).

Park, S.N., Kim, J.K., Suh, H. Evaluation of antibiotic-loaded collagen-hyaluronic acid matrix as a skin substitute. *Biomaterials* **25**, 3689-3698 (2004).

Park, Y.D., Tirelli, N., Hubbell, J.A. Photopolymerized hyaluronic acid-based hydrogels and interpenetrating networks. *Biomaterials,* **24**, 893-900 (2003)

Payan, E., Jouzeau, J.Y., Lapicque, F., Bordji, K., Simon, G., Gillet, P., O'Regan, M., Netter, P. In-vitro drug-release from HYC-141, a corticosteroid ester of high-molecular-weight hyaluronan. *J Control Release* **34**, 145-153 (1995).

Peattie, R.A., Rieke, E.R., Hewett, E.M., Fisher, R.J., Shu, X.J., Prestwich, G.D. Dual growth factor-induced angiogenesis in vivo using hyaluronan hydrogel implants. *Biomaterials,* **27**, 1868-1875 (2006).

Peppas, N.A., Bures, P., Leobandung, W., Ichikawa, H. Hydrogels in pharmaceutical formulations. *Eur. J. Pharm. Biopharm.* **50**, 27-46 (2000).

Pike, D.B., Cai, S., Pomraning, K.R., Firpo, M.A., Fisher, R.J., Shu, X.Z., Prestwich, G.D., Peattie, R.A. Heparin-regulated release of growth factors in vitro and angiogenic response in vivo to implanted hyaluronan hydrogels containing VEGF and bFGF *Biomaterials,* **27**, 5242-5251 (2006).

Prestwich, G.D., Marecak, D.M., Marecek, J.F., Vercruysse, K.P., Ziebell, M.R. Controlled chemical modification of hyaluronic acid: synthesis, applications and biodegradation of hydrazide derivatives. *J. Control Release* **53**, 93-103 (1998).

Price, R.D., Myers, S., Leigh, I.M., Navsaria, H.A. The role of hyaluronic acid in wound healing. *Am. J. Clin. Dermatol.* **6**, 393-402 (2005).

Price, R.D., Das-Gupta, V., Leigh, I.M., Navsaria, H.A. A comparison of tissue-engineered hyaluronic acid dermal matrices in a human wound model. *Tissue Eng.* **12**, 2985-2995 (2006).

Reijnen, M.M.P.J., Bleichrodt, R.P., van Goor, H. Pathophysiology of intra-abdominal adhesion and abscess formation, and the effect of hyaluronan. *Brit. J. Surg.,* **90**, 533-541 (2003).

Revzin, A., Tompkins, R.G., Toner, M. Surface engineering with poly(ethylene glycol) photolithography to create high-density cell arrays on glass. *Langmuir* **19**, 9855-9862 (2003).

Saltzman, W.M., Olbrich, W.L. Building drug delivery into tissue engineering. *Nat. Rev. Drug Discov.* **11**, 177-186 (2002).

Sannino, A., Madaghiele, M., Conversano, F., Mele, G., Maffezzoli, A., Netti, P.A., Ambrosio, L., Nicolais, L. Cellulose derivative-hyaluronic acid-based microporous hydrogels cross-linked through divinyl sulfone (DVS) to modulate equilibrium sorption capacity and network stability. *Biomacromolecules* **5**, 92-96 (2004).

Savani, R.C., Cao, G., Pooler, P.M., Zaman, A., Zhou, Z., DeLisser, H.M. Differential involvement of the hyaluronan (HA) receptors CD44 and receptor for HA-mediated motility in endothelial cell function and angiogenesis. *J. Biol. Chem.* **276**, 36770-36778 (2001).

Schugens, Ch., Maquet, V., Grandfils, C., Jerome, R., Teyssie, Ph. Biodegradable and macroporous polylactide implants for cell transplantation: 1. Preparation of

macroporous polylactide supports by solid-liquid phase separation. *Polymer,* **37**, 1027-1038 (1996).

Shah, M.M., Sampogna, R.V., Sakurai, H., Bush, K.T., Nigam, S.K. Branching morphogenesis and kidney disease. *Development* **131**, 1449-1462 (2004).

Sharma, B., Elisseeff, J.H. Engineering structurally organized cartilage and bone tissues. *Ann. Biomed. Eng.* **32**, 148-159 (2004).

Shiedlin, A., Bigelow, R., Christopher, W., Arbabi, S., Yang, L., Maier, R.V., Wainwright, N., Childs, A., Miller, R.J. Evaluation of hyaluronan from different sources: streptococcus zooepidemicus, rooster comb, bovine vitreous, and human umbilical cord. *Biomacromolecules,* **5**, 2122-2127 (2004).

Smeds, K.A., Pfister-Serres, A., Hatchell, D.L., Grinstaff, M.W. Synthesis of a novel polysaccharide hydrogel. *J.M.S. Pure Appl. Chem.,* **A36**, 981-989 (1999).

Smeds, K.A., Grinstaff, M. Photocrosslinkable polysaccharides for in situ hydrogel formation. *J. Biomed. Mater. Res. A* **54**, 115-121 (2001).

Stern, R. Devising a pathway for hyaluronan catabolism: are we there yet? *Glycobiology,* **13**, 105R-115R (2003).

Struve, J., Maher, P.C., Li, Y., Kinney, S., Fehlings, M.G., Kuntz, C., Sherman, L.S. Disruption of the hyaluronan-based extracellular matrix in spinal cord promotes astrocyte proliferation. *Glia* **52**, 16-24 (2005).

Szeman, J., Fenyvesi, E., Szejtli, J., Ueda, H., Machida, Y., Nagai, T. Water-soluble cyclodextrin polymers – Their interaction with drugs. *J. Inclusion Phenom.* **5**, 427-431 (1987).

Szente, L., Szejtli, J. Highly soluble cyclodextrin derivatives: chemistry, properties, and trends in development. *Adv. Drug Deliver. Rev.,* **36**, 17-28 (1999).

Tawhai, M.H., Hunter, P., Tschirren, J., Reinhardt, J., McLennan, G., Hoffman, E.A. CT-based geometry analysis and finite element models of the human and ovine bronchial tree. *J. Appl. Physiol.,* **2004**, 97, 2310-2321.

Teng, Y.D., Lavik, E.B., Qu, X., Park, K.I., Ourednik, J., Zurakowski, D., Langer, R., Snyder, E.Y. Functional recovery following traumatic spinal cord injury mediated by a unique polymer scaffold seeded with neural stem cells. *PNAS,* **99**, 3024-3029 (2002).

Tessmar, J.K., Gopferich, A.M. Matrices and scaffolds for protein delivery in tissuse engineering. *Adv. Drug Deliver. Rev.,* **59**, 274-291 (2007).

Tomihata, K., Ikada, Y. Crosslinking of hyaluronic acid with water-soluble carbodiimide. *J. Biomed. Mater. Res. A* **37**, 243-251 (1997).

Tomihata, K., Ikada, Y. Crosslinking of hyaluronic acid with glutaraldehyde. *J. Polym. Sci. A. Polym. Chem.* **35**, 3553-3559 (1997).

Tsang, V.L., Bhatia, S.N. Three-dimensional tissue fabrication. *Adv. Drug. Deliver. Rev*., **56**, 1635-1647 (2004).

Tsang, V.L., Chen, A.A., Cho, L.M., Jadin, K.D., Sah, R.L., DeLong, S., West, J.L., Bhatia, S.N. Fabrication of 3D hepatic tissue by additive photopatterning of cellular hydrogels. *FASEB J.,* **21**, 790-801 (2007).

Uekama, K., Fujinaga, T., Hirayama, F., Otagiri, M., Yamasaki, M. Inclusion complexations of steroid-hormones with cyclodextrins in water and in solid-phase. *Int. J. Pharm.* **10**, 1-15 (1982).

Uekama, K. Design and evaluation of cyclodextrin-based drug formulation. *Chem. Pharm. Bull.,* **52**, 900-915 (2004).

Ulcinas, A., Butler, M.F., Heppenstall-Butler, M., Singleton, S., Miles, M.J. Direct observation of spherulitic growth stages of $CaCO_3$ in a poly(acrylic acid)-chitosan system: In situ SPM study. *J. Cryst. Growth* **307,** 378-85 (2007).

Uludag, H., de Vos, P., Trasco, P.A. Technology of mammalian cell encapsulation. *Adv. Drug Deliver. Rev*. **42**, 29-64 (2000).

West, D.C., Hampson, I.N., Arnold, F., Kumar, S. Angiogenesis induced by degradation products of hyaluronic acid. *Science* **228**, 1324-1326 (1985).

Wheeler, D.B., Carpenter, A.E., Sabatini, D.M. Cell microarrays and RNA interference chip away at gene function. *Nature Genetics*, **37**, S25-S30 (2005).

Williams, C.G., Malik, A.N., Kim, T.K., Manson, P.N., Elisseeff, J.H. Variable cytocompatibility of six cell lines with photoinitiators used for polymerizing hydrogels and cell encapsulation. *Biomaterials* **26**, 1211-1218 (2005).

Xu, C.W. High-density cell microarrays for parallel functional determinations. *Genome Res.,* **12**, 482-486 (2002).

Xu, A., Ma, Y., Colfen, H. Biomimetic mineralization. *J. Mater. Chem.* **17**, 415-449 (2007).

Yang, S.F., Leong, K.F., Du, Z., Chua, C.K. The design of scaffolds for use in tissue engineering. Part II. Rapid prototyping techniques. *Tissue Eng.,* **8**, 1-11 (2002).

Yeo, Y., Kohane, D.S. Polymers in the prevention of peritoneal adhesions *Eur. J. Pharm. Biopharm.,* **68**, 57-66 (2008).

Yoo, H.S., Lee, E.A., Yoon, J.J., Park, T.G. Hyaluronic acid modified biodegradable scaffolds for cartilage tissue engineering. *Biomaterials* **26**, 1925-1933 (2005).

Yun, Y.H., Goetz, D.J., Yellen, P., Chen, W. Hyaluronan microspheres for sustained gene delivery and site-specific targeting. *Biomaterials* **25**, 147-157 (2004).

Zhang, J., Wu, L., Jing, D., Ding, J. A comparative study of porous scaffolds with cubic and spherical macropores. *Polymer,* **2005**, 46, 4979-4985.

Ziauddin, J., Sabatini, D.M. Microarrays of cells expressing defined cDNAs *Nature*, **411**, 107-110 (2001).

Vita

Scott Andrew Zawko was born in Rochester, New York on January 12, 1980 to Stanley and Andrea Zawko. He graduated from Pope High School in 1998 and attended the Georgia Institute of Technology. In 2002 he received a Bachelor of Science degree in chemical engineering and entered the Graduate School of The University of Texas.

Permanent Address: 1016 Camino La Costa, Austin, TX 78752.

This dissertation was typed by Scott Andrew Zawko.